A Dissertation for the Degree of Doctor of Philosophy

Regulation of Stemness and Aging in Human Mesenchymal Stem Cells

인간 중간엽줄기세포의 줄기세포능 및 노화 조절 연구

By

Kyung-Rok Yu

February 2013

Department of Veterinary Public Health,

College of Veterinary Medicine,

Graduate School of Seoul National University

ABSTRACT

Regulation of Stemness and Aging in Human Mesenchymal Stem Cells

Kyung-Rok Yu

Department of Veterinary Public Health,
College of Veterinary Medicine
Graduate School of Seoul National University

Supervisor : Kyung-Sun Kang, D.V.M., Ph.D.

Adult stem cells in mammalian organs play pivotal roles in the maintenance and repair of these organs throughout the adult life of the organism, and the main function of adult stem cells is to maintain the proper homeostasis of a tissue or organ through precisely regulated molecular signaling. Thus, first part of this study mainly focused on the identification of the specific marker to maintain the stemness and enhance multipotent of human adult stem cells. I demonstrated that the expression of CD49f regulated the ability of human mesenchymal stem cells (hMSCs) to form spheres and was associated

with an activation of the PI3K/AKT signaling pathway. Furthermore, the forced expression of CD49f modulated the proliferation and differentiation potentials of hMSCs through prolonged activation of PI3K/AKT and suppressed the level of p53. The pluripotency factors OCT4 and SOX2 were recruited to the putative promoter region of CD49f, indicating that OCT4 and SOX2 play positive roles in the expression of CD49f. Indeed, CD49f expression was up-regulated in human embryonic stem cells (hESCs) compared with hMSCs. The elevated level of CD49f expression was significantly decreased upon embryoid body formation in hESCs. In hESCs, the knockdown of CD49f down-regulated PI3K/AKT signaling and up-regulated the level of p53, inducing differentiation into three germ layers. These data suggest that the cell-surface protein CD49f has novel and dynamic roles in regulating the differentiation potential of hMSCs and maintaining pluripotency.

Similar to normal somatic cells, adult stem cells experience a lifelong exposure to stressors, which leads to an age-associated decline in their number and function. The second and third part of this study showed the molecular regulatory mechanism of HMGA2 and ZMPSTE24, which are an important regulator of hMSCs aging. The human high-mobility group protein A2 (HMGA2) protein is an architectural transcription factor that transforms chromatin structure by binding to DNA. Recently, it has been reported that HMGA2 is highly expressed in fetal neural stem cells and has the capacity to promote stemness. I evaluated the direct effects of HMGA2 on the cellular aging and proliferation of hMSCs and investigated potential regulatory mechanisms responsible for

the corresponding functions. The overexpression of HMGA2 enhanced proliferation and reduced or even reversed the *in vitro* aging process of hMSCs. This effect was accompanied by the increased expression of cyclin E and CDC25A and the significantly decreased expression of cyclin-dependent kinase inhibitors. Furthermore, HMGA2 inhibition compromised cell proliferation and adipogenic differentiation in early-stage hMSCs. From the molecular/cellular functional analysis of microarray data, I found that HMGA2 overexpression induced a PI3K/Akt/mTOR/p70S6k cascade, which in turn suppressed the expression of $p16^{INK4A}$ and $p21^{CIP1/WAF1}$ in hMSCs.

ZMPSTE24 is involved in the post-translational maturation step of lamin A. Defects in ZMPSTE24 are associated with the accumulation of prelamin A in the nuclear envelope and lead to premature senescence. hMSCs down-regulated ZMPSTE24 and accumulated prelamin A during replicative or HDAC inhibitor-mediated senescence. The miR-141, which is over-expressed during the senescence process, was able to decrease the ZMPSTE24 expression levels and led to an up-regulation of prelamin A and a DNA damage marker in hMSCs. The transfection of anti-miR-141 prevented the reduction of ZMPSTE24 in VPA/SB-treated cells, resulting in the suppression of the induction of abnormal nuclear morphology. In addition, epigenetic histone markers of the chromatin configuration on the miR-141 promoter region were transcriptionally activated during senescence.

According to these results, following conclusions have been drawn:

i) CD49f, a cell-surface molecule, plays important roles in MSC sphere formation and in the determination of the differentiation potential through direct regulation of OCT4 and SOX2.

ii) HMGA2 regulates in vitro aging by repressing $p16^{INK4A}$, $p21^{CIP1/WAF1}$ expression through the PI3K/AKT/mTOR/p70S6K signaling pathway.

iii) Histone deacetylase regulates ZMPSTE24 and induces prelamin A accumulation through miR-141 up-regulation.

Taken together, these results provide novel insights into the mechanism by which CD49f, HMGA2 and ZMPSTE24 regulate the stemness and aging of human mesenchymal stem cells.

Keywords : Mesenchymal stem cell, CD49f, PI3K/AKT/p53 signaling, HMGA2, $p16^{INK4A}$, Senescence, lamin A, ZMPSTE24, miRNA-141

Student number : 2008-21748

LIST OF ABBREVIATION

hMSC	Human mesenchymal stem cell
hUCB-MSC	Human umbilical cord-derived MSC
CD49f	Integrin subunit alpha 6
PI3K	Phosphatidylinositol 3-kinase
FAK	Focal adhesion kinase
OCT4	Octamer-binding transcription factor 4
SOX2	Sex determining region Y (SRY)-box 2
HMGA2	High mobility group A2
mTOR	Mammalian target of rapamycin
ZMPSTE24	Zinc metallopeptidase STE24
HDAC	Histone deacetylase

miRNA	Micro RNA
VPA	Valproic acid
NB	Sodium butyrate
ChIP	Chromatin immunoprecipitation
RT-PCR	Reverse transcriptase-polymerase chain reaction
MTT	3-(4,5-Dimethylthiazol-2-yl)-2,5-diphenyltetrazolium bromide
CPDL	Cumulative population doubling level

TABLE OF CONTENTS

LITERATURE REVIEW

Mesenchymal Stem Cells

Human mesenchymal stem cells (hMSCs), also referred to as multipotent stromal cells or mesenchymal stromal cells, have been isolated from a variety of connective tissues including bone marrow, adipose tissue, dental pulp, amniotic fluid, Wharton's jelly and umbilical cord blood (Javazon et al., 2004; Prockop, 2009). Among these, umbilical cord blood represents a good alternative source of hMSCs, because the use of umbilical cord blood, which is routinely discarded as waste material after delivery of a baby, would be advantageous since it is an abundant source of MSCs and is obtainable by non-invasive, painless means and harmless for the mother and the baby (Chao et al., 2012). Furthermore, human umbilical cord blood-derived MSCs (hUCB-MSCs or hMSCs) exhibit higher potencies of proliferation and differentiation, and express a lower level of HLA-class I than bone marrow-derived MSCs (Baksh et al., 2007; Lu et al., 2006).

To date hMSCs are widely defined as a fibroblastic spindle shape and a plastic-adherent cell population that can be directed to differentiate *in vitro* into cells of osteogenic, chondrogenic, adipogenic, myogenic, tenogenic, or hematopoietic-supportive stromal lineages (Javazon et al., 2004; Pittenger et al., 1999; Prockop, 2009). Furthermore,

hMSCs are positive for CD73, CD90 and CD105 but negative for CD11b, CD14, CD19, CD34, CD45 or HLA-DR (Horwitz et al., 2005).

Intergrin (CD49f)-PI3K/AKT signaling pathway

Integrin-mediated cell to cell or cell to extracellular matrix (ECM) interaction is an essential part of cellular behavior, cell adhesion, migration, proliferation and differentiation (Hall et al., 2006; Meng et al., 2010). Because integrins transfer information about the chemical composition of the ECM, integrins are able to regulate signaling pathways, such as focal adhesion kinases (FAK) and the phosphatidylinositol 3-kinase (PI3K)/AKT pathways (Fig. 1). The PI3K signaling pathway initiated by the activation of integrin is important for cell migration, invasion and proliferation (Cruet-Hennequart et al., 2003; Shaw et al., 1997). Integrin subunit alpha 6 (CD49f) is prominently expressed in ESCs (Rowland et al., 2009) and may be a marker of high therapeutic potency for bone marrow derived mesenchymal stem cells (BM-MSCs) following myocardial infarction (Lee et al., 2009b), or efficiently generating the long-term multilineage grafts in hematopoietic stem cells (Notta et al., 2011). In addition, alpha6 integrin was required for endothelial progenitor cells migration, adhesion and promotions of the postischemic vascular repair (Bouvard et al., 2010), and the signaling pathways initiated by the interaction between integrin and ECM synergistically crosstalk with platelet-derived growth factor receptor (PEGFR) signaling cascades to control the migration of MSCs for vascular remodeling (Veevers-Lowe et al., 2011). Although

studies reported that FAK, PI3K/AKT singnalings are crucial for the maintenance of stem cell viability and pluripotency, little attempt had been made to demonstrate the role of integrin induced signaling on stem cell ability and reprogramming process.

Cellular aging of adult stem cells

Aging is an extremely complex process that affects most of the biological functions of an organism, culminating in disease and death due to the accumulated actions of different types of stresses (Fig. 2). Among these stresses, oxidative reactions, telomere attrition and the decline of the DNA repair and protein turnover systems are proposed to contribute to aging (Kirkwood, 2005). The down-regulation of the regenerative ability of tissues and organs, along with an increased susceptibility to infections and cancers, are prominent hallmarks of senescence (Hayflick, 1994). Similar to normal somatic cells, adult stem cells experience a lifelong exposure to stressors, which leads to an age-associated decline in their number and function. Given that the senescence-induced loss of adult stem cell stemness results in the impairment of tissue homeostasis, regeneration and repair (Janzen et al., 2006; Kasper et al., 2009; Rao and Mattson, 2001; Silva and Conboy, 2008), it is important to understand the mechanisms that underlie the regulation of adult stem cell stemness and senescence.

It is crucial to isolate and populate hMSCs *in vitro* before using them for therapeutic purpose. However, after 10-30 times of divisions, hMSCs undergo replicative

senescence *in vitro* which involves "Hayflick phenomenon (limit)"; characterized by enlargement, changes in morphology and ultimate arrest of proliferation (Hayflick, 1965). It has been reported that the mean telomere length decreased and differentiation potential dropped after hMSCs enter senescence (Bonab et al., 2006). Furthermore, replicative stress contributes to the accumulation of DNA damage in adult stem cell aging. Several lines of reports demonstrated that the replicative stress with replication fork stalling can induce the telomeric DNA damage, because telomerase exhibits fragile region of DNA which is sensitive to replication-induced DNA damage (Sperka et al., 2012).

Tumor suppressor $p16^{INK4A}$ is associated with replicative senescence through a telomere-dependent or –independent mechanism and $p16^{INK4A}$ expression gradually increase in consecutive passages of adult stem cells (Rayess et al., 2012). In hMSCs, $p16^{INK4A}$ –positive cells showed growth retardation and increased activity of senescence associated β-galactosidase. Furthermore, transfection of siRNA targeting $p16^{INK4A}$ in senescent hMSCs resulted reduced number of senescent cells and maintains the ability to proliferate, suggesting $p16^{INK4A}$ is an important regulator of hMSCs aging (Shibata et al., 2007).

HMGA2 is a non-histone chromosomal high-mobility group A (HMGA) family protein that alters chromatin structure through DNA binding (Fig. 3) (Fusco and Fedele, 2007; Thanos and Maniatis, 1992). As an architectural transcription factor, HMGA2 regulates transcription during embryogenesis and in embryonic stem cells (Chiappetta et

al., 1996; Li et al., 2006). Recently, several studies reported that HMGA2 is able to promote fetal neural stem cell self-renewal through its ability to repress $p16^{INK4A}$ and $p19^{Arf}$ expression (Nishino et al., 2008; Tzatsos and Bardeesy, 2008). Consistent with these data, Lee et al. (2011) demonstrated that HMGA2 expression decreased during the aging process, concomitant with the increased expression of $p16^{INK4A}$, $p21^{CIP1/WAF1}$ and $p27^{KIP1}$, in hMSCs (Lee et al., 2011). Taken together, HMGA2 plays an important age-associated role in the stemness of adult stem cells.

Lamin A-dependent nuclear abnormalities in aging

Nuclear lamina, a filamentous meshwork providing the regulation between the inner nuclear membrane and chromosome, is composed of the A- and B- type of lamins (Aebi et al., 1986). Two major products of A type lamins, lamin A and C, are derived from *LMNA* gene by alternative splicing. Lamin A and C are located at the nuclear envelope and also present in the nucleoplasm, where they play basic roles of DNA replication, transcriptional regulation and structural support (Hutchison and Worman, 2004; Shumaker et al., 2003). Mutation of *LMNA* gene is responsible for at least 12 distinct disorders, collectively known as “laminopathies”, and involve in different tissues including adipose, peripheral nerve, skin, muscle and bone (Mounkes et al., 2003). Hutchinson-Gilford progeria syndrome (HGPS) is well known laminopathy characterized by features of premature aging. HGPS caused by the G608G mutation within exon 11 of LMNA leading to internal truncation within the carboxyl-terminus of prelamin A

(Eriksson et al., 2003). This 50 amino acid internal deletion produces progerin and abolish cleavage site for metalloproteinase ZMPSTE24/FACE-1, resulting accumulation of farnesylated, truncated prelamin A (Young et al., 2005).

Both progerin and prelamin A accumulation in the nuclear envelope leading to premature senescence that are characterized by nuclear blebbing, heterochromatin disorganization and defects in DNA replication, transcription and repair (Candelario et al., 2011; Dechat et al., 2007; Liu et al., 2005; Shumaker et al., 2006). Mature lamin A (646 amino acids) undergoes a series of post-translational modifications from a prelamin A precursor (664 amino acids) (Fig. 4). First, protein farnesyltransferase triggers farnesylation of the cysteine in the carboxy-terminal CAAX motif. Second, the last three amino acids (i.e., the AAX) are clipped off from the protein and exposed farnesylcysteine is methylated by Icmt methyl-transferase. Third, endoproteolytic release of the last 15 amino acids from the carboxy-terminus by ZMPSTE24, a membrane zinc metalloproteinase (Corrigan et al., 2005; Young et al., 2005). ZMPSTE24 is indispensably required for the production of mature lamin A, since it performs both first cleavage step that releases –AAX and final endoproteolytic step (Corrigan et al., 2005). A deficiency of ZMPSTE24 expression can cause restrictive dermopathy (RD) with features of the severe progeroid syndrome, resulting in early neonatal death (Navarro et al., 2004). Cells lacking of ZMPSTE24 show accumulation of a farnesylated, methylated prelamin A at the nuclear lamina, which is toxic to cells induced by DNA double-strand breaks (DSBs) (Liu et al., 2006b). Although, interests in prelamin A accumulation and

ZMPSTE24 deficiency has increased, several fundamental issues related to regulation of its expression levels and activities have not been addressed. Some reports has been demonstrated that ZMPSTE24 expression level is down-regulated in aged or senescent human vascular smooth muscle cells and fibroblast cells (Ragnauth et al., 2010; Ukekawa et al., 2007). But the signaling pathway that can modulate ZMPSTE24 expression level has not been clarified (Maraldi et al., 2011).

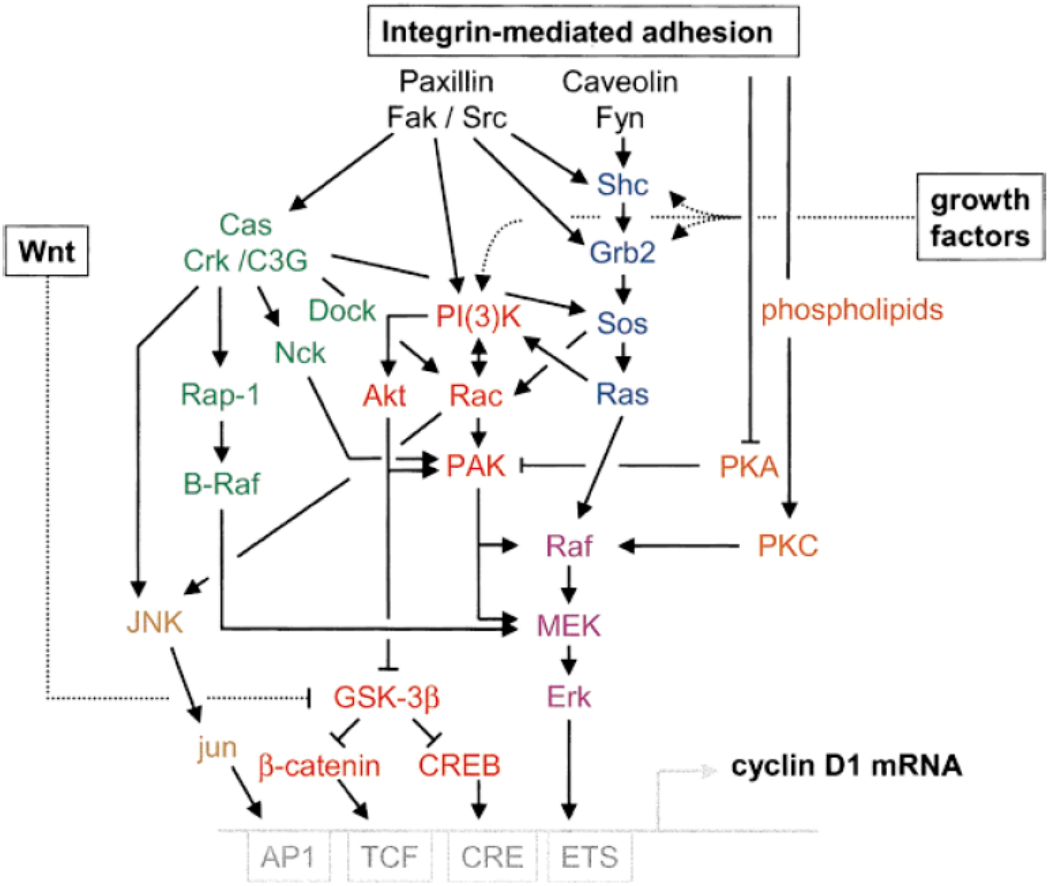

Figure 1.

Integrin-mediated signal transduction cascades (Danen and Yamada, 2001).

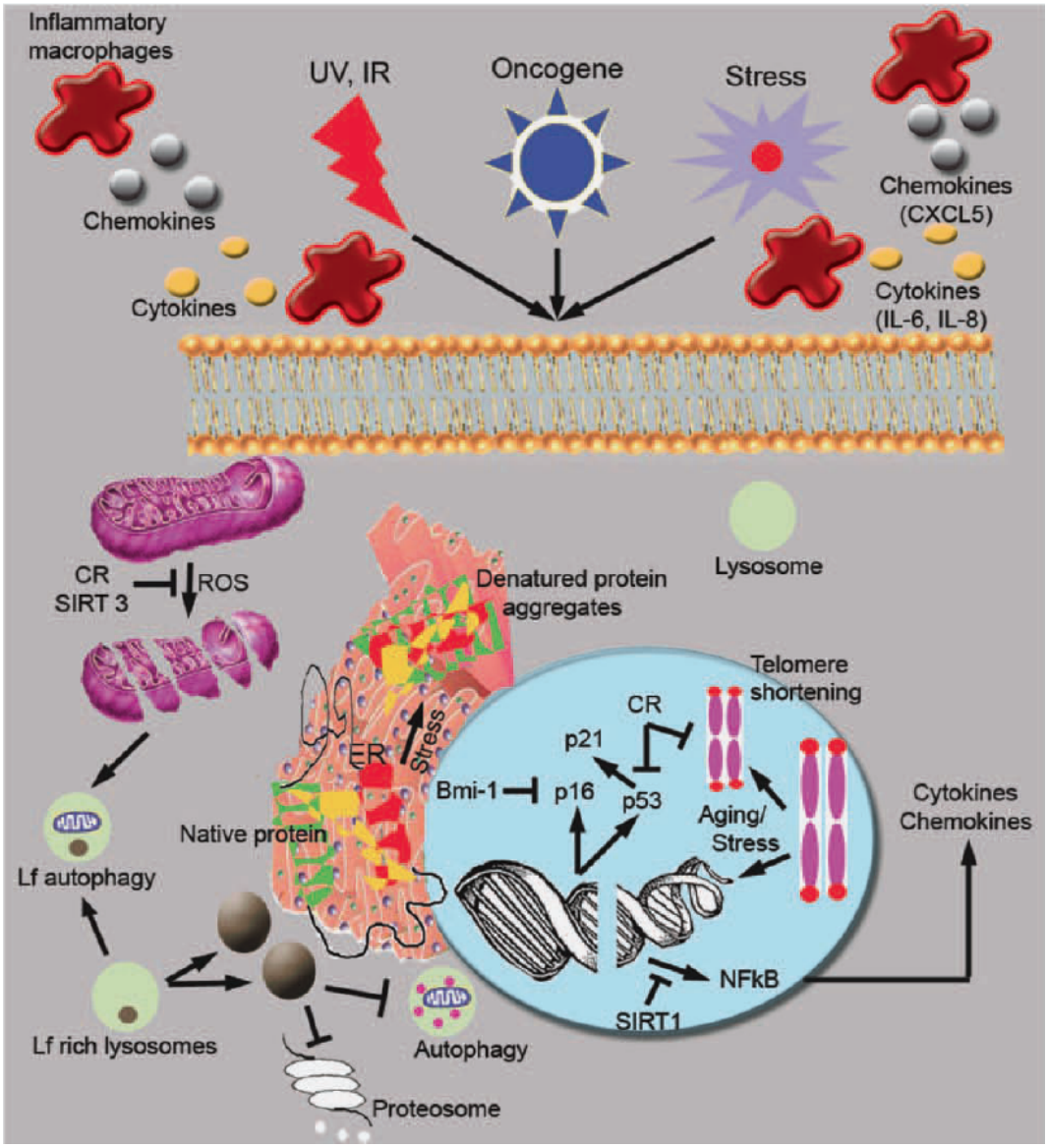

Figure 2.

Molecular mechanism of senescence (Rayess et al., 2012).

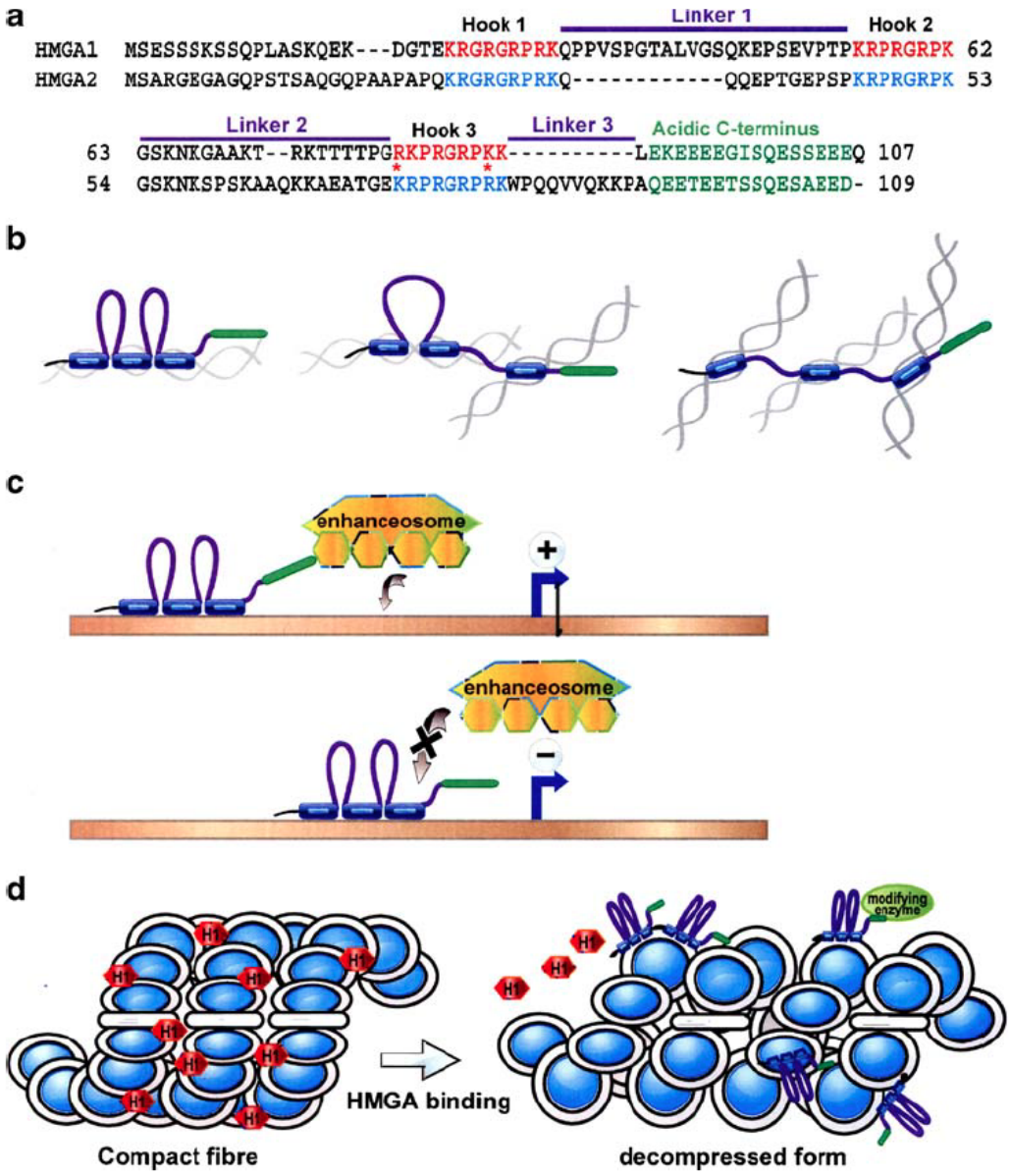

Figure 3.

HMGA structure/domain overview (Pfannkuche et al., 2009).

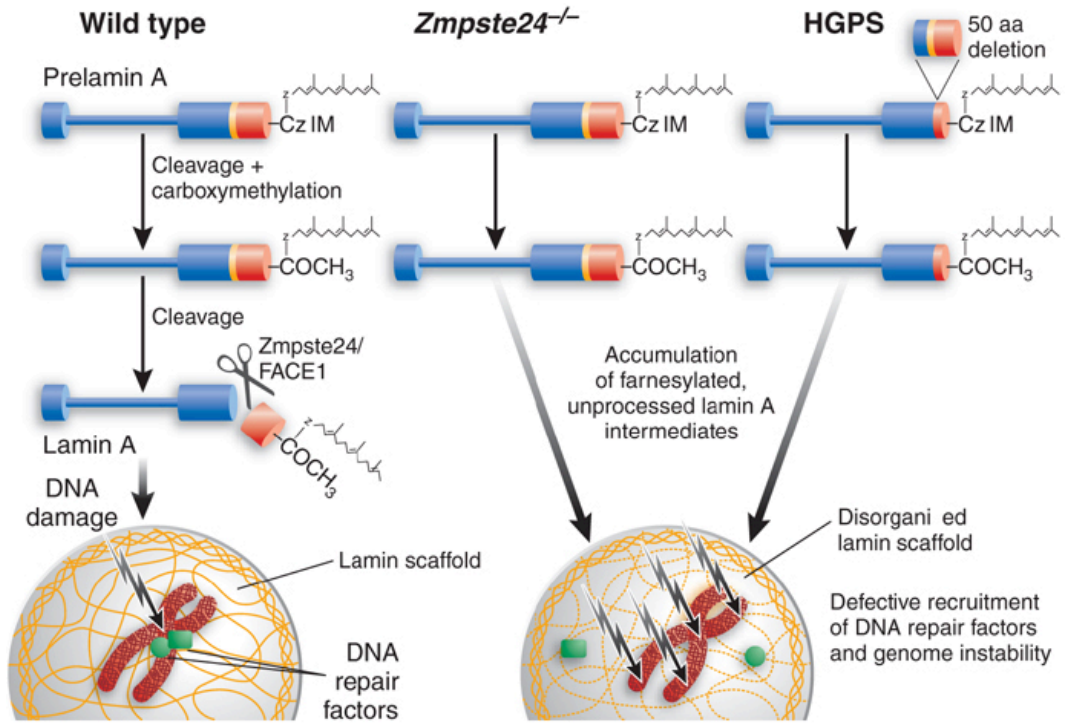

Figure 4.

Lamin A–processing defects in laminopathies (Misteli and Scaffidi, 2005).

CHAPTER I

CD49f enhances multipotency and maintains stemness through the direct regulation of OCT4 and SOX2

1.1 INTRODUCTION

hMSCs have typically been selected and expanded in two-dimensional monolayer cultures; however, cultured hMSCs are heterogeneous, making them difficult to use for therapeutic and research applications (Majore et al., 2009; Tormin et al., 2009). Understanding the cellular heterogeneity of adult stem cells, such as hMSCs, and isolating a cell population with higher cellular potency by identifying a surface marker have been major interests of the scientific community. It has been reported that non-adherent sphere culture methods can enrich self-renewal capability in many tissue-specific adult stem cells and primary cancers (Cocciadiferro et al., 2009; Liu et al., 2006a; Smukler et al., 2011). Sphere-forming ability is one of the properties of cancer stem cells capable of tumor regeneration. This characterization has been reported in leukemia and primary tumors of the breast, colon and brain (Ailles and Weissman, 2007). However, sphere-forming cells from the mouse inner ear can differentiate into vestibular and cochlear sensory epithelia (Oshima et al., 2009), and sphere-forming mesenchymal cells derived from the dermis attain hair-inducing capacity through the process of sphere formation (Shimizu et al., 2011). Therefore, it is reasonable to hypothesize that a three-dimensional culture of hMSCs is required to isolate a more homogeneous population and to increase proliferation. Recently, it has been shown that growing hMSCs in three-dimensional matrices significantly increases their ability to both expand cell populations and maintain them in an undifferentiated state (Cao et al., 2010; Frith et al., 2010).

However, the molecular mechanisms regulating how sphere-forming cells maintain stemness are still unknown.

Given the characteristic ability of hMSCs to survive under non-adherent culture conditions, it is worth studying integrins as a plausible selection marker for this population. Integrin-mediated cell-to-cell or cell-to-extracellular matrix (ECM) interaction is an essential part of cellular behavior, adhesion, migration, proliferation and differentiation (Hall et al., 2006; Meng et al., 2010). Integrin interactions cue cascades of signaling pathways involved in cell survival and proliferation, such as the focal adhesion kinase (FAK) and the phosphatidylinositol 3-kinase (PI3K)/AKT pathways (Gambaletta et al., 2000; Koul et al., 2005). The PI3K signaling pathway, initiated by the activation of integrins, is important for cell migration, invasion and proliferation (Cruet-Hennequart et al., 2003; Shaw et al., 1997). Integrins transduce survival signals from the ECM to cells, leading to the inhibition of a p53-regulated apoptotic pathway (Ilic et al., 1998). Furthermore, crosstalk between AKT and p53 has been found. The activation of AKT, which is driven through a kinase cascade from PI3K, can phosphorylate Mdm2, resulting in p53 inactivation and degradation (Ogawara et al., 2002; Oren, 2003). Additionally, p53 plays important roles in p21 induction following DNA damage and p16 induction following premature senescence (Lin et al., 1998; Macleod et al., 1995).

Integrin subunit alpha 6 (CD49f) is required for endothelial progenitor cell migration and adhesion and the activation of post-ischemic vascular repair (Bouvard et al.,

2010). $Lin^{-}Sca\text{-}1^{+}CD49f^{Hi}$ cells derived from the prostate were capable of forming spheres in three-dimensional cultures, eventually promoting the progression to prostate carcinoma (Lawson et al., 2010). In mice with myocardial infarcts, CD49f may be a marker of high therapeutic potency for bone marrow-derived multipotent stem cells (BM-MSCs) (Lee et al., 2009a). CD49f plays a role in efficiently generating long-term multi-lineage grafts in hematopoietic stem cells (Notta et al., 2011). In hESCs, integrin-ECM engagement is essential for cell proliferation and adhesion. Specifically, CD49f is prominently expressed in hESCs, and its ligand, laminin, can be used as a substrate for the expansion of undifferentiated hESCs (Meng et al., 2010; Miyazaki et al., 2008; Rodin et al., 2010; Rowland et al., 2009). However, the role of CD49f in MSC sphere formation and the maintenance of pluripotency in hESCs through PI3K/AKT signaling remains obscure.

OCT4 and SOX2 are two core components of the pluripotency circuit for maintaining the self-renewal capacity of undifferentiated ESCs (Iovino and Cavalli, 2011). These genes, expressed in ESCs and tissue-specific adult stem cells such as MSCs, help to maintain an undifferentiated state and prevent differentiation (Boiani and Scholer, 2005; Orkin et al., 2008). Together with other factors, transduced OCT4 and SOX2 may co-occupy each other's promoters and activate auto-regulatory loops, resulting in the activation of endogenous pluripotency markers and the induction of pluripotency (Alon, 2007; Boyer et al., 2005). Here, I demonstrate that CD49f can be regulated through an auto-regulatory circuit through the direct binding of OCT4 and SOX2 on the CD49f

promoter.

In this study, I show that CD49f plays crucial roles in maintaining the stemness of hMSCs and hESCs. Specifically, CD49f regulates proliferation and differentiation capacities through PI3K/AKT/p53 activity. Furthermore, I reveal crosstalk between the pluripotency genes OCT4 and SOX2 and CD49f in hMSCs and hESCs.

1.2 MATERIALS AND METHODS

1.2.1 Cell culture

The umbilical cord blood (UCB) samples were obtained with the written informed consent of the mother approved by the Boramae Hospital Institutional Review Board (IRB) and the Seoul National University IRB (IRB No. 0603/001-002-07C1) from the umbilical vein immediately following delivery. Briefly, the UCB samples were mixed with Hetasep solution (StemCell Technologies, Vancouver, Canada) at a ratio of 5:1 and then incubated at room temperature to deplete the erythrocytes. The supernatant was carefully collected, and the mononuclear cells were isolated using Ficoll density-gradient centrifugation at 2,500 rpm for 20 min. The cells were washed twice in PBS and were seeded at a density of 2×10^5 to 2×10^6 cells/cm^2 on plates in growth medium consisting of D-media (Formula No. 78-5470EF, Gibco BRL, USA) containing EGM-2 SingleQuot and 10% fetal bovine serum (Gibco BRL). After 3 days, the non-adherent cells were removed. For long-term culture, the cells were seeded at a density of $4x10^5$ cells/10 cm plate, and the cells were subcultured upon reaching 80~90% confluency.

1.2.2 MSC sphere formation

To generate MSC spheres, 1.5 x 10^5 hMSCs were plated on 100-mm culture dishes (Nunc, Rochester, NY) coated with 1% agarose to prevent cells from attaching to the bottom of the plastic dish. A total of 15,000 cells were plated per ml of medium, and

the MSC spheres were cultured for 7 days. After 7 days, MSC spheres were collected using a 40-μm-pore cell strainer. The collected MSC spheres were washed with PBS and gently centrifuged (60 x g/5 min) before further experimentation.

1.2.3 Immunocytochemistry

The immunocytochemical analysis of CD49f, OCT4 and SOX2 was performed as follows. Cultured cells were fixed in 4% paraformaldehyde and permeabilized with 0.2% Triton X-100 (Sigma Aldrich, USA). The cells were incubated with 10% normal goat serum (Zymed Laboratories Inc., USA) and then labeled with primary antibodies against CD49f (1:200; Abcam, ab20142), OCT4 (1:200; Abcam, ab19857) and SOX2 (1:200; Abcam, ab59776), followed by a 1-hr incubation with Alexa 488- or Alexa 594-labeled secondary antibody (1:1,000; Molecular Probes, USA). Nuclei were stained with Hoechst 33258 (1 μg/ml; 10 min). Images were captured using a confocal microscope (Nikon, Eclipse TE200, Japan).

1.2.4 Overexpression of CD49f, OCT4, SOX2, NANOG, and LIN28

To overexpress of the CD49f protein, the coding sequence of full-length human CD49f was cloned into the pCMV6 expression vector and transfected using Fugene 6 transfection reagent (Roche, Indianapolis, IN, USA). To overexpress OCT4, SOX2, NANOG, and LIN28, hMSCs were infected with lentiviruses expressing these genes. The viral production and transduction process was performed as previously described . Briefly, plasmids, including pSin-EF2-Oct4-Pur, pSin-EF2-Sox2-Pur, pSin-EF2-Nanog-Pur, or

pSin-EF2-Lin28-Pur (Addgene, Cambridge, USA), were transfected into 293T cells together with the MISSION lentiviral packaging mix (Sigma), and viral supernatants were collected 48 and 72 hr post-transfection. The viral supernatants were used to infect human MSCs in the presence of 5 μg/mL polybrene (Sigma).

1.2.5 siRNA and shRNA inhibition study

To specifically inhibit OCT4, SOX2, CD49f and p53, siRNA knockdown studies were performed using commercial siRNA targeting OCT4, SOX2, CD49f and p53 (Dharmacon, ON Target plus SMART pool) along with a non-targeting siRNA (Dharmacon, ON Target plus SMART pool, Cat# D-001810-01, Lafayette, CO, USA). The siRNA transfections were performed according to the manufacturer's instructions. Briefly, the cells were seeded at a concentration of 5 x 10^4/well, and siRNA-containing media (without added antibiotics) were added when the cells reached 50% confluence. The cells were incubated with 50 nM siRNA for 48 hr to evaluate mRNA expression and for 72 hr to evaluate protein expression. After these incubations, RNA and protein extractions were performed for genetic and proteomic analyses. Control shRNA lentiviral particles and integrin α6 shRNA lentiviral particles were used to infect hMSCs in the presence of 5 μg/mL polybrene (Sigma-Aldrich, MO, USA).

1.2.6 Chromatin immunoprecipitation (ChIP) assays

To prepare for ChIP testing, hMSCs and Tera-1 cells (1 - 2 x 10^7 cells per IP) were fixed with 1% formaldehyde for 10 min; the solution was then neutralized by the

addition of 1/20 volume of 2.5 M glycine for 5 min. Cells were washed with enough ice-cold PBS and scraped with SDS lysis buffer (1% SDS, 10 mM EDTA, 50 mM Tris, pH 8.1) containing protease inhibitors. Lysates were sonicated to shear the DNA to lengths between 200 and 1000 base pairs. Samples were centrifuged for 10 min at 15,000 x g and 4°C to remove insoluble material. The supernatant was diluted 10 fold in ChIP dilution buffer (0.01% SDS, 1.1% Triton X-100, 1.2mM EDTA, 16.7mM Tris-HCL, pH8.1, 167mM NaCl). The chromatin solution was precleared with the addition of Salmon Sperm DNA/Protein A Agarose-50% Slurry (Upstate Biotechnology, #16-157C, Lake Placid, NY, USA). The anti-OCT4 antibody-ChIP grade (Abcam, ab19857, Cambridge, MA, USA) and anti-SOX2 antibody-ChIP grade (Abcam, ab59776) were used to precipitate chromatin. A negative control was performed with a non-specific IgG control. Cross-linking was reversed by incubation of the elute with 5 M NaCl for 4 hr at 65°C. Afterwards, 0.5 M EDTA, 1 M Tris-HCL, pH 6.5, and 10 mg/ml Proteinase K were added and incubated for 1 hr at 45°C. DNA was purified by extraction with phenol/chloroform and ethanol precipitation. PCR reactions were performed with a final template dilution of 1:50. The PCR products were analyzed by gel electrophoresis on 1.5–2% agarose gels with ethidium bromide staining, followed by fluorescence digitization using a Bio-Rad GelDoc XR system (Bio-Rad, Hercules, CA, USA).

1.2.7 In vitro differentiation assay

For *In vitro* differentiation into osteogenic, adipogenic, cells from normal cultured and MSC spheres were cultured in adipogenic medium (DMEM supplemented

with 5% FBS, 1 μM dexamethasone, 10 μM insulin, 200 μM indomethacin, and 0.5 mM isobutylmethylxanthine) or osteogenic medium (DMEM supplemented with 5% FBS, 50 μM L-ascorbate-2-phosphate, 0.1 μm dexamethasone, and 10 mM glycerophosphate). Intracellular lipid accumulation, an indicator of adipogenic differentiation, was visualized by oil red O staining. After being photographed, the oil red O was eluted with 100% isopropyl alcohol and quantified with an ELISA plate reader (EL800, Bio-Tek Instruments, USA) at OD500. Osteogenic differentiation was noted by positive staining with Alizarin Red stain, which is specific for calcium. Alizarin Red S staining was quantified using 100 mM of cetylpyridinium chloride (Sigma-Aldrich) for 1 h. The release of solubilized alizarin red S was measured at 570nm using a spectrophotometer.

1.2.8 Reverse transcription polymerase chain reaction (RT-PCR) and real-time PCR

Total cellular RNA was extracted from cells with TRIzol reagent™ (Invitrogen) according to the manufacturer's instructions. cDNA was synthesized by adding the purified RNA and oligo-dT primers to SuperScript iii First-Strand Synthesis System for RT-PCR (Invitrogen) according to the manufacturer's instructions. PCR was performed using Accupower PCR premix (Bioneer, Daejeon, Republic of Korea). The primer sets used for this study are listed in Table 1. All PCR products were analyzed by gel electrophoresis on 1.5% agarose gels with ethidium bromide staining, followed by fluorescence digitization using a Bio-Rad GelDoc XR system (Bio-Rad). Real-time PCR was performed by mixing cDNA with each primer and the SYBR Green PCR Master Mix (Applied Biosystems, Foster City, CA). According to the manufacturer's instructions, an

ABI 7300 sequence detection system with supplied software (Applied Biosystems) was used to quantify gene expression. Each gene was normalized with β-actin or RPL13A as housekeeping controls. At least three independent analyses were done for each gene.

1.2.9 Statistical analysis

All experiments were conducted at least in triplicate (n = 3), and the results are expressed as the mean ± SD. The statistical analyses were conducted using an analysis of variance (ANOVA) followed by Duncan's multiple range tests or Student's t-test. A value of $P < 0.05$ was considered significant (*, $P < 0.05$; **, $P < 0.01$).

Table 1. Names and sequences of the primers for RT-PCR and qRT-PCR assays		
Gene name	Primer sequence	
β-ACTIN	Forward:	AGA GCT ACG AGC TGC CTG AC
	Reverse:	AGC ACT GTG TTG GCG TAC AG
C/EBP-β	Forward:	GCG CGC TTA CCT CGG CTA CC
	Reverse:	TGG CCT TGT CGC GGC TCT TG
AP2	Forward:	GGG TCA CAG CAC CCT CCT GA
	Reverse:	GGT TTG GCC ATG CCA GCC AC
PPAR-γ	Forward:	CCT CCG GGC CCT GGC AAA AC
	Reverse:	CTC CTG CAC AGC CTC CAC GG
LEPTIN	Forward:	GAA GAC CAC ATC CAC ACA CG
	Reverse:	AGC TCA GCC AGA CCC ATC TA
OSTEOCALCIN	Forward:	CCT ATT GGC CCT GGC CGC AC
	Reverse:	GAC ACC CTA GAC CGG GCC GT
RUNX2	Forward:	CTT GAC CAT AAC CGT CTT CA
	Reverse:	GTC ATC AAT CTT CTG TCT GT
Paxillin	Forward:	AAC TGG TTG AAG GGT GTT GC
	Reverse:	AGG TTC AGT GGG TTC ACA GG
FAK	Forward:	CGA GAG ATT GAG ATG GCA CA
	Reverse:	TAC TCT TGC TGG AGG CTG GT
ILK	Forward:	AAG GTG CTG AAG GTT CGA GA
	Reverse:	ATA CGG CAT CCA GTG TGT GA
VDR	Forward:	CGG CCG GAC CAG AAG CCT TT
	Reverse:	CTG GCA GTG GCG TCG GTT GT
MSX2	Forward:	CCC TGG AGC GCA AGT TCC GT
	Reverse:	GGC GGG ATG GGA AGC ACA GG
CD49f	Forward:	TCA TGG ATC TGC AAA TGG AA
	Reverse:	AGG GAA CCA ACA GCA ACA TC
OCT4	Forward:	GTG GAG GAA GCT GAC AAC AA
	Reverse:	ATT CTC CAG GTT GCC TCT CA
SOX2	Forward:	TGG CGA ACC ATC TCT GTG GT

	Reverse:	CCA ACG GTG TCA ACC TGC AT
LIN28	Forward:	GGG GAA TCA CCC TAC AAC CT
	Reverse:	CTT GGC TCC ATG AAT CTG GT
NANOG	Forward:	ACC TTG GCT GCC GTC TCT GG
	Reverse:	AGC AAA GCC TCC CAA TCC CAA
CMYC	Forward:	AAG ACA GCG GCA GCC CGA AC
	Reverse:	TGG GCG AGC TGC TGT CGT TG
KLF4	Forward:	GGC TGC ACA CGA CTT CCC CC
	Reverse:	GGT GGC GGT CCT TTT CCG GG
CK18	Forward:	AAT GGG AGG CAT CCA GAA CGA GAA
	Reverse:	GGG CAT TGT CCA CAG TAT TTG CGA
FOXA2	Forward:	TGG GAG CGG TGA AGA TGG AA
	Reverse:	TCA TGC CAG CGC CCA CGT AC
PEPCK	Forward:	TTA GAT GGG ACA AAG CCT G
	Reverse:	GCA AGA CGG TGA TTG TAA CT
HNF4a	Forward:	GGA ACA TAT GGG AAC CAA CG
	Reverse:	AAC TTC CTG CTT GGT GAT GG
AFP	Forward:	GAA TGC TGC AAA CTG ACC AC
	Reverse:	TGG CAT TCA AGA GGG TTT TC
TUJ-1	Forward:	CAG TGA CCT GCA ACT GGA GA
	Reverse:	GAT TGG CCA AAC ACG AAG TT
MUSASHI	Forward:	GCC CAA GAT GGT GAC TCG
	Reverse:	ATG GCG TCG TCC ACC TTC
NESTIN	Forward:	AAC AGC GAC GGA CTG TCT CTA
	Reverse:	TTC TCT TGT CCC GCA GAC TT
MAP2	Forward:	CCA ATG GAT TCC CAT ACA GG
	Reverse:	TCT CCG TTG ATC CCA TTC TC
PAX6	Forward:	ACC CAT TAT CCA GAT GTG TT
	Reverse:	ATG GTG AAG CTG GGC ATA GG
MSX1	Forward:	CGA GAG GAC CCC GTG GAT GC
	Reverse:	GGC GGC CAT CTT CAG CTT CT
BRACHYURY	Forward:	GCC CTC TCC CTC CCC CTC CAC

	Reverse:	GGC GCC GTT GCT CAC AGA CC
Col1A2	Forward:	CTG GTG CTG CTG GCC GAG TC
	Reverse:	GGG ACC AGG GGG ACC ACG TT

Table 2. Names and sequences of the primers for ChIP assays

CD49f primer-1	Forward:	AGAACAACGGGCTCATTCAG
	Reverse:	CGACAGGTAGAGCAAGCACA
CD49f primer-2	Forward:	TAGGAAAGAACGGCATCGTC
	Reverse:	CTAGGATTTTGCCCAGGTGA
CD49f primer-3	Forward:	AACCCCTGCAGGATAAGGTT
	Reverse:	AGTTGTGGGGAGAACTGCTG
CD49f primer-4	Forward:	TGATGTTCACGCAGCTTTTC
	Reverse:	GGAATCTGACATCCCTGCAT
CD49f primer-5	Forward:	ACATGGGGATATCCAAGCAG
	Reverse:	TGCCCTTAGTTCCTCACAGG
CD49f primer-6	Forward:	CTGGCCAAAACTTGATGGTT
	Reverse:	CCATCGCAAATGGAAAACTT

1.3 RESULTS

1.3.1 MSC spheres retain hMSC properties with improved potential for differentiation and proliferation

hMSCs displayed a flattened and spindle-shaped morphology in monolayer culture (MSC monolayers), while under non-adherent conditions, hMSCs formed floating spheroid colonies (MSC spheres), which are characteristic of hMSCs (Fig. 1A). Under non-adherent conditions, 30 to 50 spheres per $1x10^4$ cells were formed, and the mean diameter of the spheres was 50 to 150 μm. Both MSC monolayers and MSC spheres were positive for hMSC markers (CD44 and CD90) but negative for the hematopoietic stem cell markers CD34 and CD117, indicating that MSC spheres retained the properties of hMSCs.

To compare the differentiation capacity of MSC monolayers and MSC spheres, we induced the *in vitro* differentiation of both populations into adipogenic and osteogenic lineages. After adipogenic induction, MSC sphere-derived cells showed a higher adipogenic differentiation potential than MSC monolayer cells, as evidenced by Oil Red O staining (Figs. 1B, 1C, 1F). The expression levels of adipogenic genes, such as C/EBP-β, aP2, PPAR-γ and leptin, were significantly up-regulated in sphere-derived cells compared to monolayer-cultured cells (Supporting Information Fig. S2A). Sphere-derived MSCs were also more effective at osteogenic differentiation, as shown by Alizarin Red S staining (Figs. 1D, 1E, 1G). The sphere-derived cells also showed elevated expression

levels of Runx2 and osteocalcin after osteogenic induction (Supporting Information Fig. S2B). To compare the proliferative potency of hMSCs derived from monolayers and MSC spheres, the cumulative population doubling level (CPDL) was measured. The sphere-derived cells showed an increased proliferation rate (CPDL 7.7 after 2 weeks) compared with the cells from the MSC monolayers (Fig. 1H). Taken together, these data suggest that the MSC sphere-derived cells have increased proliferation rates and a greater potential to differentiate towards both the adipogenic and osteogenic lineages.

1.3.2 The PI3K/AKT/GSK3β pathway modulates the formation of MSC spheres

I next treated the hMSCs with BIO or LY294002, a GSK3-specific inhibitor and a PI3K inhibitor, respectively, to determine whether the PI3K/AKT/GSK3 and the p53, p21 and p16 pathways were involved in the formation of MSC spheres. As shown in Figure 1I, phospho-PI3K and phospho-AKT activities were dramatically increased in MSC spheres that were either untreated or treated with BIO compared to MSC monolayers, whereas supplementation with LY294002 led to the dephosphorylation of constitutively active PI3K (Tyr458,199), AKT (Ser473) and GSK3β (Ser9). The levels of endogenous p53, p21 and p16 were reduced in MSC spheres and BIO-treated spheres. I next assessed the efficiency of sphere formation after treatment with BIO or LY294002 to confirm whether the PI3K/AKT/GSK3β pathway was involved in MSC sphere formation. After 7 days of sphere induction under non-adherent conditions, supplementation with BIO significantly increased both the number and size of spheres formed, suggesting that GSK3β activity inhibits sphere formation (Figs. 1J and 1K). Furthermore, treatment with

one of the most selective inhibitors of GSK3β, CHIR99021, increased MSC sphere-forming efficiency (Fig. 1L). In contrast, treatment with LY294002 at concentrations of 30 μM to 50 μM significantly reduced both the number and size of MSC spheres (Figs. 1M and 1N). MSC sphere formation was significantly inhibited by treatment with 1 μM wortmannin, which is a specific and direct inhibitor of PI3 kinase (Fig. 1O). Taken together, these results indicate that the PI3K/AKT/GSK3β signaling pathway is critical for MSC sphere formation.

1.3.3 Up-regulation of CD49f contributes to MSC sphere formation via the phosphorylation of FAK/Paxillin

Integrins are one of the key molecules that interact with the extracellular matrix. They initiate survival and activate growth-associated signal transduction pathways (e.g., PI3K/AKT) via local protein kinases, which include FAK and Paxillin. Therefore, I performed flow cytometry analysis to determine the integrin expression profiles in both the MSC monolayers and the MSC spheres. The expression levels of CD49a and CD49b showed no significant difference between the two culture conditions, while CD49e was slightly decreased in MSC spheres. However, both CD49f and CD104, which form a heterodimer, were up-regulated in MSC sphere-derived cells (Fig. 2B). In line with the flow cytometry data, immunostaining showed an increase in CD49f-positive cells in the MSC spheres. Both an elevated CD49f expression level and an increase in the number of cells positive for this marker were observed in the MSC sphere cultures compared to the MSC monolayer cultures (Fig. 2A). Using western blot analysis, high levels of phospho-

Paxillin, phospho-FAK and CD49f were observed in MSC spheres (Fig. 2C). To confirm that integrin expression affected the efficiency of sphere formation, I purified CD49f-positive and CD49f-negative hMSCs using flow cytometry and compared the efficiency of sphere formation for these two distinct populations. The gene expression levels of Paxillin, FAK and ILK, which are tyrosine kinases downstream of the integrins, were increased in the CD49f-positive population (Fig. 2D). The CD49f-positive cells were more efficient at forming spheres, and the mean diameter of the spheres was increased approximately 2.4-fold compared to the CD49f-negative cells (Figs. 2E, 2F and 2G). To determine the mechanism responsible for the increased tendency toward sphere formation in the CD49f-positive cells, I investigated the molecular signaling. Western blotting results showed that FAK, PI3K and AKT were activated and that the protein levels of p53, p21 and p16 were lower in MSC spheres derived from CD49f-positive cells compared to hMSCs from monolayer or MSC spheres derived from CD49f-negative (Fig. 2H). Furthermore, transfection with siRNA targeting CD49f resulted in a decrease in the number and size of MSC spheres (Fig. 2I-2L). In contrast, p53 inhibition increased the number and size of MSC spheres (Fig. 3C, 3D). Taken together, these data suggest that the improvement in sphere formation is associated with the activation of CD49f and the PI3K/AKT/p53 signaling pathway.

1.3.4 Overexpression of CD49f regulates cellular proliferation and differentiation via regulation of the PI3K/AKT/p53 pathway

To further assess whether CD49f gene expression was dependent upon the

activation of the PI3K/AKT/GSK3β pathway, CD49f-overexpressing hMSCs were treated with LY294002 or BIO for 24 or 48 hr. In the CD49f-overexpressing hMSCs, MTT assays revealed that the growth rates of BIO-treated hMSCs were higher than those of the untreated hMSCs, whereas LY294002 inhibited cell proliferation (Fig. 4A). Because p53 is closely related to the CD49f-PI3K/AKT/GSK3β signaling pathway, the influence of p53 inhibition on the cell cycle was assessed using flow cytometry. The inhibition of p53 increased the number of cells in S phase and decreased the number of cells in G0/G1 phase (Fig. 3B). These results suggest that p53 inhibition activates the cell cycle. In the sphere formation assay, BIO treatment consistently increased the number of MSC spheres, whereas LY294002 inhibited the sphere formation of the CD49f-overexpressing hMSCs (Fig. 4B). Western blot analysis showed that CD49f overexpression led to increased levels of PI3K, AKT and GSK3β phosphorylation in the hMSCs. BIO treatment led to the induction of AKT and GSK3β phosphorylation, whereas LY294002 treatment suppressed AKT phosphorylation in the CD49f-overexpressing hMSCs (Fig. 4C). I also found that active CD49f expression was sufficient to reduce p53, p21 and p16 levels, but the decrease in p53, p21 and p16 levels was blocked by LY294002, suggesting that PI3K/AKT is required for p53, p21 and p16 regulation in hMSCs. These data suggest that the up-regulation of CD49f enhances cell proliferation and sphere formation via regulation of the PI3K/AKT pathway. The CD49f-overexpressing hMSCs had a significantly enhanced osteogenic differentiation potential when compared to wild-type hMSCs. Strikingly, osteogenic differentiation was further boosted in the presence of BIO, as evidenced by an increased level of mineral deposition

measured using Alizarin Red S staining. In contrast, treatment with LY294002 dramatically reduced the osteogenic differentiation potential of CD49f-overexpressing hMSCs (Figs. 4D and 4E). The gene expression levels of osteogenic markers, such as osteocalcin, Runx2, VDR and MSX2, were consistently and significantly increased in the presence of BIO. However, LY294002 treatment inhibited osteogenic marker expression, as determined using conventional RT-PCR (Fig. 4F). Under adipogenic differentiation conditions, CD49f-overexpressing cells showed significantly increased levels of lipid accumulation with Oil Red O staining compared to wild-type hMSCs, indicating that the overexpression of CD49f could also enhance the adipogenic differentiation potential of hMSCs. However, both BIO and LY294002 treatments suppressed lipid accumulation (Figs. 4G and 4H). Similarly, the gene expression levels of the adipogenic transcription factors, including C/EBP-β, aP2, PPARγ and leptin, were significantly increased in the CD49f-overexpressing cells. However, both BIO and LY294002 treatments inhibited the transcription of adipogenic-specific markers (Fig. 4I). I further assessed the osteogenic and adipogenic differentiation capabilities of the p53-inhibited hMSCs. The inhibition of p53 led to increases in the osteogenic and adipogenic differentiation potentials (Fig. 3E and 3F). Therefore, these data suggest that the PI3K/AKT/p53 pathway regulates hMSC differentiation.

1.3.5 Overexpression of OCT4 and SOX2 enhances CD49f expression by binding to the CD49f promoter.

The enhancement of hMSC multi-potential by CD49f prompted us to investigate

the relationship between CD49f and the pluripotency marker genes OCT4 and SOX2. First, I analyzed the expression of pluripotency markers in MSC spheres. In MSC spheres, the mRNA levels of OCT4, SOX2, NANOG and LIN28 were increased compared with MSC monolayers (Fig. 5A). To determine whether OCT4 and SOX2 directly regulated CD49f, I introduced siOCT4 and siSOX2 into hMSCs. OCT4 and SOX2 siRNA blocked OCT4 and SOX2 expression, respectively (Figs. 5B and 5C). In addition, the siRNA targeting of either OCT4 or SOX2 significantly repressed CD49f expression, resulting in decreased sphere formation (Figs 5D and 5E). To determine how OCT4 and SOX2 regulated CD49f expression, I overexpressed either OCT4 or SOX2 in hMSCs and examined OCT4, SOX2 and CD49f expression using immunocytochemistry. The overexpression of both OCT4 and SOX2 led to increased CD49f expression (Fig. 5G). The overexpression of CD49f in hMSCs was also confirmed using flow cytometry analysis. As shown in Figure 5H, OCT4 and SOX2 overexpression led to a larger CD49f-positive subpopulation. To clarify how OCT4 and SOX2 regulated CD49f expression, I performed ChIP analysis to investigate the direct binding of both OCT4 and SOX2 to putative CD49f promoter regions. For ChIP, Tera-1 cells, hMSCs and OCT4/SOX2/LIN28/NANOG-overexpressing hMSCs were crosslinked with formaldehyde, and the fragmented chromatin lysates were used for immunoprecipitation using the OCT4 and SOX2 antibodies. Sequentially located primers (Table 2) along the entire conserved promoter region of CD49f were used to analyze OCT4- and SOX2-binding DNA sites. As shown in Figure 5F, specific regions within the CD49f promoter were enriched with OCT4 and SOX2 protein. I found that the CD49f promoter region has

the classic canonical octamer sequence (CD49f-1, ATTTGCAT) and the partially conserved sequence (CD49f-2, ATGTAAA) for the OCT4-binding site and the SOX2-binding site (CD49f-3, CATTATT). A negative control (IgG control) showed no significant enrichment in the surveyed region. These data suggest that OCT4 and SOX2 bind directly to the CD49f promoter and induce the expression of CD49f. I next investigated whether CD49f expression was also regulated by other reprogramming factors in hMSCs, such as LIN28 and NANOG. I introduced OCT4, SOX2, LIN28 and NANOG into hMSCs in different combinations and determined the expression level of CD49f. Again, introducing OCT4/SOX2 increased CD49f expression. Overexpressing all four factors (OCT4/SOX2/LIN28/NANOG) further enhanced the transcription level of CD49f (Fig. 5I). As observed using western blot analysis, the protein levels of both CD49f and phosphor-FAK were increased in OCT4/SOX2- and OCT4/SOX2/LIN28/NANOG-overexpressing hMSCs (Fig. 5J). Therefore, these data suggest that OCT4, SOX2, LIN28 and NANOG form a positive feedback loop that regulates CD49f expression and integrin signaling pathway in hMSCs.

1.3.6CD49f maintains cellular pluripotency through the PI3K/AKT/p53 pathway

I next investigated the effect of CD49f on pluripotency maintenance through embryoid body formation and the depletion of CD49f in hESCs using siRNA and shRNA. Embryoid bodies were generated from hESCs for 8 days in suspension culture and were attached to gelatin-coated dishes for another 8 days to induce differentiation (Fig. 6A). The hESCs showed significantly up-regulated expression of CD49f, OCT4, SOX2 and

NANOG compared to hMSCs, whereas CMYC mRNA levels were comparable in both cell lines. CD49f expression and pluripotency markers decreased upon differentiation, which suggests that CD49f expression is closely related to pluripotency. In contrast, the gene expression of CMYC was not influenced by differentiation (Fig. 6B). To determine the role of CD49f in the maintenance of the pluripotency of hESCs, I treated the hESCs with siRNA against CD49f. After three rounds of consecutive transfection with siCD49f, the hESCs gradually showed typical differentiated morphologies and reduced alkaline phosphatase (AP) activity (Figs. 6C and 6D). Furthermore, a significant reduction in AP-positive colonies was observed after the two rounds of control and CD49f-targeting shRNA lentiviral particles (Fig.5E).

To determine whether the inhibition of CD49f affected hESC pluripotency in addition to AP activity, I performed immunocytochemistry. The siCD49f-transfected hESCs showed significant down-regulation of OCT4 and SOX2 expression (Fig. 6F). Next, I performed real-time PCR to explore pluripotency markers and lineage markers. In agreement with the immunocytochemistry results, siCD49f-transfected hESCs displayed a substantial reduction in the levels of the pluripotency marker genes. In contrast, lineage-specific marker genes were up-regulated in siCD49f-transfected hESCs, demonstrating that CD49f plays a role in the maintenance of pluripotency in hESCs (Fig. 6G). In line with my observations in the MSC spheres, CD49f knockdown led to an inhibition of the PI3K/AKT/GSK3β pathway and an increase in p53, p21 and p16 expression in hESCs (Fig. 6H). To further determine whether CD49f, through the PI3K pathway, was required for maintaining the undifferentiated status of hESCs, I treated the cells with a selective

PI3K/AKT inhibitor, LY294002. PI3K/AKT inhibition significantly reduced the expression of both NANOG and CD49f in a dose-dependent manner (Fig. I). Taken together, these findings indicate that CD49f plays a pivotal role in maintaining cellular pluripotency through the PI3K/AKT/p53 pathway.

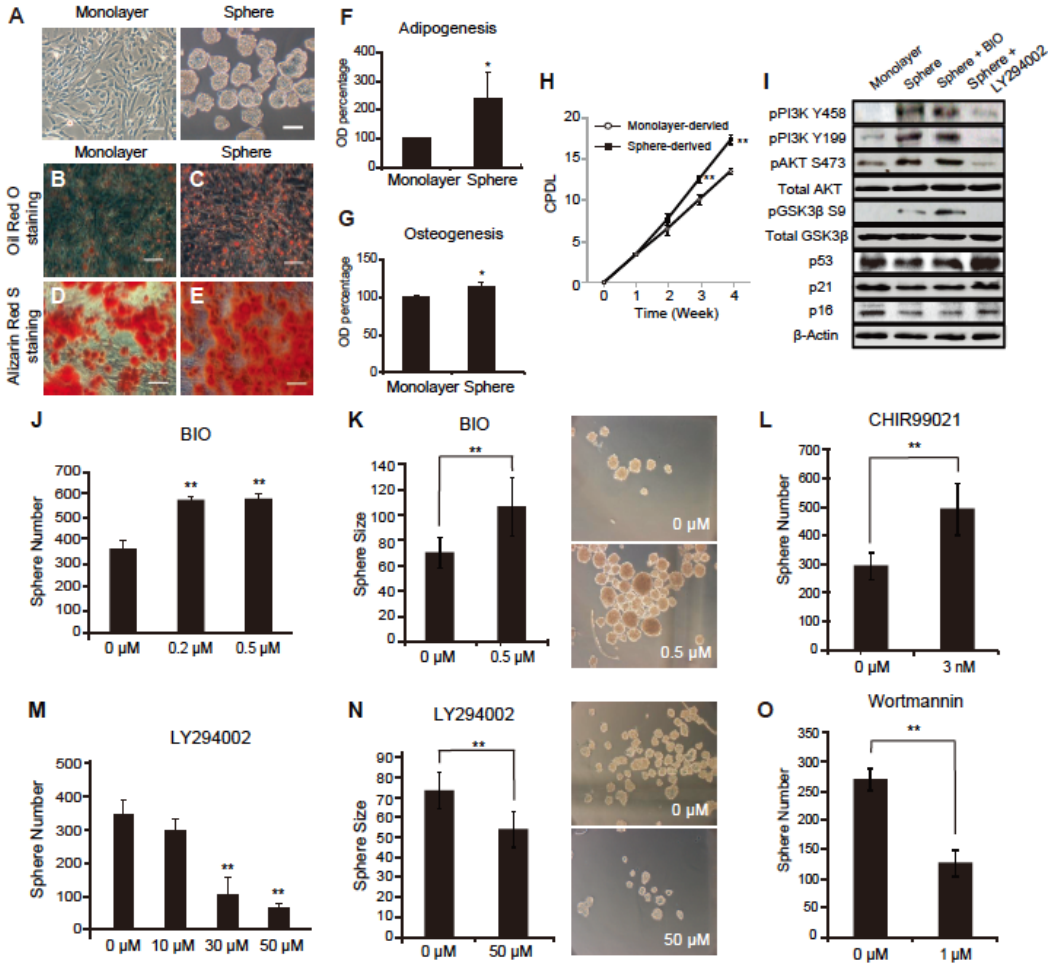

Figure 1. Enhancement of adipogenic and osteogenic differentiation and PI3K pathway activation in sphere-derived cells.

(A) Phase-contrast images of hMSCs cultured in a plastic culture dish or an agarose-coated dish. On average, 15,000 cells were seeded per 1 ml of medium. Scale bar = 100 μm. **(B-E)** Phase-contrast images of monolayer cells (left panel) and sphere-derived cells (right panel) after induction into specific tissues. The lipid droplet accumulation in differentiated cells was visualized using Oil Red O staining after 3 weeks of adipogenic induction (B, C). Mineral deposition was stained with Alizarin Red S after 3 weeks of osteogenic induction (D, E). **(F)** Oil Red O-stained dye was eluted using 100% isopropanol, and the absorbance was measured at a wavelength of 500 nm. (*, $P < 0.05$) **(G)** A total of 100 mM cetylpyridinium chloride were used for the elution of Alizarin Red S dye, and the absorbance was measured at a wavelength of 570 nm. (*, $P < 0.05$) **(H)** The cumulative population doubling level was assessed in monolayer-derived cells and sphere-derived cells. (**, $P < 0.01$, n = 3) **(I)** Western blot analysis was conducted after 7 days of sphere-inducing culture. MSC spheres were collected using a 40-μm strainer and washed twice. The phosphorylation levels of PI3K and its sequential downstream effectors AKT, GSK3β, p53, p21 and p16 were analyzed and compared between monolayer cells, spheres, 0.2 μM BIO-treated spheres and 30 μM LY294002-treated spheres. **(J)** The numbers of MSC spheres cultured in growth medium containing 0 μM, 0.2 μM or 0.5 μM BIO, a GSK3 inhibitor. (**, $P < 0.01$) **(K)** The sphere size of 0 μM or 0.5 μM BIO-treated MSC spheres was measured. Phase- contrast images of the MSC spheres cultured with BIO at the indicated concentrations. (**, $P < 0.01$) **(L)** The

numbers of MSC spheres cultured in growth medium containing 0 μM or 3 μM CHIR99021, a GSK3 β inhibitor. (**, $P < 0.01$) **(M)** The numbers of MSC spheres cultured in growth medium containing 0 μM, 10 μM, 30 μM or 50 μM LY294002, a PI3K inhibitor. (**, $P < 0.01$) **(N)** The sphere size of the 0 μM or 50 μM BIO-treated MSC spheres was measured. Phase-contrast images of the MSC spheres cultured with LY294002 at the indicated concentrations. (**, $P < 0.01$) **(O)** The numbers of MSC spheres cultured in growth medium containing 0 μM or 1 μM wortmannin, a PI3K inhibitor. (**, $P < 0.01$)

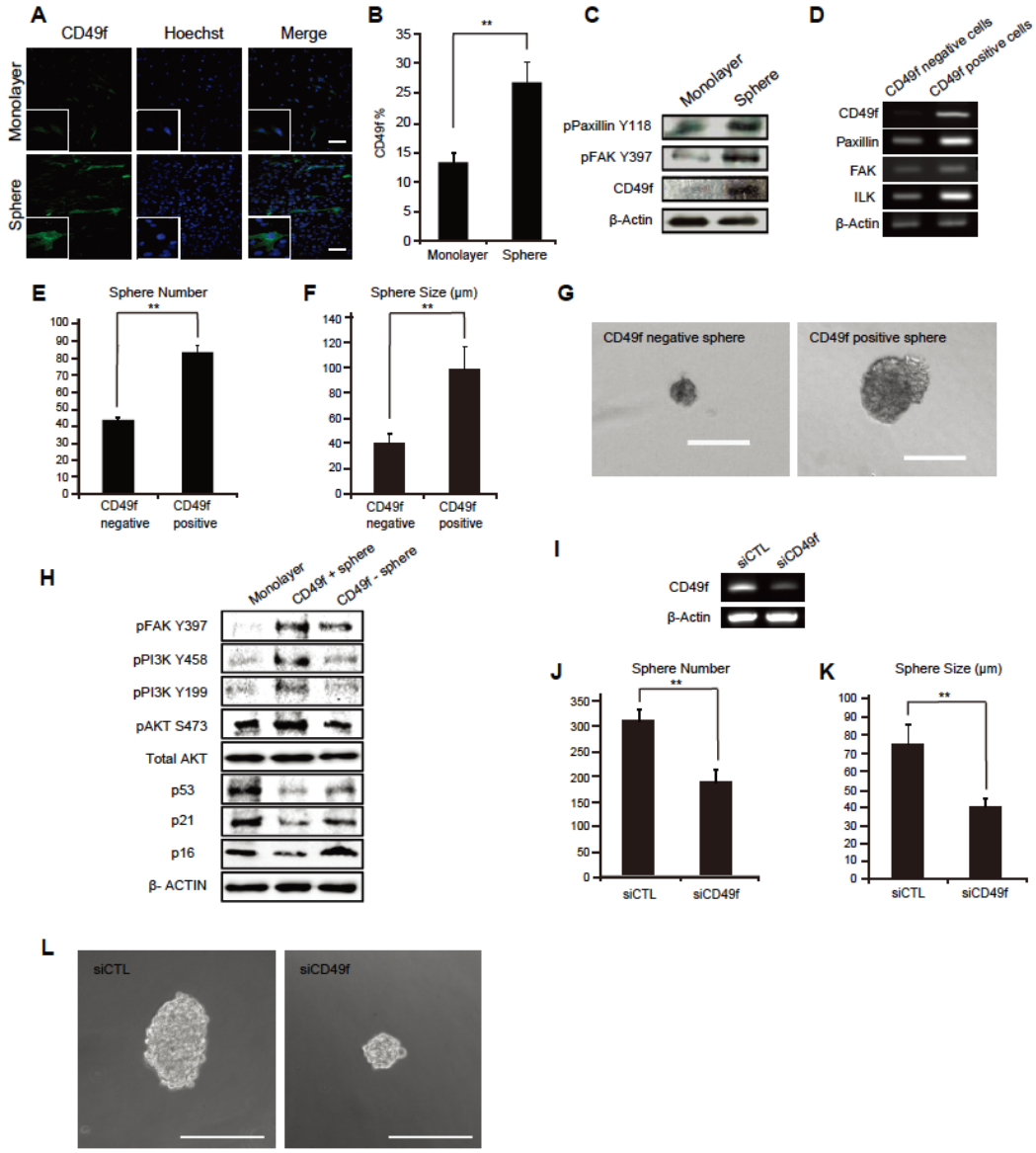

Figure 2. Up-regulation of CD49f in sphere-derived cells and its regulation of sphere-forming efficiency.

(A) Immunocytochemical analysis of CD49f expression in monolayer-cultured and sphere-derived hMSCs. Monolayer MSCs and dissociated MSC spheres were seeded with the same starting number of cells into 4-well chamber slides. After 3 days, the cells were fixed and analyzed with the indicated antibodies. Scale bar = 100 μm. **(B)** The expression level of CD49f was analyzed using flow cytometry with a FITC-conjugated antibody. Measurements were performed in triplicate. (**, $P < 0.01$) **(C)** The activities of downstream signal transducers of integrin, such as FAK and Paxillin, were estimated using western blotting. **(D)** The expression levels of the integrin-related markers CD49f, Paxillin, FAK and ILK were analyzed in both CD49f-negative and CD49f-positive populations using RT-PCR. **(E)** After flow cytometry sorting into CD49f-negative and CD49f-positive cell populations, the sphere-forming efficiency of 20,000 cells from each population was assessed. (**, $P < 0.01$) **(F)** The sphere size was measured in the CD49f-negative and CD49f-positive populations. For the assessment of sphere-size, 50 spheres were randomly selected and analyzed statistically. (**, $P < 0.01$) **(G)** Phase-contrast images of a single representative sphere derived from CD49f-negative or CD49f-positive cells. **(H)** Western blot analysis was conducted on monolayer cells and MSC spheres from CD49f-positive and CD49f-negative populations. The phosphorylation levels of PI3K and its sequential downstream effectors AKT, GSK3β, p53, p21 and p16 were analyzed. **(I)** The expression level of CD49f was analyzed using RT-PCR 3 days after transfection with siCTL or siCD49f. **(J)** After transfection with control siRNA or the siRNA targeting CD49f, the sphere-forming efficiency of each population was assessed. (**, $P < 0.01$) **(K)** Sphere size was measured in the control siRNA- and the siRNA

targeting p53-transfected MSC spheres. For the assessment of sphere size, 50 spheres were randomly selected and analyzed statistically. (**, $P < 0.01$) **(L)** Phase-contrast images of a single representative sphere derived from hMSCs transfected with the control siRNA or the siRNA targeting CD49f. Scale bar = 100 μm.

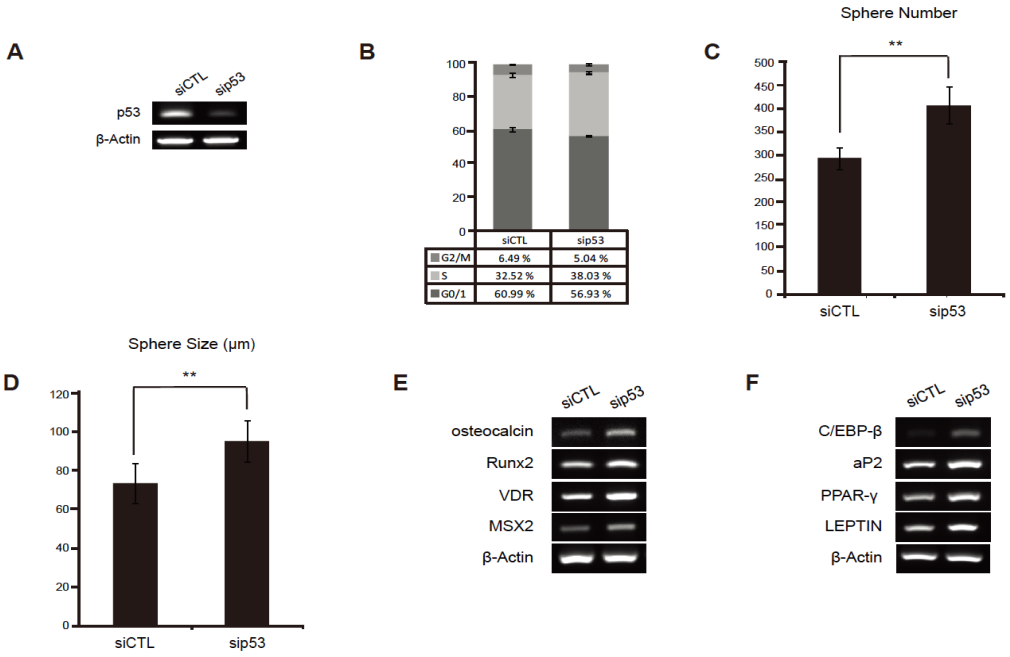

Figure 3. Significance of p53 on the formation of spheres and the differentiation potential of hMSCs

The hMSCs were analyzed after transfection with either control siRNA (siCTL) or the siRNA targeting p53 (sip53)**. (A)** The expression levels of p53 were analyzed using RT-PCR 3 days after siRNA transfection. **(B)** After siRNA transfection, hMSCs were stained with propidium iodide, and their cell cycle distribution was determined using flow cytometry (n = 3). **(C, D)** After siRNA transfection, hMSCs were subjected to sphere-forming conditions. The sphere-forming efficiency (C) and sphere size (D) of each population were assessed. (**, $P < 0.01$, n = 50) **(E, F)** The efficiency of osteogenic (E) and adipogenic (F) differentiation was evaluated through the expression of osteogenic and adipogenic marker genes, respectively. β-actin was used for the loading control.

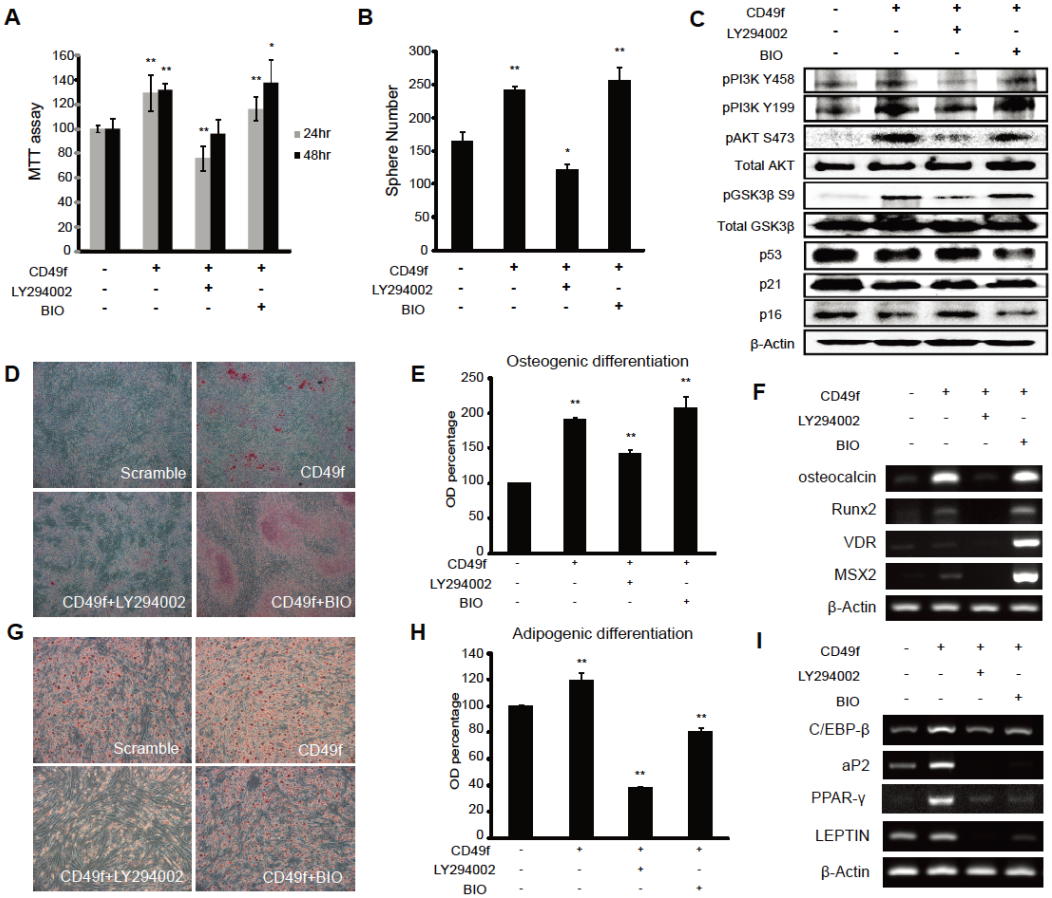

Figure 4. CD49f overexpression enhances the proliferation, sphere-forming efficiency and differentiation of hMSCs and activates the PI3K/AKT/GSK3β pathway

(A) An MTT cell proliferation assay was performed in the presence or absence of CD49f, LY294002 or BIO. Cells were seeded in 24-well culture plates, and the optical density was measured at 24 and 48 hr. (*, $P < 0.05$; **, $P < 0.01$) **(B)** Sphere numbers were measured in the presence or absence of CD49f, LY294002 or BIO. (*, $P < 0.05$; **, $P <$

0.01) **(C)** A western blot analysis of PI3K/AKT/GSK3β, p53 and p16 was performed. Cells were transfected with a CD49f expression vector and treated with LY294002 and BIO. The phosphorylation levels of the protein kinases were determined using western blot with phospho-specific antibodies against each protein. Each well was loaded with 20 μg of protein lysate. **(D)** hMSCs were cultured in osteogenic-induction media in the presence or absence of CD49f, LY294002 or BIO. Osteogenesis was determined using Alizarin Red S staining. **(E)** An Alizarin Red S-stained dish was incubated with cetylpyridinium chloride. The levels of eluted Alizarin Red S solution were determined using an ELISA at 570 nm. (**, $P < 0.01$) **(F)** The efficiency of osteogenic differentiation was evaluated by the expression of osteogenic marker genes, including osteocalcin, RUNX2, VDR and MSX2 **(G)** hMSCs were cultured in adipogenic induction media in the presence or absence of CD49f, LY294002 or BIO. The accumulation of lipid droplets in the cytosol was visualized using Oil Red O staining after 2 weeks of induction. **(H)** Oil Red O was eluted using 100% isopropanol, and the absorbance was measured via spectrometry at 500 nm. (**, $P < 0.01$) **(I)** The efficiency of adipogenic differentiation was evaluated through the expression of adipogenic marker genes, including CEBP-β, aP2, PPAR-γ and leptin.

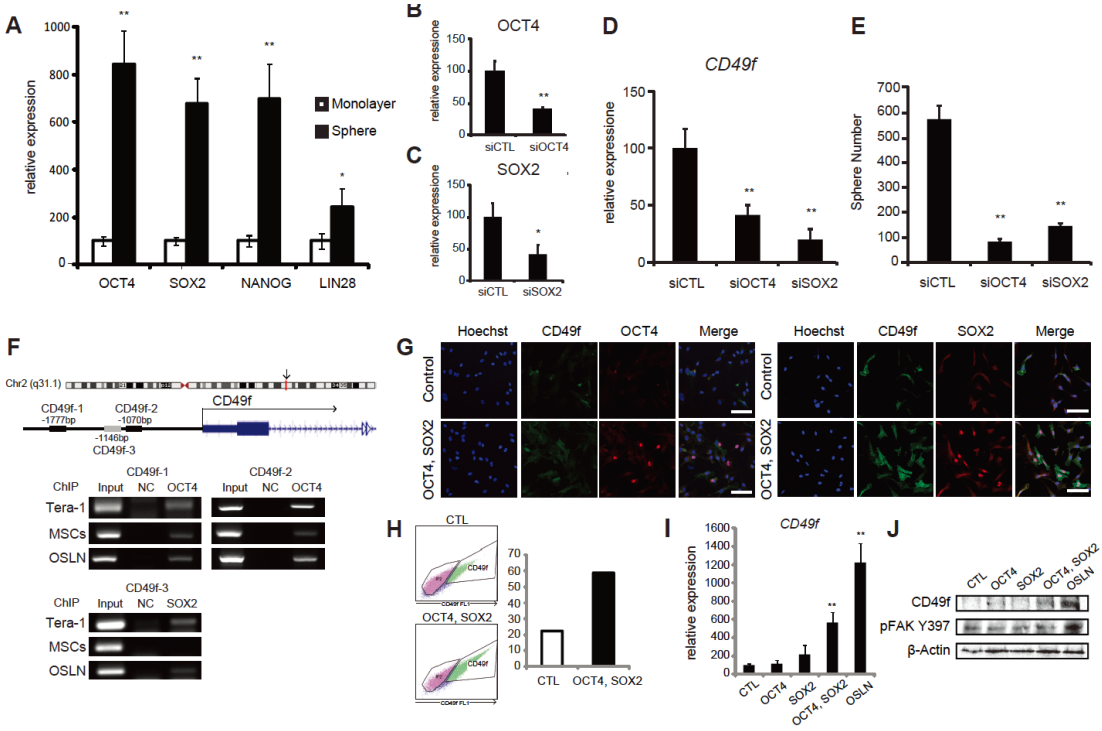

Figure 5. OCT4 and SOX2 bind to and regulate CD49f transcription through the CD49f promoter region

(A) A quantitative estimation of mRNA expression as detected using real-time PCR. Relative mRNA expression levels of pluripotency markers are presented for monolayer cells and MSC spheres. All analyses were performed in triplicate and normalized to endogenous β-actin. (*, $P < 0.05$; **, $P < 0.01$) **(B, C)** hMSCs were transfected with siRNAs targeting OCT4 or SOX2. Non-targeting siRNA (siCON) was used as a control. The expression levels of *OCT4* and *SOX2* were analyzed using real-time PCR. (*, $P < 0.05$; **, $P < 0.01$) **(D)** After 48 h of transfection, the cells were collected, and real-time

PCR was performed to assess CD49f expression (**, $P < 0.01$) **(E)** Sphere-forming efficiency was measured in siRNA-transfected cells and control-transfected cells. (**, $P < 0.01$) **(F)** Chromatin immunoprecipitation was performed using anti-OCT4 and anti-SOX2 antibodies. Three regions on the CD49f promoter were targeted using specific primer sets, as described in Table 2. "NC" indicates negative control (IgG control). **(G)** Immunocytochemical analyses of CD49f, OCT4 and SOX2 were performed on both control virus- and OCT4 and SOX2 virus-infected cells. Nuclei were stained using Hoechst (blue). Scale bar = 50 μm. **(H)** The CD49f-positive population was estimated using flow cytometry for control and OCT4- and SOX2-overexpressing cells. **(I)** Quantitative estimates of CD49f mRNA expression were determined in control cells and cells overexpressing the indicated combinations of OCT4, SOX2, LIN28 and NANOG. (**, $P < 0.01$) **(J)** Western blotting was performed to determine CD49f and phospho-FAK expression in the indicated combinations of virus-infected cells.

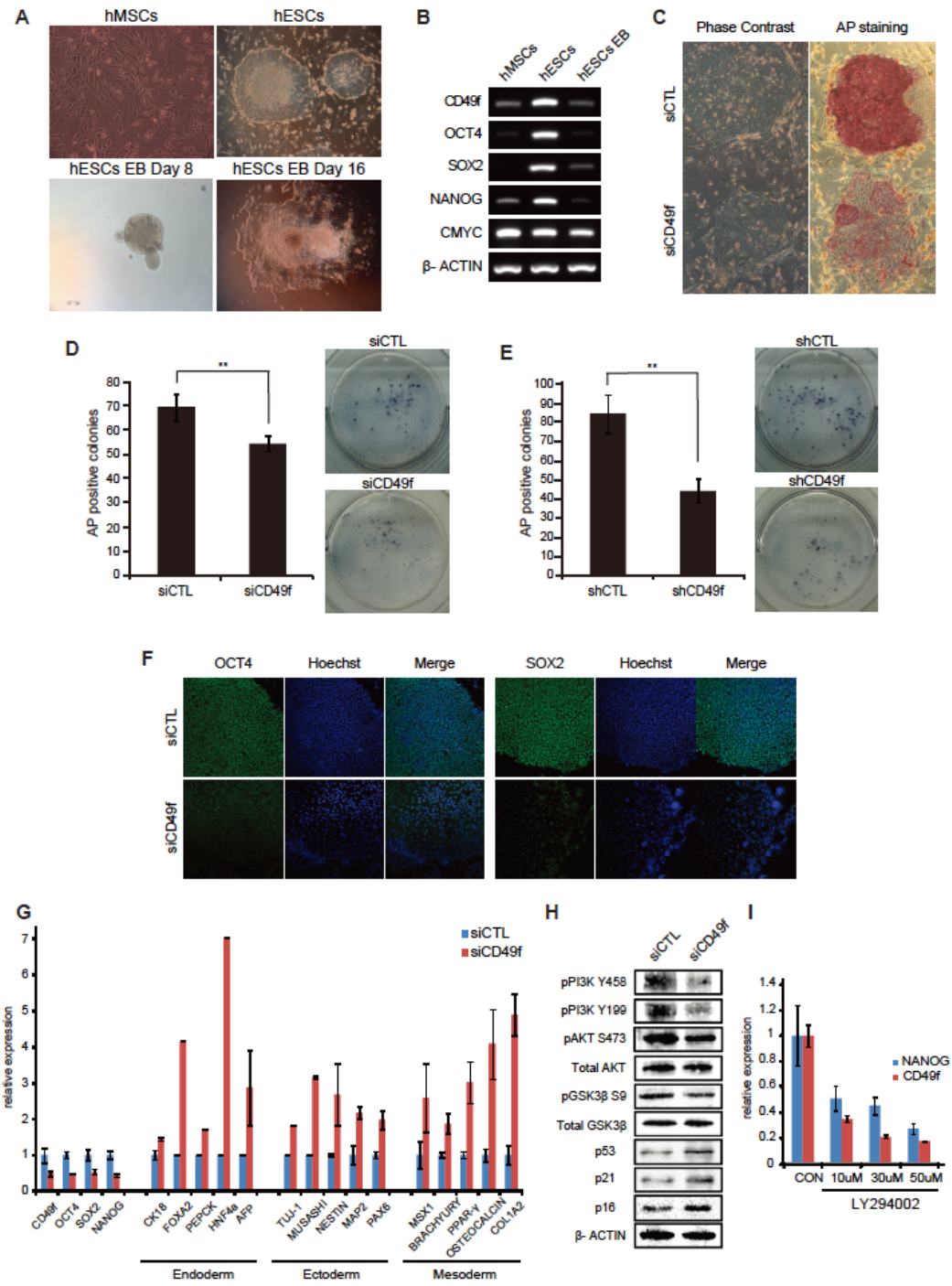
A
hMSCs
hESCs
hESCs EB Day 8
hESCs EB Day 16
B
hMSCs
hESCs
hESCs EB
CD49f
OCT4
SOX2
NANOG
CMYC
β- ACTIN
C
Phase Contrast
AP staining
siCTL
siCD49f
D
AP positive colonies
siCTL
siCD49f
E
AP positive colonies
shCTL
shCD49f
F
OCT4
Hoechst
Merge
SOX2
Hoechst
Merge
siCTL
siCD49f
G
siCTL
siCD49f
relative expression
CD49f
OCT4
SOX2
NANOG
CK18
FOXA2
PEPCK
HNF4a
AFP
TUJ-1
MUSASHI
NESTIN
MAP2
PAX6
MSX1
BRACHYURY
PPARγ
OSTEOCALCIN
COL1A2
Endoderm
Ectoderm
Mesoderm
H
siCTL
siCD49f
pPI3K Y458
pPI3K Y199
pAKT S473
Total AKT
pGSK3β S9
Total GSK3β
p53
p21
p16
β- ACTIN
I
relative expression
NANOG
CD49f
CON
10uM
30uM
50uM
LY294002

Figure 6. CD49f maintains the pluripotency of hESCs through the PI3K/AKT/GSK3β pathway

(A) Phase-contrast images of hMSCs, hESCs and EBs. For spontaneous differentiation, the EBs were generated from hESCs after 8 days in suspension culture. To trigger further differentiation, the EBs were transferred to gelatin-coated dishes and maintained for another 8 days. **(B)** RT-PCR analysis was performed to determine the expression levels of pluripotency marker genes, CD49f and β-actin in hMSCs, hESCs and hESC EBs. **(C)** Phase-contrast images and alkaline phosphatase staining images of hESCs transfected with the control siRNA and the siRNA targeting CD49f. **(D)** A representative image and quantitative analysis of alkaline phosphatase-positive colonies of hESCs transfected with the control siRNA and siCD49f. The expression levels were normalized to cells transfected with non-targeting siRNA (siCTL). (**, $P < 0.01$) **(E)** A representative image and quantitative analysis of alkaline phosphatase-positive colonies of hESCs infected with control shRNA and shCD49f viruses. (**, $P < 0.01$) **(F)** Immunocytochemical analyses of OCT4 and SOX2 were performed on both control siRNA- and siCD49f-transfected cells. Nuclei were stained using Hoechst (blue). **(G)** The expression levels of CD49f, pluripotency marker genes and additional markers for the three germ layers in the siRNA control- and siCD49f-transfected hESCs. **(H)** hESCs were transfected with non-targeting siRNA or siRNA targeting CD49f. After three rounds of consecutive transfection, cell lysates were collected and used for western blot analysis of PI3K/AKT/GSK3β and p53, p21 and p16. **(I)** hESCs were treated with the indicated concentration of LY294002, a PI3K inhibitor. NANOG and CD49f expression was measured using real-time PCR.

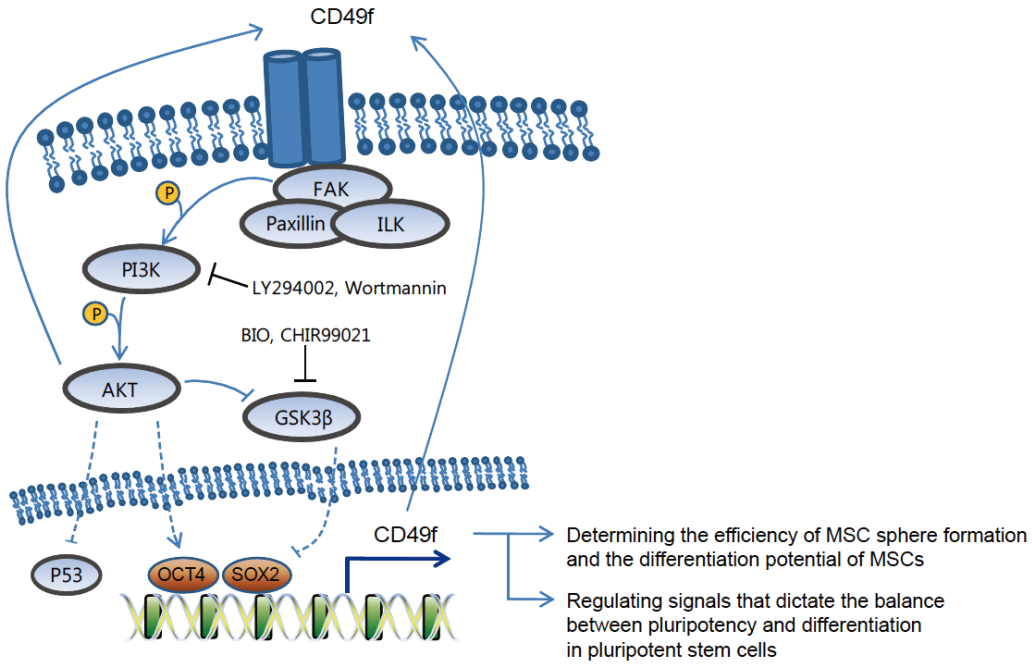

Figure 7. Schematic diagram of the role of CD49f in MSC sphere formation and reprogramming

This schematic summarizes the proposed role of CD49f in hMSCs. This diagram illustrates how the activation of CD49f can lead to the phosphorylation of PI3K/AKT, which in turn leads to an enhancement of MSC sphere formation and hMSC cellular potency. Additionally, CD49f expression can contribute to the maintenance of stem cell pluripotency.

1.4 DISCUSSION

In this study, I have isolated and characterized sphere-forming cells from hMSCs. The sphere-forming hMSCs showed higher proliferation and differentiation capabilities via activation of the PI3K/AKT/p53 axis, which is important for cell-cell and cell-ECM interactions. Integrins are a cell adhesion-related family that form heterodimeric complexes between the alpha and beta subunits (Hynes, 1987). Among the integrins, I have shown that CD49f and CD104 are up-regulated in sphere-derived cells. The CD49f/CD104 (integrin alpha 6/beta 4) complex plays an important role in cell proliferation and PI3K/AKT activation via interactions with laminin and the anchoring filament protein kalinin (Gambaletta et al., 2000; Hynes, 1987). Downstream signal transducers of integrin, such as FAK and Paxillin, were activated in sphere cells, suggesting that integrin signaling is sufficient for triggering the PI3K/AKT/GSK3β signaling pathways. Moreover, both sphere-forming efficiency and sphere size were significantly increased in the CD49f-positive population compared to the CD49f-negative population. Interestingly, there was a difference between the MSC spheres created from the distinct populations. I found that MSC spheres generated from CD49f-positive cells showed a higher activation of the FAK, PI3K and AKT signaling pathways compared with MSC spheres from CD49f-negative cells. Consistent with a previous report that survival signals from FAK could suppress the p53-regulated cell death pathway, I showed that p53, p21 and p16 were inhibited in MSC spheres from CD49f-positive cells with an

activated FAK signaling pathway(Ilic et al., 1998). This result is compatible with previous reports that cancer cells grown under sphere-forming conditions showed preferential activation of the PI3K/AKT signaling pathway and displayed preferential sensitivity to AKT inhibition (Lawson et al., 2010; Ma et al., 2008). Given my observation that CD49f knockdown inhibited sphere formation in hMSCs, CD49f may be a potential molecular target for interrupting cancer stem cell activity through the inhibition of PI3K/AKT signaling.

Although CD49f activates the PI3K/AKT pathway in carcinoma cells (Gambaletta et al., 2000; Shaw et al., 1997), whether the CD49f-mediated PI3K/AKT pathway is conserved in both the proliferation and cellular potency of adult stem cells is unknown. I found that CD49f overexpression activated the PI3K/AKT pathway and led to an up-regulation of sphere-forming efficiency and adipogenic and osteogenic differentiation potentials. In addition, CD49f overexpression down-regulated p53 levels in hMSCs. Because the pivotal regulatory proteins PI3K/AKT can both regulate p53 and be regulated by it, I investigated p53 and its downstream effector p21, which play regulatory roles in the p53 and CDK4 in cell cycle progression (Ohtani et al., 2004). Recently, studies describing the various roles of p53 in cellular processes, including self-renewal, differentiation and reprogramming, have emerged. Cicalese et al. reported that the mammary glands of p53-knockout mice had higher number of mammosphere-forming cells that could repopulate the glands in vivo and that the p53-null mammospheres showed increased replicative potential compared to wild-type (Cicalese et al., 2009; Tao

et al., 2011). Furthermore, it has been demonstrated that p53 regulates the proliferation and differentiation of mouse MSCs (Armesilla-Diaz et al., 2009). In agreement with those studies, my data showed that p53 levels regulated the proliferation and differentiation of hMSCs; furthermore, the down-regulation of p53 through PI3K/AKT signaling was induced by CD49f.

Consistent with previous studies reporting that the PI3K/AKT network is critical for both osteogenic differentiation and bone growth (Fujita et al., 2004; Mukherjee and Rotwein, 2009), I observed that the activation of the PI3K/AKT/GSK3β pathway mediated by CD49f appeared to promote the osteogenic differentiation of hMSCs. Furthermore, I found that hMSCs treated with BIO, an inhibitor of GSK3, showed an increased propensity for osteogenic differentiation without an effect on viability. In previous studies, it has been shown that constitutively activated PI3K/AKT induces spontaneous adipocyte differentiation (Kohn et al., 1996; Xu and Liao, 2004). However, the inhibition of GSK3 blocks adipogenic differentiation by inhibiting PPARγ, the master regulator of adipogenesis (Kang et al., 2007). In agreement with this, I observed that the treatment of BIO up-regulated a set of osteogenic marker genes, while a set of adipogenic marker genes was substantially decreased, indicating that CD49f preferentially stimulates the differentiation of hMSCs into the osteogenic lineage by regulating the PI3K/AKT/p53 pathway (Cicalese et al., 2009; Tao et al., 2011). Fig. 7 shows a schematic representation of the CD49f-PI3K/AKT/p53 pathway.

According to recent studies, OCT4 and other pluripotency marker genes can regulate the proliferative capacity, colony formation and lineage differentiation potencies of MSCs (Greco et al., 2007; Liu et al., 2009; Tondreau et al., 2005). In this study, I found that sphere-derived hMSCs showed an increased expression of OCT4/SOX2/LIN28/NANOG. This result suggests that the increased proliferation and differentiation potentials of sphere-forming MSCs may be mediated, at least in part, by the higher expression of these pluripotency-enhancing genes. Furthermore, I showed that the silencing of OCT4 or SOX2 led to the down-regulation of CD49f activity, whereas the endogenous transcripts and proteins of CD49f were activated by the forced expression of OCT4 and SOX2. The effects of OCT4 and SOX2 siRNA and overexpression may have been indirect because changes in endogenous OCT4 and SOX2 levels may have led to different cellular states (i.e., differentiation or reprogramming). To determine whether the regulation of CD49f by OCT4 and SOX2 was due to direct binding, I performed chromatin immunoprecipitation. Using specific antibodies against OCT4 and SOX2, I showed that these two transcription factors bound to the putative promoter region of the CD49f gene (Fig. 5F). Because hMSCs display much lower expression levels of endogenous OCT4 and SOX2 than hESCs (Fig 6B), hMSCs showed a weak enrichment of OCT4 and SOX2 in the CD49f promoter region compared to Tera-1 cells.

In this study, I elucidated the role of CD49f in the maintenance of the differentiation potential of both hMSCs and hESCs. To my knowledge, we are the first group to report that CD49f plays a significant role in the maintenance of the hMSC

differentiation potential. In the case of hESCs, it has previously been reported that these cells express a broad range of integrins, including CD49f, which interacts with laminin (Meng et al., 2010; Miyazaki et al., 2008; Rodin et al., 2010; Rowland et al., 2009). The laminin recognized by alpha 6 beta 1 ($\alpha 6\beta 1$) integrin or alpha 6 beta 4 ($\alpha 6\beta 4$) can be used as a substrate for the adhesion and expansion of undifferentiated hESCs (Meng et al., 2010; Miyazaki et al., 2008; Rodin et al., 2010; Rowland et al., 2009). However, the role of CD49f in the maintenance of pluripotency and the regulation of the PI3K/AKT/GSK3β signaling pathway had yet to be elucidated in hESCs. Regarding the role of CD49f in hESCs, I showed that the depletion of CD49f led to a loss of pluripotency, as suggested by the decreased expression of OCT4 and SOX2 and the induction of differentiation in hESCs. I also showed that the CD49f-mediated maintenance of differentiation potential was linked to the PI3K/AKT/GSK3β signaling pathway in both hMSCs and hESCs. Blocking CD49f inhibited the PI3K/AKT/GSK3β pathway, which is crucial for the maintenance of pluripotency and/or viability of hESCs (Armstrong et al., 2006; Watanabe et al., 2006). Because active AKT can reduce the levels of p53 (Ogawara et al., 2002), blocking CD49f in hESCs promotes the up-regulation of p53, p21 and p16. These observations suggest that CD49f helps to maintain a more stem-like state, and the loss of CD49f might trigger the progression into the differentiated state. Taken together, these findings suggest that CD49f crosstalks with OCT4 and SOX2 and may contribute to the maintenance of pluripotency through the activation of the CD49f-PI3K/AKT/p53 signaling pathway.

In summary, I conclude that CD49f, a cell-surface molecule, plays important roles in MSC sphere formation and in the determination of the differentiation potential of hMSCs. I showed that the pluripotency factors OCT4 and SOX2 bound directly to the CD49f promoter, indicating that OCT4 and SOX2 play positive roles in the expression of CD49f. In addition, the CD49f-induced activation of the PI3K/AKT/p53 pathway contributes to the maintenance of pluripotency in hESCs.

CHAPTER II

HMGA2 regulates the *in vitro* aging and proliferation of human umbilical cord blood-derived stromal cells through the mTOR/p70S6K signaling pathway

2.1 INTRODUCTION

HMGA2 is a non-histone chromosomal high-mobility group A (HMGA) family protein that binds to the minor groove of AT-rich DNA sequences (Fusco and Fedele, 2007; Grosschedl et al., 1994). The HMGA2 protein does not have direct transcriptional activity but rather transforms the chromatin structure through its DNA binding (Thanos and Maniatis, 1992); these changes in chromatin architecture can alter the local transcription. In general, HMGA2 is highly expressed during embryogenesis and is nearly undetectable in adult tissues (Chiappetta et al., 1996). In many cases, HMGA2 is up-regulated in tumor cells in adult tissues (Fedele et al., 2010; Young and Narita, 2007); overexpression studies have generally shown that HMGA2 induces oncogenesis (Fedele et al., 2010). However, there are some exceptions, particularly in adult stem cells. Recent studies have proposed the possibility that HMGA2 is intimately involved in the regulation of adult stem cells. HMGA2 was highly expressed in neural stem cells (NSCs) and regulated the self-renewal of NSCs in young mice (Nishino et al., 2008). In humans, normal CD34-positive hematopoietic stem cells (HSCs) express HMGA2, and the proliferation and differentiation of HSCs are governed by HMGA2 (Rommel et al., 1997). These data suggest that HMGA2 may have critical roles in regulating stemness in NSCs or HSCs and also in hMSCs. My previous study showed that the expression of HMGA2 , $p16^{INK4A}$, $p21^{CIP1/WAF1}$ and $p27^{KIP1}$ was strongly affected by the aging of MSCs (Lee et al., 2011). These results indicate that HMGA2 has crucial roles in adult stem cells, especially MSCs, and can regulate stem cell aging in addition to proliferation and differentiation.

Phosphatidylinositol 3-kinases (PI3Ks) are lipid kinases that are involved in the control of stem cell proliferation (Welham et al., 2011). Previously, I reported that the PI3K signaling pathway determines the self-renewal and differentiation potential of hMSCs (Yu et al., 2012). PI3K is one component of an intracellular signaling cascade that also involves AKT and mammalian target of rapamycin (mTOR). The PI3K/AKT/mTOR pathway regulates several cellular functions, such as proliferation, growth, survival, mobility and tumorigenesis (Morgensztern and McLeod, 2005), and several studies have investigated the PI3K/AKT/mTOR pathway within the context of adult stem cell regulation (Le Belle et al., 2011; Martelli et al., 2011). However, the interactions between PI3K/AKT/mTOR and HMGA2 in adult stem cells remain uncharacterized.

$p16^{Ink4a}$ and $p19^{Arf}$, also known as cyclin-dependent kinase inhibitors, are well-known tumor suppressor genes. There is considerable evidence that $p16^{Ink4a}$ and $p19^{Arf}$ promote cellular aging (Bennecke et al., 2010; Collado et al., 2007), and previous studies have shown that HMGA2 modulates self-renewal and aging by reducing $p16^{Ink4a}$ and $p19^{Arf}$ expression in adult stem cells (Nishino et al., 2008). However, it remains unknown whether HMGA2 regulates $p16^{Ink4a}$ and $p19^{Arf}$ directly or indirectly in adult stem cells. In this study, I elucidate the mechanistic relationship among $p16^{Ink4a}$, $p19^{Arf}$ and HMGA2 within the context of the PI3K/AKT/mTOR/p70S6K pathway. Moreover, my results confirm that HMGA2 regulates the proliferation and aging of mesenchymal stem cells.

2.2 MATERIALS AND METHODS

2.2.1 Cell culture

hMSCs were isolated and cultured as previously described (Park et al., 2012). Briefly, hMSCs were obtained from umbilical cord blood immediately after the full-term delivery of newborns from 20- to 30-year-old mothers; each mother provided written informed consent for the procedure. The blood samples were processed within 24 hr of collection. The UCB samples were mixed with HetaSep solution (Stem Cell Technology, Vancouver, Canada) at a ratio of 5:1 (v/v) and were then incubated at room temperature until the red blood cells were depleted. The supernatant was collected and centrifuged through a Ficoll density-gradient at 600 x g for 20 min. Mononuclear cells were harvested and seeded on culture dishes under normal culture conditions. The hMSCs were maintained in endothelial cell growth medium-2 (EGM-2, Lonza, Basel, Switzerland) containing 10% fetal bovine serum (FBS). The isolation and research protocols were approved by the Boramae Hospital Institutional Review Board (IRB). All of the procedures were approved by the IRB of Seoul National University (hMSC, #0603/001-002).

2.2.2 Transfection

To overexpress the HMGA2 protein, the coding sequence of full-length human HMGA2 was cloned into the pMX retroviral vector. Viral production and transduction

were performed as previously described (Yu et al., 2012). Briefly, the HMGA2 plasmid was transfected into 293T cells along with the VSV-G and gag/pol plasmids. The viral supernatants were collected at 48 and 72 hr post-transfection and used to infect human hMSCs in the presence of 5 μg/mL polybrene (Sigma-Aldrich, Sigma, Ronkonkoma, NY, USA).

2.2.3 Microarray

Total RNA was purified and amplified using the Ambion Illumina RNA amplification kit (Ambion, Austin, TX), according to the manufacturer's instructions, to yield biotinylated cRNA. Briefly, 550 ng of total RNA was reverse-transcribed to cDNA using a T7 oligo(dT) primer. Second-strand cDNA was synthesized, *in vitro* transcribed, and labeled with biotin-NTP. After purification, the cRNA was quantified using the ND-1000 Spectrophotometer (NanoDrop, Wilmington, NC), and 750 ng of labeled cRNA was hybridized to each humanHT-12 expression v.4 bead array for 16-18 hr at 58°C, as indicated by the manufacturer (Illumina, Inc., San Diego, CA). The array signal was detected using Amersham FluoroLink Cy3-streptavidin (GE Healthcare Bio-Sciences, Little Chalfont, UK) following the protocol described in the bead array manual. The arrays were scanned using an Illumina Bead Array Reader confocal scanner. The array data export processing and analysis was performed using Illumina Bead Studio v3.1.3 (Gene Expression Module v3.3.8).

2.2.4 Immunocytochemistry

The cells were fixed in 4% paraformaldehyde for 10 min at room temperature. The cells were then permeabilized by exposure to 0.5% Triton X-100 for 10 min at room temperature and then blocked for 2 hr with 10% normal goat serum (Zymed, San Francisco, CA) at room temperature. The primary antibodies were used at the manufacturer's recommended dilution in 5% normal goat serum. Rabbit anti-HMGA2 (ab41878, Abcam, Cambridge, MA) was used for the immunostaining. The secondary antibody, goat anti-rabbit Alexa Fluor 594 (Invitrogen, Carlsbad, CA), was used at a 1:1000 dilution. The nuclei were counterstained with 4',6-diamidino-2-phenylindole (DAPI; Sigma-Aldrich).

2.2.5 Reverse transcription polymerase chain reaction (RT-PCR) and real-time PCR

Total RNA was isolated from cells using the TRIzol reagent following the protocol provided by the manufacturer (Invitrogen) and used for cDNA synthesis using the Superscript III First-Strand Synthesis System (Invitrogen). For RT-PCR, the cDNA and primers were combined with a PCR premix (Bioneer, Sung Nam, Rep. of Korea) and analyzed by gel electrophoresis on 1.5% agarose gels with ethidium bromide staining, followed by fluorescence digitization using a Bio-Rad GelDoc XR system (Bio-Rad). Real-time PCR was performed by mixing cDNA with each primer and the SYBR Green PCR Master Mix (Applied Biosystems, Foster City, CA). According to the manufacturer's instructions, an ABI 7300 sequence detection system with supplied software (Applied Biosystems) was used to quantify gene expression. Each gene was

normalized with β-actin as a housekeeping control. At least three independent analyses were done for each gene. The primer sets used for this study are listed in Table 1.

2.2.6 Western blotting

Whole-cell protein lysates were extracted in a solution containing 1% Triton X-100, 20 mM Tris HCl (pH 8), 137 mM NaCl, 10% glycerol and 2 mM EDTA (Sigma-Aldrich). Nuclear and cytoplasmic lysates were extracted using NE-PER reagents (Thermo, Rockford, IL), and the protein concentrations were determined using a DC assay kit (Bio-Rad, Hercules, CA). The proteins were separated by 10% sodium dodecyl sulfate-polyacrylamide gel electrophoresis (SDS-PAGE), transferred to nitrocellulose membranes at 100 V and 350 mA for 2 hr, and probed with primary antibodies. The secondary antibodies were used according to the manufacturer's specifications, and binding was detected using an enhanced chemiluminescence (ECL) detection kit (Amersham, Piscataway, NJ) according to the manufacturer's instructions.

2.2.7 siRNA inhibition study

Transient transfection assays were performed using specific, commercially available siRNA targeting HMGA2 (Dharmacon, ON Target plus SMART pool, Cat# L-013495-00-0005, Lafayette, CO, USA) along with a non-targeting siRNA (Dharmacon, ON Target plus SMART pool, Cat# D-001810-01). The siRNA transfections were performed according to the manufacturer's instructions. Briefly, the cells were seeded at a concentration of 5 x 10^4/well, and siRNA-containing media (without added antibiotics)

were added when the cells reached 50-60% confluence. The cells were incubated with 50 nM siRNA for 48 hr. The cells were subcultured 48-72 hr following the siRNA transfection to evaluate mRNA expression and protein expression. After these incubations, RNA and protein extractions were performed for genetic and proteomic analyses.

2.2.8 Senescence-associated beta-galactosidase (SA-β-gal) staining

SA β-gal staining was performed as previously described (So et al., 2011). Briefly, the hMSCs were seeded in 6-well plates at a density of 1×10^5/well for late-stage cells and 5×10^4/well for early-stage cells. The cells were incubated for 3 days until they reached the appropriate confluence and were then washed twice with PBS and fixed with 0.5% glutaraldehyde in PBS (pH 7.2) for 5 min at room temperature. The cells were then washed with PBS containing 1 mM MgCl2 (pH 7.2) and stained with X-gal solution (1 mg/ml X-gal, 0.12 mM K3Fe[CN]6 (potassium ferricyanide), 0.12 mM K4Fe[CN]6 (potassium ferrocyanide) and 1 mM MgCl2 in PBS, pH 6.0) overnight at 37°C.

2.2.9 Flow cytometry

hMSCs were triturated into single cells and labeled with monoclonal mouse anti-human fluorochrome-conjugated antibodies (CD34-FITC, CD45-FITC, CD73-PE and CD105-FITC, all from BD Bioscience, San Jose, CA). The labeled cells were analyzed on a fluorescence-activated cell sorter, FACSAria (BD Biosciences), using FACSDiva software (BD Biosciences).

2.2.10 MTT assay

The proliferation potential was measured using the MTT assay, which is based on the ability of live cells to convert tetrazolium salt into purple formazan. Briefly, the cells (1×10^4 cells per well) were seeded in 24-well microplates in 450 μl of medium. After 48 hr, 50 μl of MTT stock solution (5 mg/ml, Sigma-Aldrich) was added to each well, and the plates were further incubated for 4 h at 37°C. The supernatant was removed, and 200 μl DMSO was added to each well to solubilize the purple formazan crystals. The absorbance at a wavelength of 540 nm was measured using an EL800 microplate reader (BIO-TEK Instruments, Winooski, VT).

2.2.11 *In vitro* differentiation assay

In vitro differentiation into the adipogenic and osteogenic lineages was performed as described previously (Yu et al., 2012). Briefly, hMSCs (1×10^5) were plated in six-well plates. After the cells had attained 70%-80% confluence, they were treated with an adipogenic induction medium (DMEM supplemented with 5% FBS, 1 μM dexamethasone, 10 μM insulin, 200 μM indomethacin and 0.5 mM isobutylmethylxanthine) or an osteogenic induction medium (DMEM supplemented with 10% FBS and 200 μM indomethacin, 1 μM dexamethasone, 0.5 mM isobutyl methylxanthine and 0.5 μg/mL insulin). DMEM supplemented with 10% FBS was used as a control. Media were changed twice weekly. After two weeks of induction, the cells were stained to confirm adipogenic or osteogenic differentiation. Intracellular lipid accumulation, an indicator of adipogenic differentiation, was visualized by Oil Red O

staining. Osteogenic differentiation was noted by positive staining with Alizarin Red stain, which is specific for calcium.

For chondrogenic differentiation, 5×10^5 cells were added to a 15-mL polypropylene tube and incubated with 1 mL of chondrocyte differentiation medium (Lonza, Wakersville, MD, USA) for three weeks. The round pellets were embedded in paraffin and cut into 3-μm sections. The sections were stained with toluidine blue.

2.2.12 Inhibitor studies

To assess the effect of PI3K/AKT signaling on HMGA2 overexpression, an inhibition study was conducted. HMGA2-overexpressing hMSCs were treated with 30 μM of LY294002 (Calbiochem, La Jolla, CA) for inhibition of the PI3K signaling pathway (Yu et al., 2012).

2.2.13 Statistical analyses

The data were analyzed using Student's t-test in Excel software. The results are expressed as the mean ± the standard error, and statistically significant data are indicated with asterisks (**$P < 0.01$).

Table 1. Names and sequences of the primers for RT-PCR and qRT-PCR assays

Gene name	Accession	Primer sequence	base numbers within the sequence
β-ACTIN	NM_001101.3	Forward : AGAGCTACGAGCTGCCTGAC	797-816
		Reverse : AGCACTGTGTTGGCGTACAG	980-961
HMGA2	NM_003483.4	Forward: CCTAAGAGACCCAGGGGAAG	944-963
		Reverse: TCCAGTGGCTTCTGCTTTCT	1027-1008
PPAR-γ	NM_138712.3	Forward: CCTCCGGGCCCTGGCAAAAC	877-896
		Reverse: CTCCTGCACAGCCTCCACGG	1132-1113
aP2	NM_001442.2	Forward: GGGTCACAGCACCCTCCTGA	1-20
		Reverse: GGTTTGGCCATGCCAGCCAC	187-168
C/EBP-β	NM_005194.2	Forward: GCGCGCTTACCTCGGCTACC	816-835
		Reverse: TGGCCTTGTCGCGGCTCTTG	1072-1053
Cyclin F	NM_01761.2	Forward: GTCCAGCCAGGAGGAGACCG	1867-1884
		Reverse: CCGCTGGGAGCTGTCACGTC	1989-1970
Cyclin E1	NM_001238.2	Forward: CCCCGCCACAGAGCGGTAAG	1367-1386
		Reverse: CATCGGGAGCACGCACTGGT	1664-1645
CDC25A	NM_001789.2	Forward: TCTCGTGGCTGCCTGCACTC	830-849
		Reverse: CTTGCCATGCACGAGGGGGT	960-941
EID2B	NM_152361.1	Forward: TTGTTCCGCGAGTATCTGGA	335-354
		Reverse: GCTACCGTAAACGCGACAG	498-480
CDKN2A IPNL	NM_080656.2	Forward: AGCAGTTCCGCTCCTACTCA	127-146
		Reverse: ATCCCATCGGCCATTTCCAT	340-321
C9orf80	NM_021218.1	Forward: AGCATATTGCAGCCCAACAG	362-381
		Reverse: TGCAGAGTCTTGAGTGATGA	444-425
C14orf153	NM_032374.3	Forward: TGCCATGATTGGATAGGACC	194-213
		Reverse: GGTTTGCCCAGAACTGTTGA	341-322
ZNF394	NM_032164.2	Forward: ACGGCTGTGTCTCTAACCTG	639-658
		Reverse: ACTCTGCTTTCCAAACTCGG	760-741
$p21^{CIP1/WAF1}$	NM_000389.4	Forward: ATTAGCAGCGGAACAAGGAGTCAGACAT	1776-1803
		Reverse: CTGTGAAAGACACAGAACAGTACAGGGT	2093-2066
$p19^{ARF}$	NM_058195.3	Forward: CCCTCGTGCTGATGCTACTG	291-310
		Reverse: ACCTGGTCTTCTAGGAAGCG	355-336
$p16^{INK4A}$	NM_000077.4	Forward: GAAGGTCCCTCAGACATCCCC	751-771
		Reverse: CCCTGTAGGACCTTCGGTGAC	844-824

Table 2. List of the up-and down-regulated genes in HMGA2 overexpressed cells compared to controls.

Number	Symbol	Accession	fold change (HMGA2/CTL)	fold change (siHMGA2/siCTL)
Up-regulated genes				
1	FKBP1A	NM_054014.1	2.56	
2	HMGA2	NM_003483.4	2.01	
3	RAB5C	NM_201434.1	1.83	
4	F3	NM_001993.2	1.75	
5	FKBP10	NM_021939.2	1.71	
6	FBXO3	NM_033406.2	1.68	
7	CCND2	NM_001759.2	1.68	
8	ECE2	NM_032331.3	1.68	
9	SLC25A10	NM_012140.3	1.66	
10	SLC7A5	NM_003486.5	1.65	
11	TGM2	NM_004613.2	1.64	
12	ANGPTL4	NM_139314.1	1.64	
13	TRIB3	NM_021158.3	1.64	
14	CTSZ	NM_001336.2	1.59	
15	GOLGA7B	NM_001010917.1	1.59	
16	PPP3R1	NM_000945.3	1.58	
17	PLAT	NM_000930.2	1.57	
18	NGF	NM_002506.2	1.49	
19	IGFBP1	NM_001013029.1	1.43	
20	HBEGF	NM_001945.1	1.30	
21	EGFR	NM_005228.3	1.19	
22	FGFRL1	NM_021923.3	1.12	
23	CCNE1	NM_059182.1	1.18	-1.14
24	CCNF	NM_001761.1	1.16	-1.14
25	CDC25A	NM_001789.2	1.03	-1.14
Down-regulated genes				
1	EID2B	NM_152631.1	-1.90	1.79
2	CDKN2AIPNL	NM_080656.1	-1.75	1.58
3	ZNF394	NM_032164.2	-1.70	1.53
4	C9orf80	NM_021218.1	-1.69	1.57
5	C14orf153	NM_032374.2	-1.66	1.57

2.3 RESULTS

2.3.1 Charaterization of hMSCs

To determine the multilineage differentiation potential of hMSCs, I induced the in vitro differentiation of the adipogenic, osteogenic and chondrogenic lineages. The condition medium-induced hMSCs were positive for Oil Red O, Alizarin Red S and Toluidine Blue staining (Figs. 1A, B, Fig. 5E). The hMSCs were positive for the hMSCs markers (CD73 and CD105) but negative for the hematopoietic cell and leukocyte markers (CD34 and CD45; Fig. 1C).

2.3.2 HMGA2 target identification using microarray analyses

To demonstrate the role of HMGA2 in regulating proliferation and senescence, early-stage (fewer than 8 passages) hMSCs were transduced with control GFP or HMGA2 virus. I observed that the transduction efficiency was higher than 80%, which was sufficient to overexpress the target gene (Fig. 2A). The elevation of the HMGA2 expression level in the HMGA2-overexpressing hMSCs was confirmed by immunocytochemical analyses (Fig. 2B). To investigate the role of HMGA2 in hMSCs, I compared the gene expression pattern in HMGA2-overexpressing and -non-overexpressing cells using microarray analyses. A GFP expression vector was used as the control. These results showed that HMGA2 overexpression produces distinct gene

expression patterns in early-stage hMSCs (Fig. 2C). The list of the detected genes and their fold changes between the HMGA2-overexpressing and -non-overexpressing cells are given in Table 2.

2.3.3 HMGA2 enhances hMSC proliferation and reduces β-gal activity

hMSCs showed gradually decreased expression of HMGA2 following consecutive passages (Fig. 2D). Late-stage (more than 16 passages) hMSCs were followed the induction of replicative senescence by repeated subculture. The late-stage hMSCs showed flattened or lengthened morphology, which is considered a phenotype of senescent cells. However, the overexpression of HMGA2 slightly reduced the senescent morphology in the late-stage hMSCs (Fig. 2E). I also compared the gene expression pattern in late-stage hMSCs using microarray analyses. A GFP expression vector was used as the control in the same manner. The results demonstrated that HMGA2 overexpression causes also distinct gene expression patterns even in late-stage hMSCs (Fig. 2F). Next, I assayed the proliferation by MTT and performed SA-β-gal staining to confirm the senescent state of the hMSCs. The late-stage hMSCs showed both elevated SA-β-gal activity and decreased proliferation (Fig. 2G, Fig. 4E). However, the overexpression of HMGA2 in these cells reduced the SA-β-gal activity and enhanced the proliferation rate (Figs. 2G, H).

2.3.4 HMGA2 activates PI3K/AKT and its sequential downstream effectors mTOR/p70S6K

To better characterize gene expression patterns, I used IPA software and identified several canonical signaling pathways and molecular/cellular functions that were related to HMGA2 overexpression (Figs. 3A, B). Both eIF4 and p70S6K signaling, which are associated with translational regulation, were highly ranked among the canonical signaling pathways activated (Fig. 3A). Moreover, eIF4- and p70S6K-related signaling, such as mTOR and PI3K/AKT signaling, were also highly ranked. Functional analysis showed that, overall, cellular growth- and death-associated functions were highly ranked (Fig. 3B). To determine the role of HMGA2 in regulating the PI3K/AKT signaling pathway, a western blot analysis was conducted in the presence or absence of the PI3K inhibitor LY294002 (Fig. 3C). The phosphorylation of AKT, mTOR and p70S6K were induced by HMGA2 and inhibited by the treatment with LY294002, whereas the expression of total proteins was unaffected. However, the expression levels of the cyclin-dependent kinase inhibitors $p16^{INK4A}$ and $p21^{CIP1/WAF1}$ were inhibited by HMGA2 overexpression. The treatment of LY294002 restores protein levels of $p16^{INK4A}$ and $p21^{CIP1/WAF1}$ to baseline level, suggesting that the PI3K/AKT/mTOR/p70S6K pathway is sufficient for reducing the $p16^{INK4A}$ and $p21^{CIP1/WAF1}$ expression. These results suggest that HMGA2 activation was associated with the activation of the PI3K/AKT/mTOR/p70S6K signaling pathway and the inhibition of $p16^{INK4A}$ and $p21^{CIP1/WAF1}$ expression.

2.3.5 HMGA2 inhibition down-regulates cell proliferation and adipogenic differentiation potential

To elucidate the precise role of HMGA2 in early-stage hMSCs, I conducted inhibition studies using siRNA. Further microarray analyses showed that the HMGA2-inhibited early-stage hMSCs, siHMGA2 transfected cells, have different gene expression patterns than the control siRNA-treated cells (Fig. 5A). Following the inhibition of HMGA2 by transfection of siRNA, I assayed proliferation by MTT and performed SA-β-gal staining to confirm the senescent state of the hMSCs. The siHMGA2 transfected hMSCs showed elevated SA-β-gal activity and a decrease in proliferation (Figs. 5B, C). I next performed western blot analysis to determine wether the PI3K/AKT/mTOR pathway was involved in HMGA2 expression. As shown in Figure 3D, phospho-AKT (Ser473), phospho-mTOR (Ser2448) and phospho-p70S6K (Thr421/Ser424) activities were dramatically decreased, whereas $p16^{INK4A}$ and $p21^{CIP1/WAF1}$ activities were increased in siHMGA2 transfected cells. To compare the adipogenic differentiation capacity of the control siRNA and siHMGA2 transfected cells, I induced the *in vitro* differentiation of both populations into the adipogenic lineage. After adipogenic induction, the HMGA2 down-regulated hMSCs showed a reduced adipogenic differentiation potential when compared to the control siRNA-treated hMSCs, as evidenced by Oil Red O staining (Fig. 5E). The gene expression levels of adipogenic transcription factors, including PPARγ, aP2 and C/EBP-β, were significantly decreased in the siHMGA2 transfected cells compared to the control siRNA transfected cells (Figs. 5F-H). Taken together, these data

suggest that the down-regulation of HMGA2 compromised cell proliferation and adipogenic differentiation via regulation of the PI3K/AKT/mTOR pathway.

2.3.6 HMGA2 regulates cell cycle-related genes and other genes

There were several genes that exhibited directly opposite patterns in the HMGA2-overexpressing and siHMGA2 hMSCs (Figs. 2C, 5A, Table 2). Among these genes, I selected eight genes that were highly related to the top-rated signaling pathways defined by the Ingenuity Pathway Analysis (IPA) software (Figs. 6A, B). Three of these genes, Cyclin F, Cyclin E1 and CDC25A, were up-regulated when HMGA2 was overexpressed and down-regulated when HMGA2 was inhibited. The other five genes, C14orf153, EID2B, ZNF394, CDKN2AIPNL and C9orf80, showed the opposite expression pattern. I performed RT-PCR to quantify the actual expression of the selected genes. I found that cell cycle-related genes, such as cyclin F, cyclin E1 and CDC25A, were up-regulated after HMGA2 overexpression. In contrast, EID2B, CDKN2A IPNL, C9orf80, C14orf153 and ZNF394 were down-regulated after HMGA2 overexpression. Cyclin-dependent kinase inhibitors, such as $p16^{INK4A}$, $p19^{ARF}$ and $p21^{CIP1/WAF1}$, were up-regulated in the late-stage cells compared to the early-stage cells. However, the overexpression of HMGA2 led to a significant reduction of $p16^{INK4A}$, $p19^{ARF}$ and $p21^{CIP1/WAF1}$ expression in both the early- and late-stage hMSCs (Fig. 6C, D).

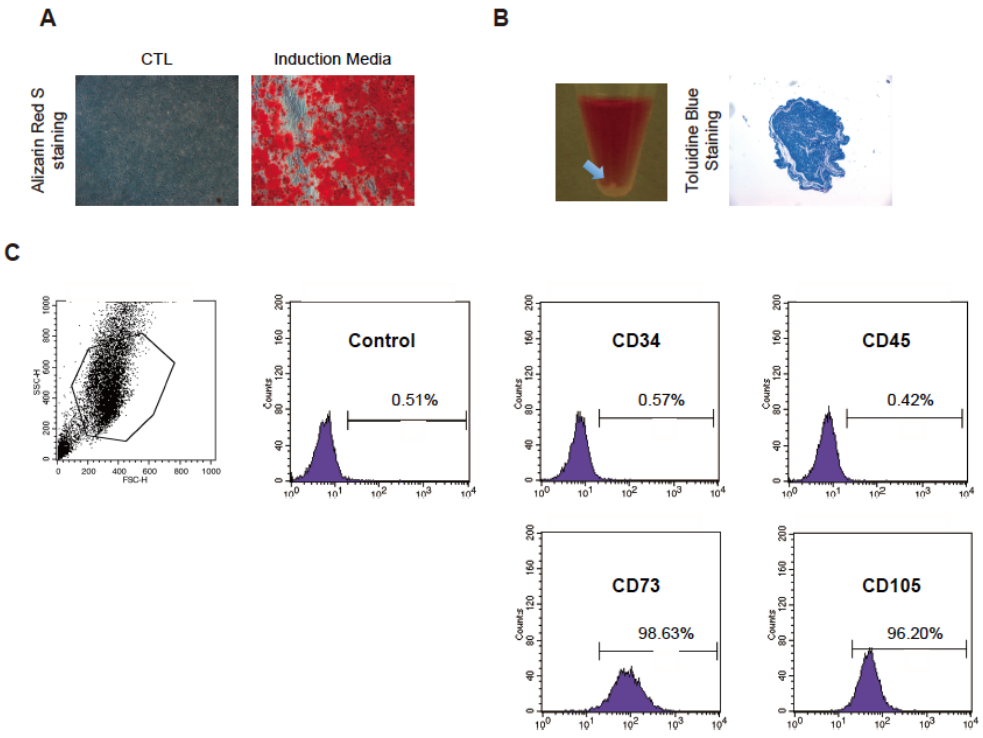

Figure 1. Differentiation capacity and immunophenotypic characterization of hMSCs

(A) hMSCs were cultured in osteogenic-induction media for two weeks. Osteogenesis was determined using Alizarin Red S staining. **(B)** A round-shaped chondrogenic pellet was formed in chondrogenic-induction media. The blue arrow indicates a pellet. Chondrogenesis was determined by Toluidine Blue staining. **(C)** Flow cytometry analysis was performed using monoclonal antibodies directed against the hMSCs-negative surface markers CD34 and CD45 and the hMSCs–positive surface markers CD73 and CD105.

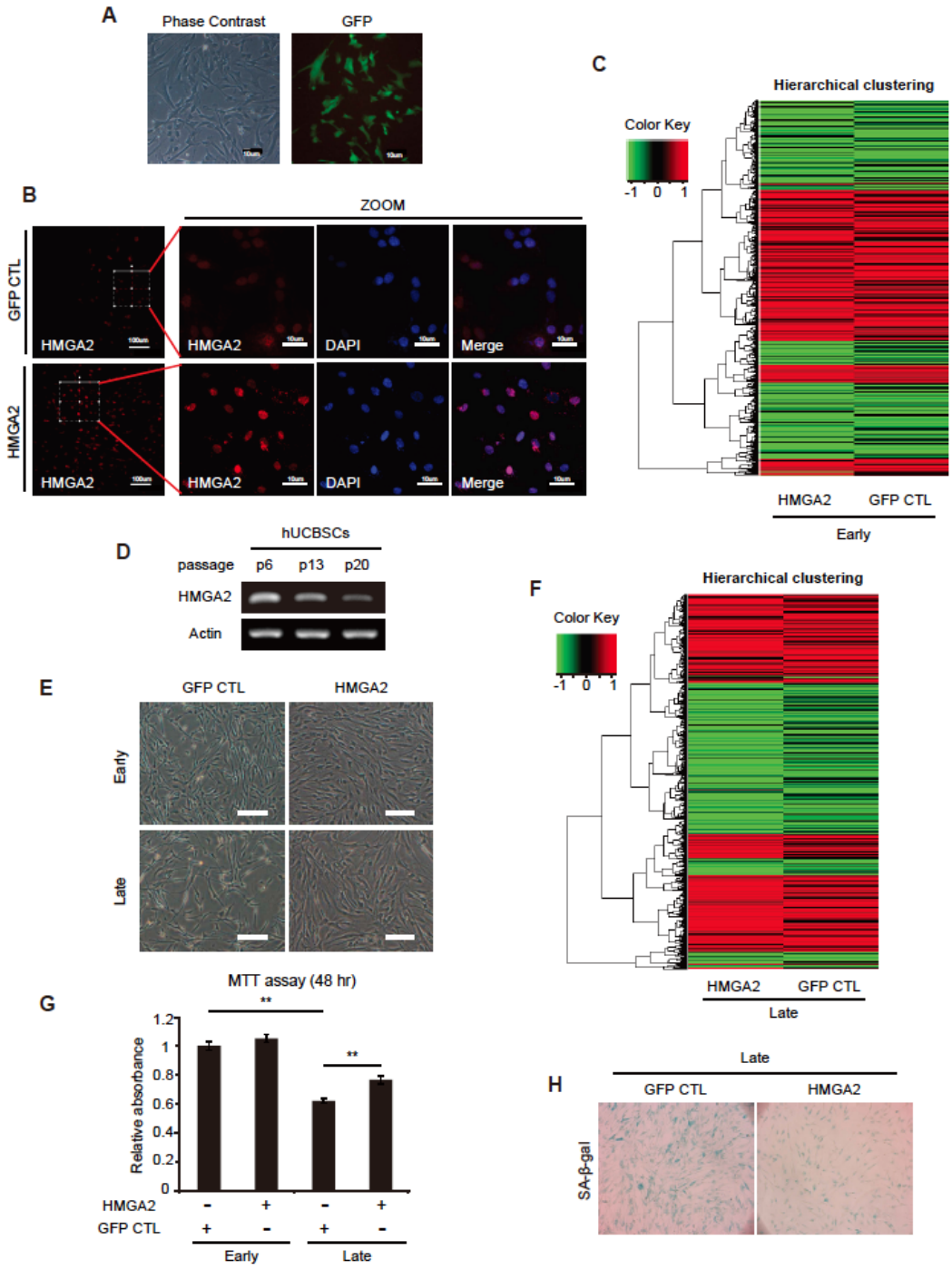
A
Phase Contrast
GFP
B
ZOOM
GFP CTL
HMGA2
HMGA2
HMGA2
DAPI
Merge
HMGA2
HMGA2
HMGA2
DAPI
Merge
C
Hierarchical clustering
Color Key
-1 0 1
HMGA2
GFP CTL
Early
D
hUCBSCs
passage p6 p13 p20
HMGA2
Actin
E
GFP CTL
HMGA2
Early
Late
F
Hierarchical clustering
Color Key
-1 0 1
HMGA2
GFP CTL
Late
G
MTT assay (48 hr)
**
**
Relative absorbance
1.2
1
0.8
0.6
0.4
0.2
0
HMGA2 - + - +
GFP CTL + - + -
Early
Late
H
Late
GFP CTL
HMGA2
SA-β-gal

Figure 2. HMGA2 overexpression enhances cell proliferation and reduces β-gal activity

(A) Viral transduction efficiency was determined using a GFP virus. Scale bar = 10 μm. **(B)** Immunocytochemical analyses of HMGA2 were performed using both the control virus- or HMGA2 virus-infected cells. Nuclei were stained using DAPI (blue). Scale bar = 100 μm or 10 μm. **(C)** Heat map of the mRNAs in early-stage hMSCs after transformation with the GFP control or HMGA2 overexpression viruses. **(D)** The expression level of HMGA2 was analyzed during repeated subculture-induced senescence of hMSCs, as shown by RT-PCR **(E)** Phase contrast images of the GFP control and HMGA2-overexpressing early- and late-stage hMSCs. Scale bar = 100 μm. **(F)** Heat map of the mRNAs in late-stage hMSCs after transformation with the GFP control or HMGA2 overexpression viruses. **(G)** The MTT cell proliferation assay was performed in the GFP control and HMGA2-overexpressing early- and late-stage hMSCs. (**$P < 0.01$) **(H)** β-gal staining was performed in the GFP control and HMGA2-overexpressing late-stage hMSCs to confirm their senescence.

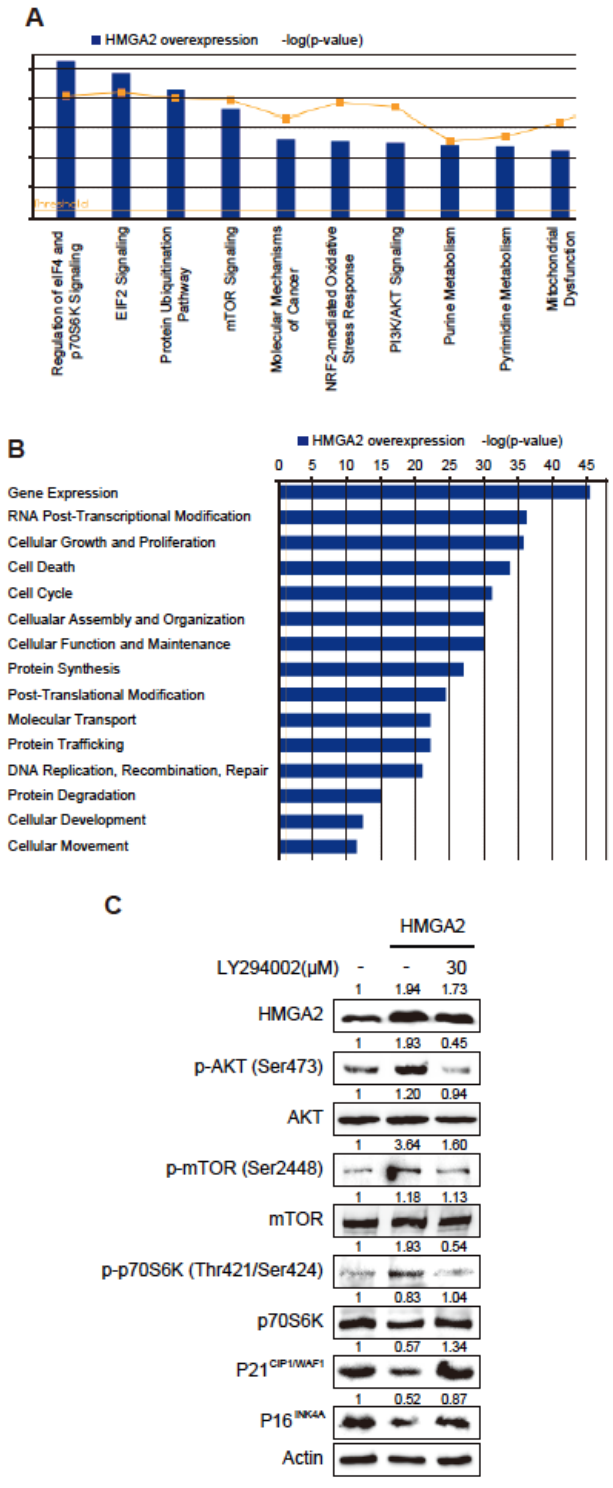
A
HMGA2 overexpression
-log(p-value)
Regulation of eIF4 and p70S6K Signaling
EIF2 Signaling
Protein Ubiquitination Pathway
mTOR Signaling
Molecular Mechanisms of Cancer
NRF2-mediated Oxidative Stress Response
PI3K/AKT Signaling
Purine Metabolism
Pyrimidine Metabolism
Mitochondrial Dysfunction
B
HMGA2 overexpression
-log(p-value)
0 5 10 15 20 25 30 35 40 45
Gene Expression
RNA Post-Transcriptional Modification
Cellular Growth and Proliferation
Cell Death
Cell Cycle
Cellualar Assembly and Organization
Cellular Function and Maintenance
Protein Synthesis
Post-Translational Modification
Molecular Transport
Protein Trafficking
DNA Replication, Recombination, Repair
Protein Degradation
Cellular Development
Cellular Movement
C
HMGA2
LY294002(μM) - - 30
1 1.94 1.73
HMGA2
1 1.93 0.45
p-AKT (Ser473)
1 1.20 0.94
AKT
1 3.64 1.60
p-mTOR (Ser2448)
1 1.18 1.13
mTOR
1 1.93 0.54
p-p70S6K (Thr421/Ser424)
1 0.83 1.04
p70S6K
1 0.57 1.34
P21CIP1/WAF1
1 0.52 0.87
P16INK4A
Actin

Figure 3. HMGA2 overexpression activates the PI3K/AKT and mTOR/p70S6K pathways

(A) Canonical signaling pathways activated in HMGA2-overexpressing hMSCs, as determined by IPA. **(B)** Molecular/cellular functions activated in HMGA2-overexpressing hMSCs by IPA. **(C)** A western blot analysis was conducted using the GFP control, HMGA2-overexpressing, HMGA2-overexpressing and LY294002-treated hMSCs. The phosphorylation of AKT and its downstream effectors mTOR, p70S6K, $p21^{CIP1/WAF1}$ and $p16^{INK4A}$ were analyzed.

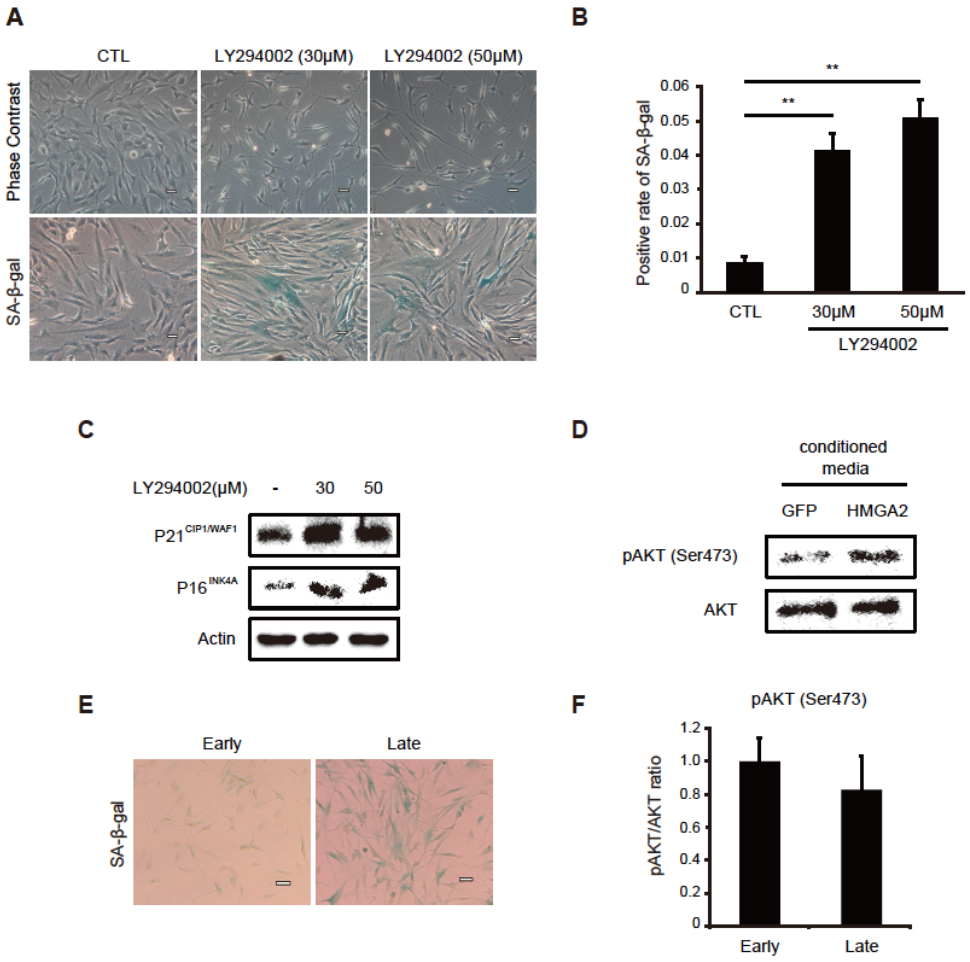

Figure 4. LY294002 induces β-gal activity and senescence-associated markers

(A) phase contrast images and β-gal activity were shown after 24hr LY294002 treatment in indicated concentrations. Scale bar = 100 μm **(B)** The graph represents the ratio of β-gal positive cells per total cells. (**P < 0.01) **(C)** $p21^{CIP1/WAF1}$ and $p16^{INK4A}$ protein expression levels were confirmed by western blot analysis in control and LY294002-treated hMSCs **(D)** The phosphorylation levels of AKT in the GFP- and HMGA2-

conditioned medium-treated cells were compared. Each conditioned medium was harvested after 5 days. The collected conditioned media were centrifuged to remove all cell debris and used to treat non-HMGA2 expressing cells. **(E)** Early- and late-stage hMSCs were subjected to β-gal staining to confirm their senescence. Scale bar = 100 μm **(F)** Densitometric analysis showed the pAKT/AKT ratio in the early- and late-stage hMSCs.

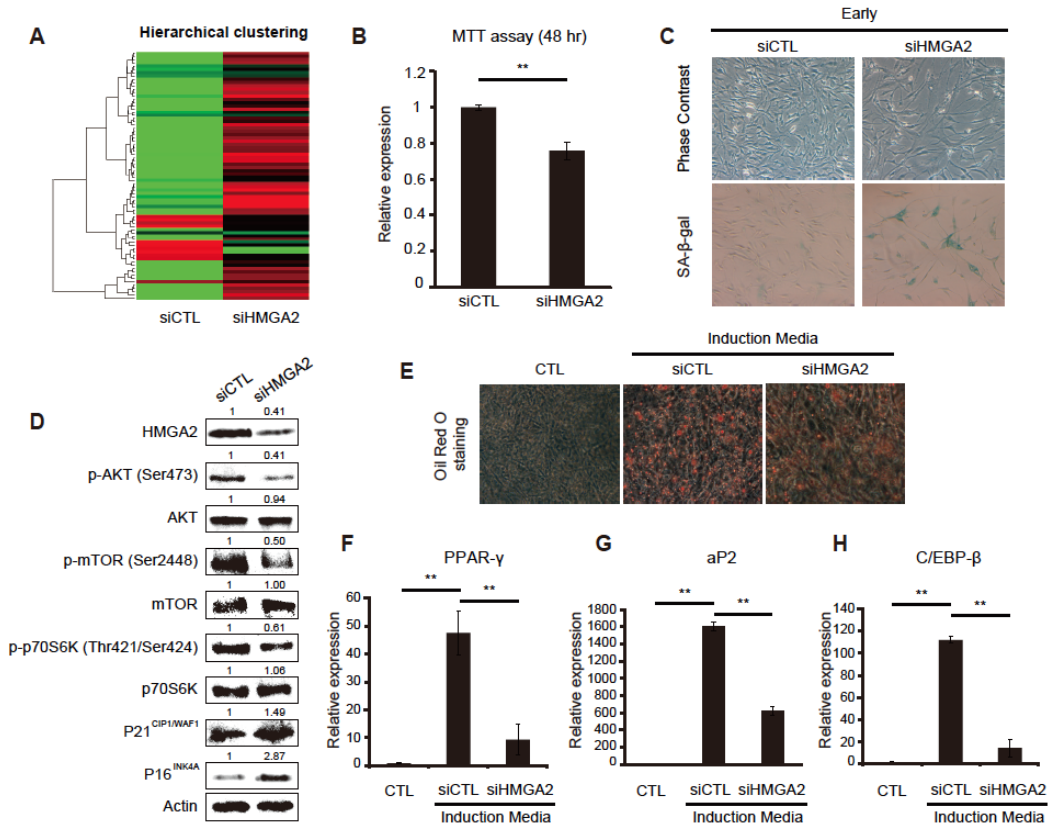

Figure 5. HMGA2 inhibition compromised cell proliferation and adipogenic differentiation.

(A) Heat map of the mRNAs in the control siRNA and siHMGA2-transfected hMSCs. **(B)** The MTT cell proliferation assay was performed in the siHMGA2-treated cells and the control siRNA-treated cells. (**$P < 0.01$) **(C)** β-gal staining was performed in the siHMGA2-treated cells and the control siRNA-treated cells to confirm their senescence. **(D)** A western blot analysis was conducted using the siHMGA2-treated cells and the control siRNA-treated cells. The phosphorylation of AKT and its downstream effectors

mTOR, p70S6K, $p21^{CIP1/WAF1}$ and $p16^{INK4A}$ were analyzed. **(E-H)** The siHMGA2-treated cells and the control siRNA-treated cells were cultured in adipogenic induction media. The lipid droplet accumulation in differentiated cells was visualized using Oil Red O staining after two weeks of adipogenic induction (E) The efficiency of adipogenic differentiation was evaluated by the expression of adipogenic marker genes including PPAR-γ, aP2 and CEBP-β (F-H). Each gene was normalized with β-actin as a housekeeping control. (**$P < 0.01$)

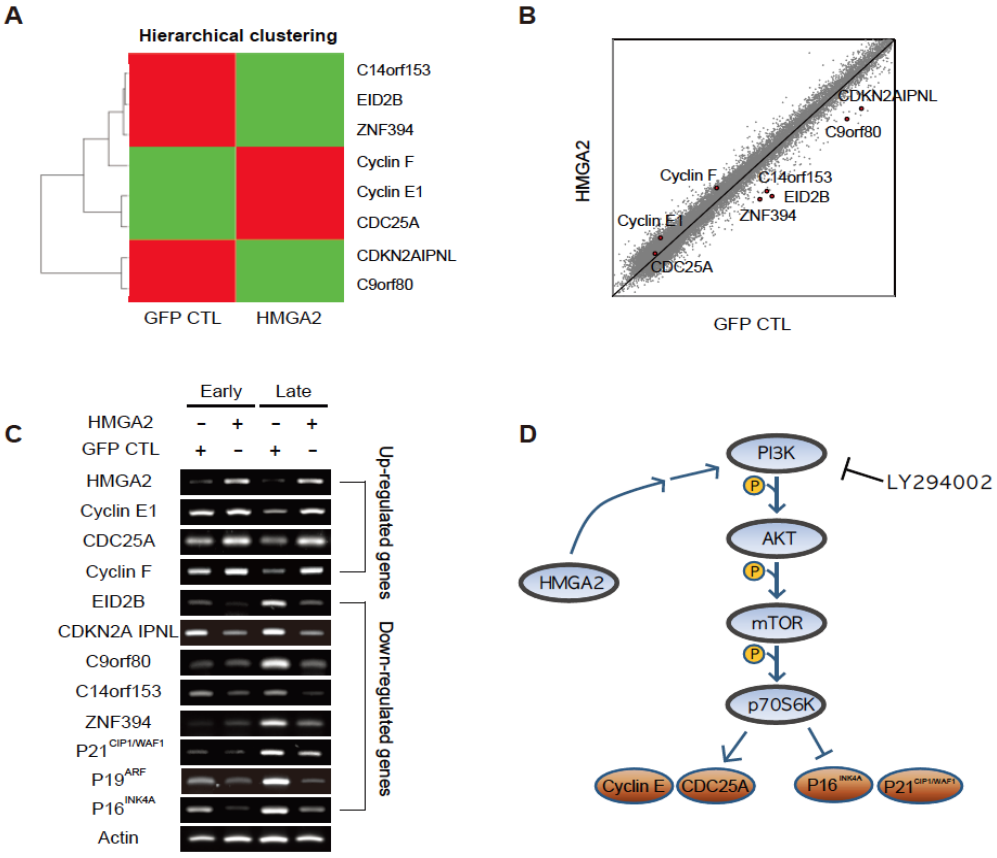

Figure 6. HMGA2 overexpression enhances the expression of Cyclin F, Cyclin E1 and CDC25A and reduces the cell cycle regulatory genes p16, p19 and p21 in hMSCs

(A) Heat map of the genes that are differentially expressed between siHMGA2- and HMGA2-overexpressing hMSCs. **(B)** Scatter plot of the genes that are differentially expressed between siHMGA2- and HMGA2-overexpressing hMSCs. **(C)** The expression of genes that were found to be up- or down-regulated in the microarray analyses were

evaluated in the GFP control and HMGA2-overexpressing early- and late-stage hMSCs. **(D)** Schematic representation of the HMGA2-induced signaling pathway.

2.4 DISCUSSION

The DNA-binding protein HMGA2 is abundantly expressed in embryonic stem cells and during embryogenesis (Chiappetta et al., 1996; Li et al., 2006). Furthermore, HMGA2 was highly expressed in fetal and young adult stem cells, such as hematopoietic stem cells or neural stem cells, and its expression was decreased upon aging. However, the role of HMGA2 in adult stem cells has not been fully elucidated. To investigate the role of HMGA2, I up-regulated and down-regulated HMGA2 expression in hMSCs and analyzed the subsequent gene expression pattern by microarray assays. Because HMGA2 proteins act as both activators and repressors of gene expression by altering chromatin structure, the expression of many genes was altered by HMGA2 expression. Among the biological functions revealed by IPA analysis, HMGA2 significantly affected factors involved in gene expression, RNA post-transcriptional modification and cellular growth and proliferation. I confirmed that cell growth-related genes, such as Cyclin F, Cyclin E1 and CDC25A, were up-regulated in the HMGA2-overexpressing cells. Conversely, certain genes of unknown function, such as CDKN2AIPNL, C9orf80, C14orf153, EID2B and ZNF394, were down-regulated.

It has been reported that HMGA2 represses the transcription of *CDKN2A*, $p16^{INK4A}$ and $p19^{ARF}$ in fetal and adult neural stem cells (Nishino et al., 2008). HMGA2 contributes to adult stem cell self-renewal by repressing the expression of $p16^{INK4A}$ and $p19^{ARF}$, but the expression of HMGA2 declines with age. In agreement with this model, I confirmed that HMGA2 overexpression down-regulated cyclin-dependent kinase inhibitors, such as $p16^{INK4A}$ and $p19^{ARF}$. Furthermore, I demonstrated that HMGA2 inhibited another cyclin-dependent kinase inhibitor, $p21^{CIP1/WAF1}$, in hMSCs. In my previous study, I demonstrated the down-regulation of HMGA2 and the up-regulation of $p16^{INK4A}$ in both replicative and HDAC inhibitor-mediated senescence in hMSCs (Lee et al., 2011). In the present study, I showed that the overexpression of HMGA2 increased proliferation and decreased the SA-β-gal activity in replicative senescent hMSCs (Figure 2). Furthermore, I found that knockdown of HMGA2 in early-stage hMSCs compromised cell proliferation and adipogenic differentiation and led to enhanced SA-β-gal activity and $p16^{INK4A}$ and $p21^{CIP1/WAF1}$ expression. My results indicated that preventing the decline in HMGA2 expression during the aging process may increase hUCB-MSC self-renewal, in part, by repressing cyclin-dependent kinase inhibitors.

To understand the molecular mechanisms by which HMGA2 inhibits $p16^{INK4A}$, $p19^{ARF}$ and $p21^{CIP1/WAF1}$, it is essential to identify the signaling pathways that are directly regulated by HMGA2. To this end, I analyzed the gene expression patterns in hUCB-MSC cell lines expressing GFP (control), exogenous HMGA2 or siRNA against HMGA2. Microarray data sets were analyzed using IPA software. Among the signaling pathways

related to HMGA2 overexpression, I confirmed that PI3K/AKT signaling is the major target signaling pathway that is activated by HMGA2 activation (Figure 3A). A previous report also suggested that *Hmga2* constitutively activates AKT in bone marrow cells from Δ*Hmga2* mice, in which the 3' untranslated region of *Hmga2* was removed (Ikeda et al., 2011). In Δ*Hmga2* mice, HMGA2-mediated PI3K/AKT activation may play an important role in controlling the proliferative hematopoiesis. However, the molecular mechanism of HMGA2-mediated PI3K/AKT activation has yet to be elucidated. In normal cells, HMGA2 is mainly confined to the nucleus (Fusco and Fedele, 2007; Grosschedl et al., 1994), and therefore, HMGA2 exerts its effects by regulating the expression of transcription factors (Mantovani et al., 1998) and growth factors that are related to the PI3K/AKT signaling pathway. Indeed, I found that IGFBP1 (insulin-like growth factor-binding protein), NGF (nerve growth factor), EGFR (epidermal growth factor receptor), HBEGF (heparin-binding EGF-like growth factor), ANGPTL4 (angiopoietin-related protein 4) and FGFRL1 (fibroblast growth factor receptor-like 1) were up-regulated after HMGA2 overexpression in hMSCs (Table 2). Indeed, I showed the concentrated cell culture supernatants of HMGA2-overexpressing hMSCs induced the phosphorylation of AKT by secreted factors in a paracrine manner (Fig. 4D). Therefore, it is certainly important for future study to determine which factors regulate HMGA2-mediated PI3K/AKT activation.

I demonstrated that the PI3K/AKT signaling pathway plays important roles in regulating hUCB-MSC self-renewal and maintaining the pluripotency of hESCs (Yu et al.,

2012). Furthermore, mTOR/p70S6K, a major downstream effector of PI3K/AKT signaling, was found to be phosphorylated, suggesting that HMGA2 effectively activates the PI3K/AKT/mTOR/p70S6K signaling pathway (Figure 3C). It has been reported that the up-regulation of the mTOR/p70S6K pathway leads to increases in cyclin E and CDC25A activities (Chou et al., 2003) and decreases the expression of $p16^{INK4A}$ (Gao et al., 2004) and $p21^{CIP1/WAF1}$ (Gao et al., 2003). To exclude the possibility that the effect of HMGA2 on the PI3K/AKT pathway is indirect, I determined that PI3K/AKT phosphorylation was not changed followed by consecutive passages (Fig. 4F).

I then performed experiments with the PI3K inhibitor, LY294002 to confirm the control of the PI3K/AKT pathway by HMGA2. Targets for LY294002 would be known downstream targets for PI3K/AKT, which would include mTOR/p70S6K, in the potential control of the expression of cyclin E, CDC25A, $p16^{INK4A}$ and $p21^{CIP1/WAF1}$. I found that LY294002 treatment was sufficient to reduce the PI3K/AKT/mTOR/p70S6K pathway and further increased the number of SA-β-gal positive cells and the expression of $p16^{INK4A}$ and $p21^{CIP1/WAF1}$ (Figs. 4A-C). However, HMGA2 expression was not attenuated by LY294002 treatment. These results suggest that HMGA2 regulates the PI3K/AKT/mTOR/p70S6K pathway. Furthermore, HMGA2-mediated down-regulation of $p16^{INK4A}$ and $p21^{CIP1/WAF1}$ expression was reversed by LY294002 treatment, indicating that the HMGA2-PI3K/AKT/mTOR/p70S6K pathway regulates gene expression rather than HMGA2 having a direct influence on transcription.

Together, my data suggest the existence of a novel signaling pathway that is induced by HMGA2 overexpression. Given the previously reported interaction between histone modification and miRNAs related to HMGA2 expression (Lee et al., 2011), future studies should further evaluate the roles of epigenetic regulatory mechanisms in HMGA2-regulated signaling pathways. However, the data in this study clearly demonstrate an important *in vitro* aging and proliferation regulatory role for HMGA2 in inducing PI3K/AKT/mTOR/p70S6K signaling, resulting in the inhibition of $p16^{INK4A}$ and $p21^{CIP1/WAF1}$ expression in hMSCs.

CHAPTER III

Histone deacetylase regulates ZMPSTE24 and induces prelamin A accumulation through miR-141 in human adult stem cell senescence

3.1 INTRODUCTION

Adult stem cells in mammalian organs play pivotal roles in the maintenance and repair of these organs throughout the adult life of the organism. Similar to normal somatic cells, adult stem cells experience a lifelong exposure to stressors, which leads to an age-associated decline in their number and function. Given that the senescence-induced loss of adult stem cell stemness results in the impairment of tissue homeostasis, regeneration and repair (Janzen et al., 2006; Kasper et al., 2009; Rao and Mattson, 2001; Silva and Conboy, 2008), it is important to understand the mechanisms that underlie the regulation of adult stem cell stemness and senescence. In previous studies, I have demonstrated that epigenetic elements are fundamentally involved in the regulation of the adult stem cell senescence mechanism (Jung et al., 2010; Lee et al., 2011; So et al., 2011). The dynamic balance between epigenetic elements, such as chromatin structure, DNA methylation, and microRNAs, is considered a crucial mechanism for the maintenance of stemness and the regulation of cellular senescence because these elements control chromatin modification and translational regulation (Bibikova et al., 2008; Narita, 2007). Furthermore, histone tails with different modifications, including acetylation, methylation or phosphorylation, dictate gene expression by inducing the repressive (heterochromatin) or permissive (euchromatin) configuration of chromatin (Shukla et al., 2008).

The nuclear lamina, a filamentous meshwork that provides the regulation between the inner nuclear membrane and chromosomes, is composed of the A- and B-types of lamins (Aebi et al., 1986). Two major A-type lamins, lamin A and C, are derived from the *LMNA* gene by alternative splicing. Lamins A and C are both located at the nuclear envelope and are also present in the nucleoplasm where they play basic roles in DNA replication, transcriptional regulation and structural support (Hutchison and Worman, 2004; Shumaker et al., 2003). ZMPSTE24 is indispensably required for the production of mature lamin A, since it performs both first cleavage step that releases –AAX and final endoproteolytic step (Corrigan et al., 2005). A deficiency in ZMPSTE24 expression can lead to restrictive dermopathy (RD), with features of severe progeroid syndrome, resulting in early neonatal death (Navarro et al., 2004). Cells lacking ZMPSTE24 show an accumulation of farnesylated, methylated prelamin A at the nuclear lamina, leading to a premature senescence that is characterized by nuclear blebbing, heterochromatin disorganization and defects in DNA replication, transcription and repair (Candelario et al., 2011; Liu et al., 2005; Liu et al., 2006b). Furthermore, mice deficient in Zmpste24 exhibited a hyperactivation of the tumor suppressor, p53 (Varela et al., 2005). Although interest in prelamin A accumulation and ZMPSTE24 deficiency has increased, several fundamental issues related to the regulation of the expression and activity levels have not yet been addressed. Some reports have demonstrated that ZMPSTE24 expression levels are down-regulated in aged or senescent human vascular smooth muscle cells and fibroblast cells (Ragnauth et al., 2010; Ukekawa et al., 2007),

yet the signaling pathway that modulates the ZMPSTE24 expression levels has not been identified (Maraldi et al., 2011).

MicroRNAs (miRNAs) are small RNAs of ~22 nucleotides in length that can perform important regulatory roles through the repression of target mRNA translation by complementary binding to the 3' untranslated region (UTR) (Bartel, 2004). Through this regulatory mechanism, miRNAs are considered to play important roles in cellular functions, including proliferation, migration, differentiation and apoptosis (He and Hannon, 2004). Although a limited percentage of the functions of miRNAs have been reported, a target prediction program estimated that miRNAs target more than 5300 human genes, representing approximately 30% of all transcripts (Lewis et al., 2005).

In the current study, I assessed the impact of down-regulation of ZMPSTE24 on the proliferation defects and DNA damage responses observed in hMSCs as they progress toward replicative senescence or an inhibition of the HDAC activity. Furthermore, my results indicate that ZMPSTE24 expression can be directly regulated by specific miRNA during hMSC senescence. I anticipate that these results might provide clues to understanding the biological relevance of ZMPSTE24 in hMSCs senescence and the aging process of adult stem cell.

3.2 **MATERIALS AND METHODS**

3.2.1 Western blot analysis

Western blot analyses of lamin A, prelamin A, ZMPSTE24, HDAC1, HDAC2, DNMT1, DNMT3B, $p16^{Ink4A}$, γ-H2AX and β-actin were performed as previously described (Jung et al., 2005). The hMSCs were lysed with 50 mM Tris-HCl buffer containing 0.1% Triton X-100 and freshly supplemented with a protease/phosphatase inhibitor cocktail. The proteins were then separated using 7.5-15% SDS-PAGE and transferred to nitrocellulose membranes at 350 mA for 5 h. The primary antibodies used to detect each proteins were as follows: lamin A (monoclonal, Abcam, 1:2500); prelamin A (polyclonal, Santa Cruz, 1:500); ZMPSTE24 (polyclonal, Abcam, 1:500); HDAC1 (monoclonal, Upstate, 1:2000); HDAC2 (monoclonal, Upstate, 1:2000); DNMT1 (polyclonal, BD, 1:1000); DNMT3A (polyclonal, Millipore, 1:1000); DNMT3B (polyclonal, Abcam, 1:1000); $p16^{Ink4A}$ (polyclonal, Abcam, 1:1000); γ-H2AX (polyclonal, Abcam, 1:1000) and β-actin (monoclonal**,** Cell-signaling, 1:5000). All of the antibodies were used according to the manufacturer's instructions, and the protein bands were detected using an enhanced chemiluminescence detection kit (Amersham Pharmacia Biotech, UK).

3.2.2 Viral packaging and cell infection

Cells expressing GFP-wt-lamin A and GFP-progerin were obtained from

Addgene (Plasmid 17662, 17663) (Cambridge, MA), and the miR-141 lentiviral vector was purchased from Genecopoeia (HmiR0181) (Rockville, MD). Six micrograms of vectors using the VSVG-based package system or the Mission lentiviral packaging mix (Sigma, Ronkonkoma, NY, USA) were added to tubes containing the Fugene 6 transfection reagent (Roche, Basel, Switzerland). The plasmids were transfected into 293FT cells; after 48 and 72 hr, the viral supernatants were filtered through a 0.45 μm cellulose acetate filter and concentrated by centrifugation at 20,000 rpm for 90 min. The viral supernatants were then used to infect the human MSCs in the presence of polybrene at 5 μg/ml (Sigma).

3.2.3 Real-time quantitative PCR

Real-time qPCR analyses were performed using SYBR® Green (Applied Biosystems, USA) according to the manufacturer's protocol. For the miRNA real-time qPCR, the universal primers supplied by the NCode VILO miRNA cDNA Synthesis Kit (Invitrogen, USA) and miRNA specific primers were used. RPL13A was used as an internal control. All of the amplicons were analyzed using the Prism 7000 sequence detection system 2.1 software (Applied Biosystems, USA). The primer set sequences used for this study are supplied in Table 1.

3.2.4 siRNA, mature miRNA and anti-miRNA transfection studies

Transient transfection assays were performed using specific, commercially available siRNAs for the inhibition of ZMPSTE24 (L-006104-00-0005), along with a

non-targeting siRNA (D-001810-10) (ON Target plus SMART pool, Dharmacon, USA). The inhibition or overexpression of the miRNAs was achieved by commercial antisense miRNAs or mature miRNAs for hsa-miR-141 with an appropriate miRNA precursor-negative control (mature miRNA #PM 10860 and anti-miRNA inhibitor #AM 10860, Ambion, USA, and miRNA precursor-negative control #1, Ambion, USA). The siRNA, mature miRNA and anti-miRNA transfections were performed using the Dharmafect transfection reagent (Dharmacon) according to the manufacturer's instructions. Briefly, the cells were seeded at a concentration of $2x10^4$ cells/well, and the siRNA, miRNA and anti-miRNA-containing media (without the addition of antibiotics) were added when the cells reached 50-60% confluence. The cells were incubated with 50 nM siRNA, 50 nM anti-miRNA or 50 nM mature miRNA for 48 hr. To investigate the long-term effects of inhibition, the cells were subcultured 48-72 hr following the siRNA, anti-miRNA or mature miRNA transfection. Subcultured cells were stabilized for 24 h and incubated with siRNA, anti-miRNA or mature miRNA for 48-72 h at the same concentration. After inhibition, RNA extraction and the subsequent real-time qPCR or SA β-gal staining were performed for genetic or characteristic analyses, respectively.

3.2.5 Immunocytochemistry

Cultured cells were fixed in 4% paraformaldehyde and permeabilized with 0.2% Triton X-100 (Sigma Aldrich, USA). The cells were then incubated with 10% normal goat serum (Zymed Laboratories Inc., USA) and stained with antibodies against lamin A (monoclonal, Abcam, 1:300), prelaimin A (polyclonal, Santa Cruz, 1:200), ZMPSTE 24

(polyclonal, Abcam, 1:200), $p16^{Ink4A}$ (polyclonal, Abcam, 1:200), γ-H2AX (polyclonal, Abcam, 1:200), followed by an incubation for 1 h with an Alexa 488 or Alexa 594-labeled secondary antibody (1:1000; Molecular Probes, USA). The nuclei were stained with Hoechst 33258 (1 μg/ml; 10 min), and the images were captured using a confocal microscope (Eclipse TE200, Nikon, Japan).

3.2.6 Chromatin immunoprecipitation (ChIP) assays

The ChIP assays were performed according to the manufacturer's protocol (ChIP assay kit, Upstate Biotechnology, USA). To prepare for the ChIP testing, the hMSCs (1 - $2x10^7$ cells per IP) were fixed with 1% formaldehyde for 10 min; the solution was then neutralized by the addition of 1/20 volume of 2.5 M glycine for 5 min. The cells were washed with ice-cold PBS and scraped with SDS lysis buffer (1% SDS, 10 mM EDTA, and 50 mM Tris, pH 8.1) containing protease inhibitors. The lysates were sonicated to shear the DNA to lengths between 200 and 1000 base pairs, and the samples were centrifuged for 10 min at 15,000 x g at 4°C to remove the insoluble material. The supernatant was diluted 10-fold in the ChIP dilution buffer (0.01% SDS, 1.1% Triton X-100, 1.2 mM EDTA, 16.7 mM Tris-HCL [pH 8.1], and 167 mM NaCl), and the chromatin was immunoprecipitated using antibodies, according to the manufacturer's instructions. Real-time qPCR was performed at a final template dilution of 1:50. The primer sequences used in the ChIP assays in this study are supplied in Table 1.

3.2.7 Measurement of the proliferative potential and cell cycle distribution

The effects of replicative senescence, progerin, ZMPSTE24 inhibition and miR-141 inhibition on the hMSC proliferation were measured using the 3-(4,5-dimethylthiazol-2-yl)-2,5-diphenyltetrazolium bromide (MTT, Sigma-Aldrich, USA) assay, as described previously (Jung et al., 2005). Briefly, cells were plated on 24-well plates at a density of $2x10^4$/ml. After 24 hr, the cells were infected with virus or transfected with siRNA or miRNA. Following the incubation, 50 μl of MTT stock solution (5 mg/ml) was added, and the plates were incubated for another 4 h at 37°C. The formazan crystals were solubilized with DMSO, and the absorbance was measured using an EL800 microplate reader (BIO-TEK Instruments, USA).

Flow cytometry cell cycle analyses using propidium iodide staining was also performed as previously described. Briefly, hMSCs in the exponential growth phase were transfected with siRNA or miRNA and then harvested by trypsinization. The cells were washed with ice-cold PBS and then fixed with 70% ethanol at -20°C and stained with 50 μg／ml of propidium iodide in the presence of 100 μg／ml RNase A for 30 min. The cell cycle distribution was analyzed using the FACS Calibur system (Becton Dickinson, Franklin Lakes, NJ, USA).

3.2.8 Luciferase assays

For miRNA target validation, the entire 3'UTR sequence of human ZMPSTE24 was amplified by PCR and cloned into a T-vector (Promega, Madison, WI, USA, #A1360). The 3'UTR was subcloned into pmirGLO Dual-Luciferase vector (Promega,

#E1330) using the restriction enzymes, *Xho*I and *Sal*I. The 293FT cells were seeded 24 hr prior to transfection in 24-well plates at 50% confluence. The control constructs and ZMPSTE24 3'UTR reporter constructs were co-transfected along with 50 nM of the miRNAs (Ambion) using Dharmafect, following the manufacturer's instruction. After 24 hr of transfection, the firefly and *Renilla* luciferase activities were measured using a luminometer with Dual-Glo Luciferase Assay System (Promega, E2920). The firefly luminescence was normalized to the *Renilla* luminescence.

3.2.9 Statistical analysis

All of the experiments were conducted at least in triplicate (n = 3), and the results are expressed as the mean ± SD. Statistical analyses were conducted via an analysis of variance (ANOVA), followed by Duncan's multiple range tests or Student's t-test. A value of $P < 0.05$ was considered significant. (*$P < 0.05$; **$P < 0.01$).

Table 1. Names and sequences of the primers for RT-PCR and qRT-PCR assays		
Gene name	Primer sequence	
β-ACTIN	Forward:	AGAGCTACGAGCTGCCTGAC
	Reverse:	AGCACTGTGTTGGCGTACAG
RPL13A	Forward:	CATCGTGGCTAAACAGGTACTG
	Reverse:	GCACGACCTTGAGGGCAGCC
LMNA-1	Forward:	CAGAACACCTGGGGCTGCGG
	Reverse:	CTGCAGTGGGAGCCGTGGTG
LMNA-2	Forward:	ACCACGTGAGTGGTAGCCGC
	Reverse:	AGATTTTTGGCACGGGGAGGCTG
LMNA-3	Forward:	CCACTGGGGAAGGCTCCCACT
	Reverse:	GTTCGGGGGCTGGAGTTGCC
p16Ink4A	Forward:	GAAGGTCCCTCAGACATCCC
	Reverse:	CCCTGTAGGACCTTCGGTGA
hsa-miR-141		TAACACTGTCTGGTAAAGATGG
Names and sequences of the primers for ChIP assays		
miR-141 primer-1	Forward:	CCTGGGTCCATCTTCCAGTA
	Reverse:	AGGGGTGAAGGTCAGAGGTT
miR-141 primer-2	Forward:	ACAAGGGGTGGTTCTTGTTG
	Reverse:	GTCGACTGTGGGTTCTGGAT

3.3 **RESULTS**

3.3.1 Senescent hMSCs show prelamin A accumulation and a progeria-like abnormal nucleus

To confirm whether prelamin A accumulation is related to the normal aging of hMSCs, I compared the phenotypes of replicative senescence and progerin-induced senescence in hMSCs. Following the induction of replicative senescence by repeated subculture or the overexpression of progerin, I performed senescence-associated-β-galactosidase (SA-β-gal) staining and assayed proliferation by MTT to confirm the senescent state of the hMSCs. Both the replication-induced senescent cells and progerin-expressing hMSCs showed SA-β-gal activity and a decrease in proliferation (Figs. 1A and B). An increase of $p16^{INK4A}$, a senescence marker, expression was confirmed in both the replicative and progerin-induced senescent cells. To determine whether prelamin A accumulation is involved in the normal aging of hMSCs, I investigated the expression levels of prelaimin A in the senescent cells and found the levels to be significantly increased during the replicative senescent state (Fig. 1C). Consequently, I observed the phenotypes of the replicative senescent cells, which expressed high levels of prelamin A, and found that the cells exhibited severely wrinkled nuclei, which was remarkably similar to the nuclei of progerin-induced senescent cells (Fig. 1D). The expression level of γH2AX, a marker of double-stranded DNA damage and a feature of progerin-induced senescent cells, was also increased in the replicative senescent cells (Fig. 1E).

3.3.2 ZMPSTE24 inhibition induces cellular senescence with DNA damage accumulation

I found that the *LMNA* gene expression and lamin A protein expression were not significantly altered at later passages (Figs. 2A and B). Next, I investigated whether the expression level of ZMPSTE24, which converts prelamin A into mature lamin A, was altered during cellular senescence, and I confirmed that the expression levels of ZMPSTE24 were decreased during cellular senescence, as shown by western blot and immunocytochemistry (Fig. 1F and Fig. 2C). To test whether the disruption of ZMPSTE24 induces cellular senescence in the hMSCs, I inhibited the expression of ZMPSTE24 by siRNA. As expected, the inhibition of ZMPSTE24 expression induced the accumulation of prelamin A, which was followed by an increase of $p16^{INK4A}$ and γH2AX levels (Fig. 1G). As evidence of cellular senescence following the inhibition of ZMPSTE24, I confirmed an increase in the SA-β-gal activity (Fig. 1H) and decreases in the proliferation rate and population doubling (Fig. 1I and Fig. 2D). The hMSCs exhibiting an inhibition of ZMPSTE24 also showed features of prelamin A-accumulated senescent cells, with an increase in wrinkled nuclei and γH2AX-positive cells (Fig. 1J).

3.3.3 HDAC regulates ZMPSTE24 expression during replicative cellular senescence

The activities of DNMT and HDAC, factors that regulate the epigenetic state of genomic DNA and control transcriptional activity, were decreased during the hMSC cellular senescence in both the present and previous studies (Jung et al., 2010; So et al., 2011) (Figs. 3A and D). To confirm whether these factors are involved in the regulation of

ZMPSTE24 expression, I evaluated the effects of the DNMT inhibitor, 5-azacytidine and the HDAC inhibitors, valproic acid (VPA) and sodium butyrate (NB). The inhibition of both DNMT and HDAC induced cellular senescence in the hMSCs, as demonstrated by the SA-β-gal activity and an increase in $p16^{INK4A}$, markers of cellular senescence (Figs. 3B-C and 3E-F). However, only the HDAC inhibition induced a decrease in the expression of ZMPSTE24, followed by an increase of prelamin A (Fig. 3F). An abnormal nuclear morphology, a feature of prelamin A-accumulated senescent cells, was also increased by the application of the HDAC inhibitors (Figs. 3G and H). The inhibition of HDAC1 and HDAC2 decreased the expression levels of ZMPSTE24, followed by the accumulation of prelamin A (Fig. 3I), and the specific inhibition of HDAC1 and HDAC2 also increased $p16^{INK4A}$ expression and induced the activity of SA-β-gal (Figs. 3I and J). According to the results of the MTT assay (Fig. 2E) and the cumulative population doubling level (CPDL) (Fig. 3K), the proliferation rates were decreased following the specific inhibition of HDAC1 and HDAC2. In addition, the number of abnormal nuclei was increased, thus demonstrating the feature of progerin-induced senescent cells (Fig. 3L). Taken together, HDAC inhibition decreased ZMPSTE24 expression levels, which resulted in the accumulation of prelamin A and the induction of cellular senescence in the hMSCs.

3.3.4 miRNA-141 regulates ZMPSTE24 expression

To test whether miRNAs are involved in the mechanism of ZMPSTE24 regulation by HDAC, I investigated the miRNAs that putatively target ZMPSTE24 using a combination of predictive algorithms, including miRanda, TargetScan and PicTar

(Figure 4A); the ZMPSTE24 mRNA-targeting miRNAs predicted by at least two different database programs (miR-124, miR-141 and miR-182) were then selected for luciferase assays. Among the predicted miRNAs, miR-141 significantly reduced the firefly luciferase activity of the reporter containing the ZMPSTE24-3'UTR, as determined by *Renilla*, the control luciferase activity, suggesting that miR-141 could directly bind to the 3'UTR of the ZMPSTE24 RNA (Figs. 4B and C, Fig. 5A). In the miR-141- transfected hMSCs, the ZMPSTE24 expression was down-regulated, and the expression of prelamin A was consequently increased in comparison to the transfections with the control miRNA or miR-106b, which was predicted to not target ZMPSTE24 (Fig. 4D). The correlation between the expression of ZMPSTE24 and miR-141 was confirmed in five other hMSC cell lines (Fig. 5B), and the cells treated with miR-141 showed changes in their nuclear morphology, with many of the cells displaying folds in the nuclear envelope (Fig. 4E). To determine whether these observations could be extended to hMSCs derived from different sources, I analyzed the effects of miR-141 on the nuclear morphology of hMSCs derived from bone marrow and adipose tissue (Fig. 5C). The overexpression of miR-141 also induced increases in the SA-β-gal activity and the appearance of nuclear γH2Ax foci (Figs. 4F and G), which were also observed in the control miRNA- or miR-106b-treated cells but with weak intensity.

To demonstrate the effect of the long-term overexpression of miR-141, I infected the hMSCs with an miR-141 virus generated from a precursor miR-141 expression clone. The virally infected hMSCs showed strong GFP expression, with significantly elevated levels of miR-141, as confirmed by real-time qPCR (Figs. 6A and

B). Using the MTT assay and a cell cycle analysis, I also confirmed that proliferation was inhibited after 5 days of miR-141 over-expression (Figs. 6C and D). To examine the role of miR-141 *in vivo*, I delivered the miR-141 virus into mice via intraperitoneal (i.p.) injection. After 7 days of i.p. injection, tissues were obtained, and immunohistochemistry and western blot analyses were performed. I found that the expression of ZMPSTE24 was reduced and GFP-positive cells were observed in liver tissues (Figs. 6E-G, Fig. 7A). These results indicate that ZMPSTE24 is the direct target of miR-141 both *in vitro* and *in vivo*.

Based on these results, I evaluated whether miR-141 inhibition could up-regulate ZMPSTE24 expression. As expected, the level of ZMPSTE24 was elevated following the transfection of miR-141 inhibitors and was decreased by the transfection of miR-141 mimics. In contrast, the expression levels of prelamin A, $p16^{INK4A}$ and γH2AX were increased after the transfection of the miR-141 mimics and were decreased following the transfection of miR-141 inhibitors (Fig. 8A), which increased the expression of ZMPSTE24 in the hMSCs and also in human and mouse dermal fibroblast cells (Fig. 8B). In the miR-141- and siZMPSTE24-transfected cells, MTT assays and cell cycle analyses revealed that the growth rate was reduced by 48 hr post-transfection (Figs. 8C and D). In contrast, the transfection of hMSCs with anti-miR-141 yielded an increase in the proliferation potential. Furthermore, the transfection of anti-miR-141 rescued the HDAC inhibitor-induced inhibition of ZMPSTE24 (Fig. 8E). The up-regulation of ZMPSTE24 expression further prevented the HDAC inhibitor-induced SA-β-gal activity and changes in the hMSC nuclear morphology, with many cells displaying folds in the

nuclear envelope (Figs. 8F-H). Collectively, these results confirm the hypothesis that miR-141 modulates cellular senescence through the regulation of ZMPSTE24, which correlates with the alteration in the phenotype observed in the siZMPSTE24-treated cells.

3.3.5 Replicative and HDAC inhibitor-mediated senescent cells showed increased miR-141 expression with an active histone mark at the miR-141 promoter

To investigate miR-141 expression during replicative senescence, I performed real-time qPCR using samples from consecutive passages and, surprisingly, found that the miR-141 expression levels were strikingly elevated following consecutive passages (Fig. 9A). To elucidate the epigenetic changes responsible for the elevation of the miR-141 expression levels during replicative senescence, I examined the changes in the histone acetylation and methylation of the promoter region of miR-141 using a chromatin immunoprecipitation (ChIP) assay. In late-passage cells, the acetylation of histone H4 and the trimethylation of histone H3 at the lysine 4 residue (H3K4), modifications that are involved in activating gene transcription through the enhancement of transcription factor binding to the nucleosomal DNA, were up-regulated in the putative coding region of miR-141 (Fig. 9B). However, histone H3 trimethylation at lysines 9 (H3K9) and 27 (H3K27), both of which are described as characteristic of the formation of relatively inactive regions of nucleosomal DNA and gene silencing, were decreased. It is believed that miRNA biogenesis is elaborately controlled by RNA polymerase II, which catalyzes the transcription of genomic DNA to produce the majority of miRNAs (Lee et al., 2004). Therefore, I performed a ChIP assay to verify the enrichment of RNA polymerase II at

the miRNA coding region. In replicatively senescent cells, the ChIP assay, which followed the real-time qPCR analysis, showed an up-regulation of RNA polymerase II binding to the putative coding region of miR-141 (Fig. 9C). However, the expression of miR-106b, which was shown to not target ZMPSTE24 (see Fig. 4), was not altered after consecutive passages or VPA/NB treatment (Fig. 10). To determine whether the HDAC activity could regulate the transcription of ZMPSTE24-targeting miRNA, I investigated the expression of miR-141 during DNMT and HDAC inhibition-mediated senescence. The miR-141 expression level was not changed in the 5-AzaC treated cells (Fig. 9D). However, the miR-141 expression levels in the VPA- and NB-treated cells were approximately 25-fold and 5-fold higher, respectively, than the levels in the non-treated cells after 6 days of treatment (Figs. 9E and F). Moreover, the inhibition of HDAC1 and HDAC2 in the hMSCs induced the up-regulation of miR-141 (Fig. 8G). I further examined the histone modifications on the miR-141 coding region using a ChIP assay. The modification of histones in the HDAC inhibitor-treated groups displayed a similar pattern to those in the replicatively senescent cells. In the VPA- and NB-treated groups, the acetylation of histones H3 and H4 and H3K4Me3 were both up-regulated, whereas H3K9Me3 and H3K27Me3 were down-regulated or remained relatively unchanged in the putative coding region of miR-141 (Fig. 9H). In the HDAC inhibitor-induced senescent groups, RNA polymerase II was increased in the proximity of the miR-141 coding region, suggesting that miR-141 is actively transcribed (Fig. 9I). Taken together, these results suggest that miR-141 transcription is activated by the histone modification pattern and RNA polymerase II activity at the site of the miR-141 promoter during replicative and

HDAC inhibitor-mediated senescence.

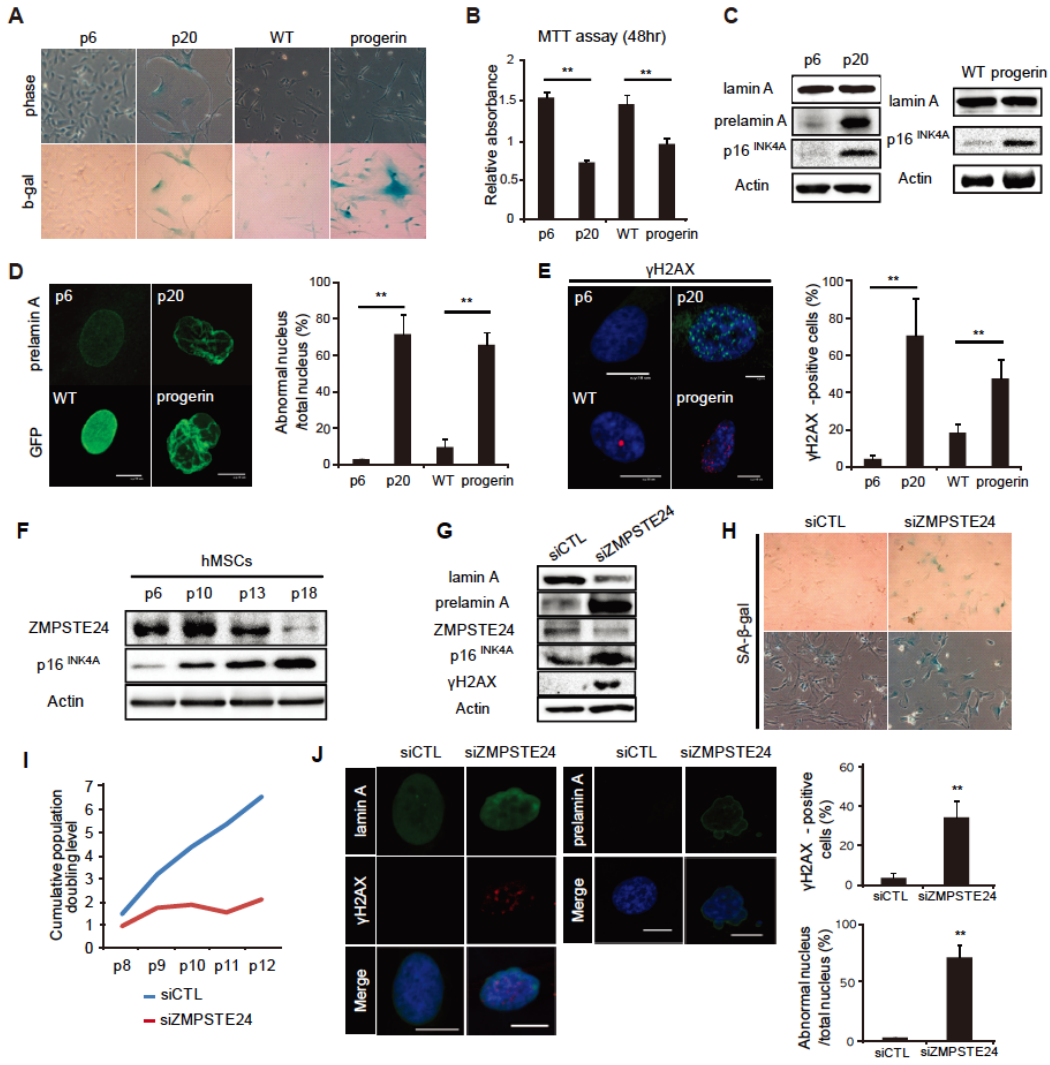

Figure 1. Senescent hMSCs show a down-regulation of ZMPSTE24 and an accumulation of prelamin A.

(A) SA β-gal staining was performed in the indicated group to confirm the state of senescence. **(B)** The proliferation rate of the hMSCs in the indicated group was measured using the MTT assay. (**$P < 0.01$) **(C)** Western blot analysis of prelamin A and $p16^{INK4A}$ was performed on early- and late-passaged cells. After transfection of progerin-GFP, the protein expression levels of lamin A and $p16^{INK4A}$ was confirmed as shown by western blot assay. **(D)** Prelamin A accumulation and the nuclear phenotype in the early- and late-passaged cells are shown by immunocytochemistry. After transfection of the lamin A-GFP and progerin-GFP vector, the GFP expression was detected by confocal microscopy. The graph represents the ratio of abnormal nuclei per total nuclei. (**$P < 0.01$) **(E)** γH2AX expression was shown by immunocytochemistry. The graph represents the ratio of cells that contained more than three γH2AX foci per nucleus. (**$P < 0.01$) **(F)** ZMPSTE24 and $p16^{INK4A}$ expression was confirmed in serially passaged cells by western blot analysis. **(G)** After the inhibition of ZMPSTE24 by siRNA, the protein expression levels of lamin A, prelamin A, ZMPSTE24, $p16^{INK4A}$ and γH2AX were confirmed by western blot analysis. **(H)** SA β-gal staining was performed, and the ZMPSTE24-inhibited cells showed β-galactosidase activity. **(I)** To confirm the effect of ZMPSTE24 inhibition on the cellular growth rate, I studied the cumulative population-doubling rate. **(J)** After the inhibition of ZMPSTE24 by siRNA, γH2AX expression was shown by immunocytochemistry. The graph represents the ratio of cells that contained more than three γH2AX foci per nucleus. (**$P < 0.01$).

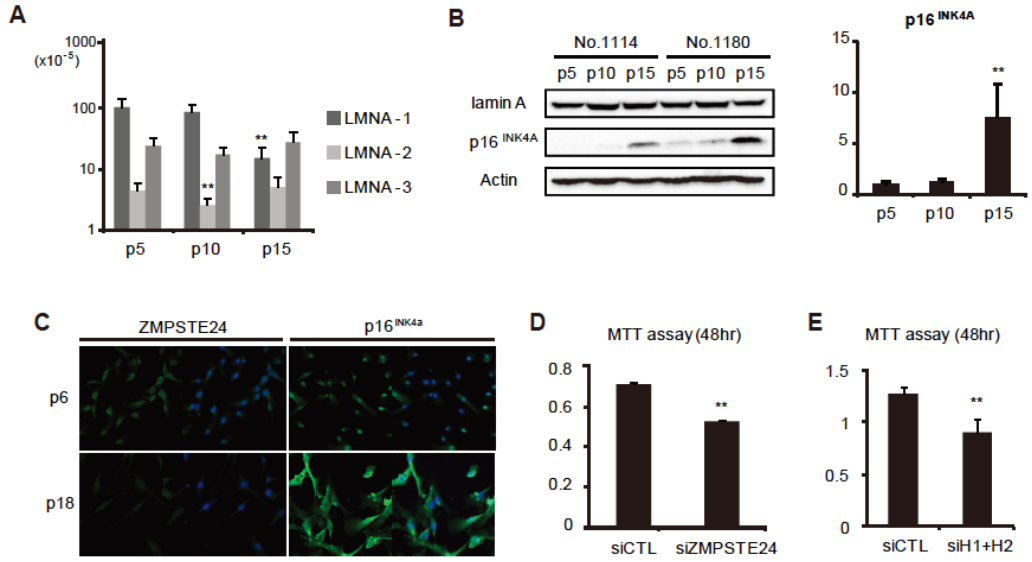

Figure 2. Lamin A expression is not altered in early/late-passaged cells.

(A) The *LMNA* mRNA expression levels of serially passaged cells was confirmed by real-time qPCR analysis. (**$P < 0.01$) **(B)** Western blot analysis and real-time PCR was performed to determine the lamin A and $p16^{INK4A}$ protein expression levels in serially passaged cells **(C)** ZMPSTE24 and $p16^{INK4A}$ expression were confirmed in early/late-passaged cells by immunocytochemistry. **(D)** MTT assay was performed to confirm the effects of ZMPSTE24 inhibition on the cellular growth rate. (**$P < 0.01$) **(E)** MTT assay was performed to confirm the effect of HDAC1 and HDAC2 inhibition on the cellular growth rate. (**$P < 0.01$)

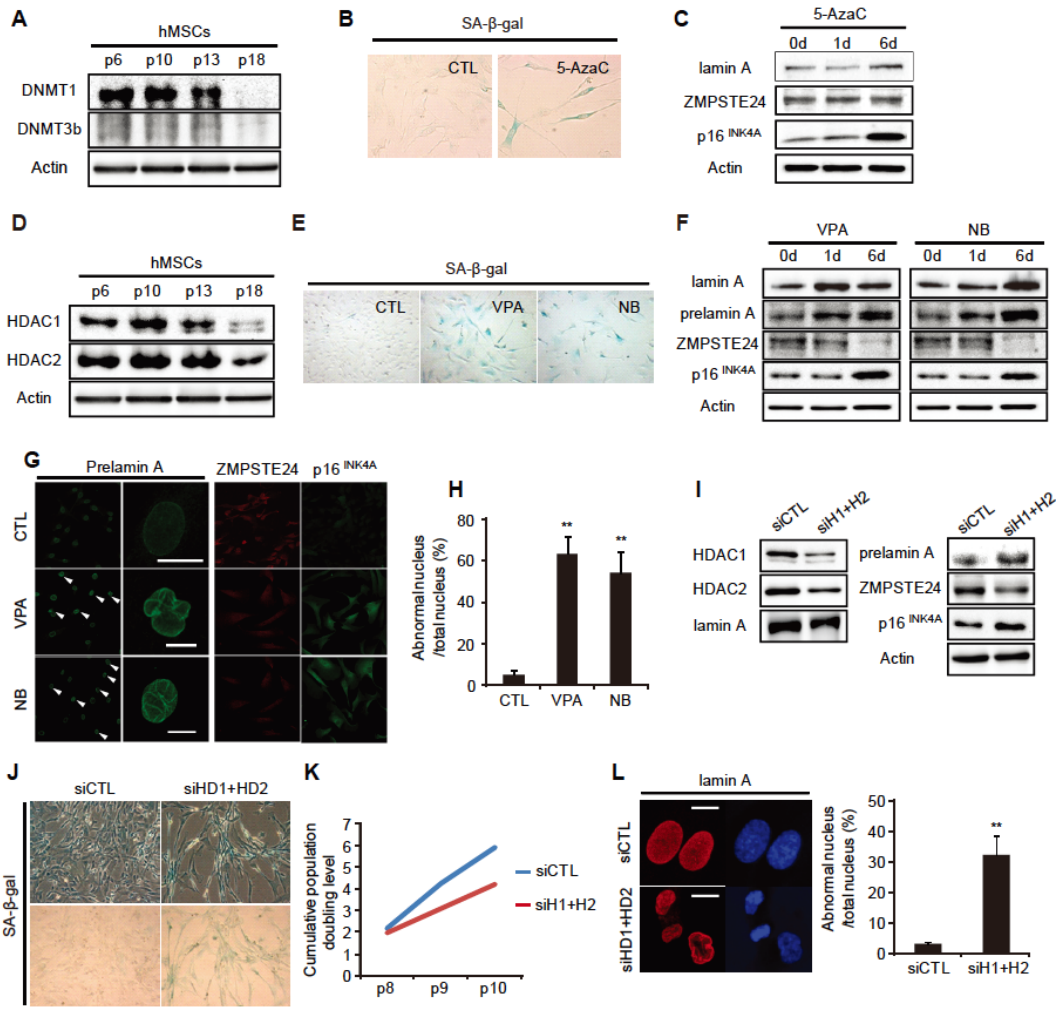

Figure 3. HDAC inhibition induces cellular senescence through a decrease in ZMPSTE24 expression and an accumulation of prelamin A.

(A) The expression levels of DNMTs were investigated during the cellular senescence of the hMSCs by western blot analysis. **(B, C)** After the inhibition of DNMT by 5-Azacytidine (5-AzaC), SA-β-gal staining (B) and western blot analysis (C) were

performed. **(D)** The changes in HDAC1 and HDAC2 expression levels during replicative cellular senescence were confirmed by western blot analysis. **(E)** After treatment with the HDAC inhibitors, valproic acid (VPA) and sodium butyrate (NB), for 6 days, SA β-gal staining was performed. **(F, G)** After treatment with VPA and NB for the indicated times, the expression levels of lamin A, prelamin A, ZMPSTE24 and $p16^{INK4A}$ were confirmed by western blot analysis (F) and immunocytochemistry (G). **(H)** The graph represents the ratio of abnormal nuclei per total nuclei. (**$P < 0.01$) **(I)** After the inhibition of HDAC1 and HDAC2 by siRNA, the protein expression levels of HDAC1, HDAC2, lamin A, prelamin A, ZMPSTE24 and $p16^{INK4A}$ were confirmed by western blot analysis. **(J)** After the inhibition of HDAC1 and HDAC2, cellular senescence was investigated by SA β-gal staining. **(K)** To confirm the effect of HDAC1 and HDAC2 inhibition on the cellular growth rate, I studied the cumulative population-doubling rate. **(L)** After the inhibition of HDAC1 and HDAC2, the nuclear phenotype was evaluated by immunocytochemistry. The graph represents the ratio of abnormal nuclei per total nuclei. (**$P < 0.01$).

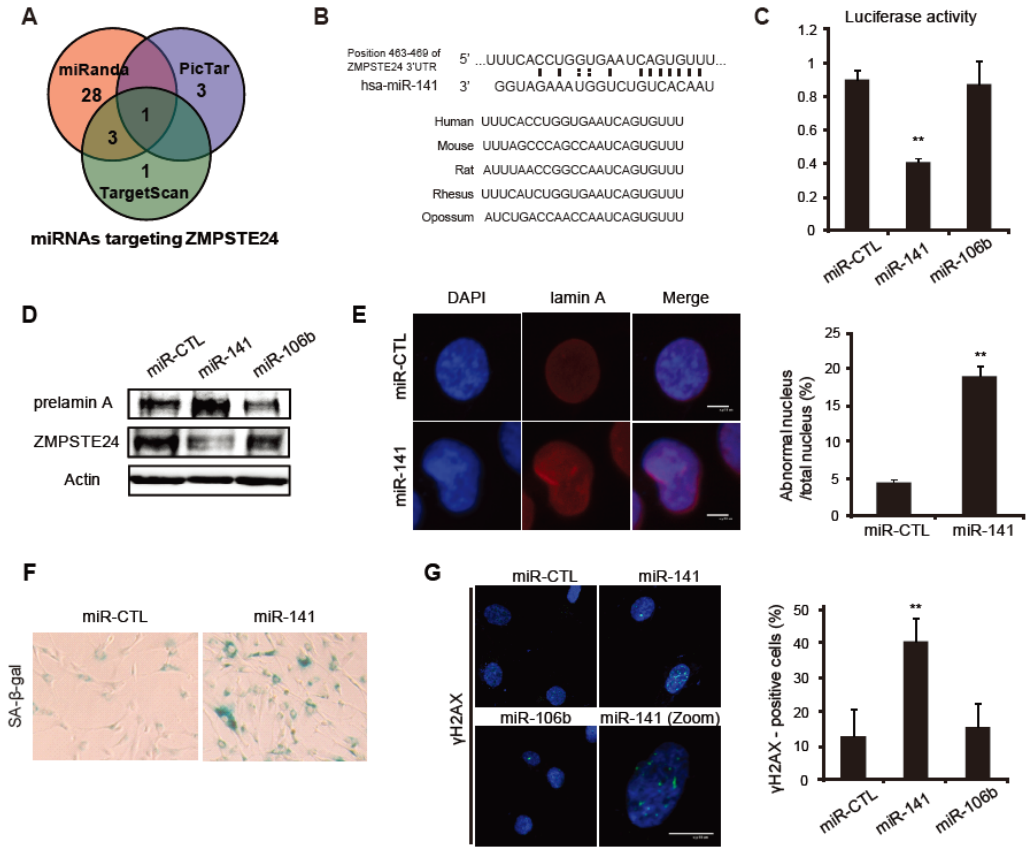

Figure 4. miRNA-141 regulates ZMPSTE24 expression directly.

(A) ZMPSTE24-targeting miRNAs were identified using a combination of the prediction algorithms at miRNA databases. **(B)** Schematic diagram of the miR-141 target site at the human ZMPSTE24 3'UTR and the 3'UTRs of representative mammals. **(C)** A reporter vector containing the ZMPSTE24 3'UTR was transfected into 293FT cells, along with miR-CTL, miR-141 or miR-106b. The luciferase activities were measured 48 hr after transfection and normalized to the *Renilla* luciferase activity. (**$P < 0.01$) **(D)** The prelamin A and ZMPSTE24 protein expression levels were confirmed by western blot

analysis in hMSCs. Three experiments were performed independently, and the representative data are shown. **(E)** hMSCs were transfected with miR-CTL or miR-141 and immunostained with lamin A antibody and DAPI (nuclei). The graph represents the ratio of cells that show an abnormal nucleus per total nuclear-stained cells. (**$P < 0.01$) **(F)** Representative images of SA β-gal activity from miR-CTL- and miR-141-transfected cells. **(G)** After transfection with miR-CTL, miR-141 or miR-106b, the γH2AX expression was determined by immunocytochemistry. The graph represents the ratio of cells that have more than three γH2AX foci per nucleus. (**$P < 0.01$)

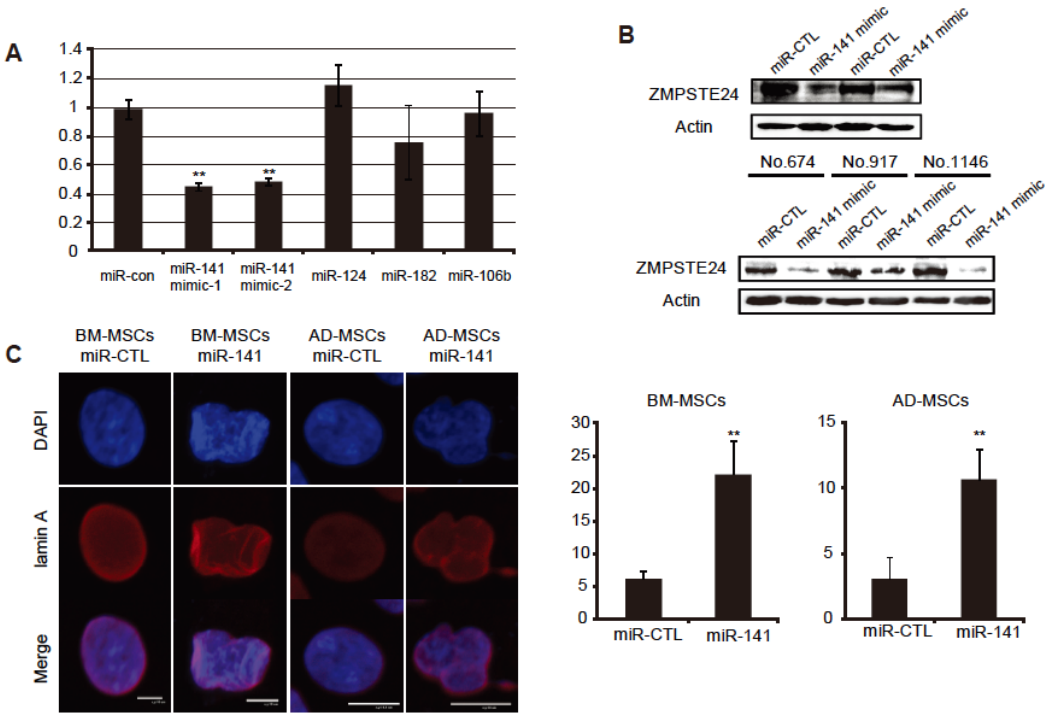

Figure 5. ZMPSTE24-target miRNA prediction and validation.

(A) A reporter vector containing the ZMPSTE24 3'UTR was transfected, along with miR-CTL, miR-141, miR-124, miR-182, miR-200a or miR-106b, into 293FT cells. The luciferase activities were measured after 48 hr of transfection and normalized to the *Renilla* luciferase activity. (**$P < 0.01$) **(B)** ZMPSTE24 protein expression levels were confirmed by western blot analysis in five different hUCB-MSC cell lines. **(C)** hBM-MSC and hAD-MSCs were transfected with miR-CTL or miR-141 and immunostained with an lamin A antibody and DAPI (nuclei). The graphs represent the ratio of cells that showed abnormal nuclei per total nuclear stained cells. (**$P < 0.01$)

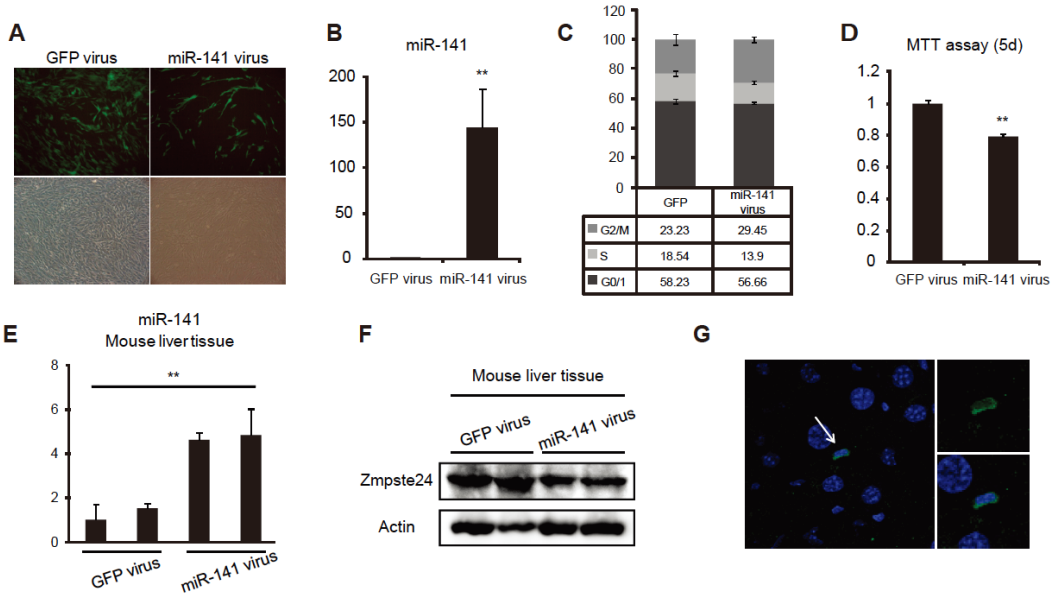

Figure 6. miRNA-141 regulates ZMPSTE24 expression *in vivo*.

(A) hMSCs were infected with miR-141 virus in-frame with a GFP tag. **(B)** miR-141 expression levels were investigated in GFP control virus- or miR-141 virus-infected cells by real-time qPCR. (**$P < 0.01$) **(C)** Panels are the cell cycle distribution profiles representing the percentage of cells in G0/G1, S, and G2/M phases for the cells infected with a GFP control virus or miR-141 virus. **(D)** MTT assay was performed after 5 days of miR-141overexpression. (*$P < 0.05$; **$P < 0.01$) **(E-G)** Following 7 days of i.p. injection of the GFP control virus or miR-141 virus into mice, liver tissues were obtained, and the miR-141 expression levels were investigated by real-time qPCR (E). Western blot analysis was performed to investigate the Zmpste24 protein expression level (F). Immunohistochemistry was performed to detect GFP expression (G). (**$P < 0.01$)

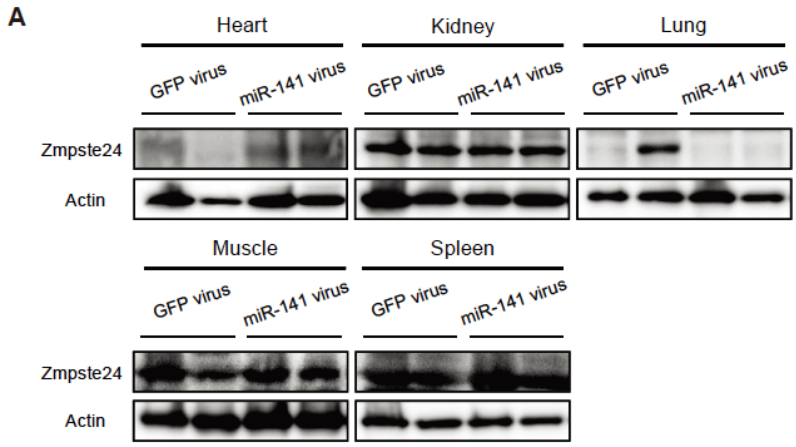

Figure 7. miRNA-141 regulates ZMPSTE24 expression *in vivo*

(A) After 7 days of i.p. injection of GFP control virus or miR-141 virus in mice, western blot analysis was performed to investigate the Zmpste24 protein expression level in the indicated tissues.

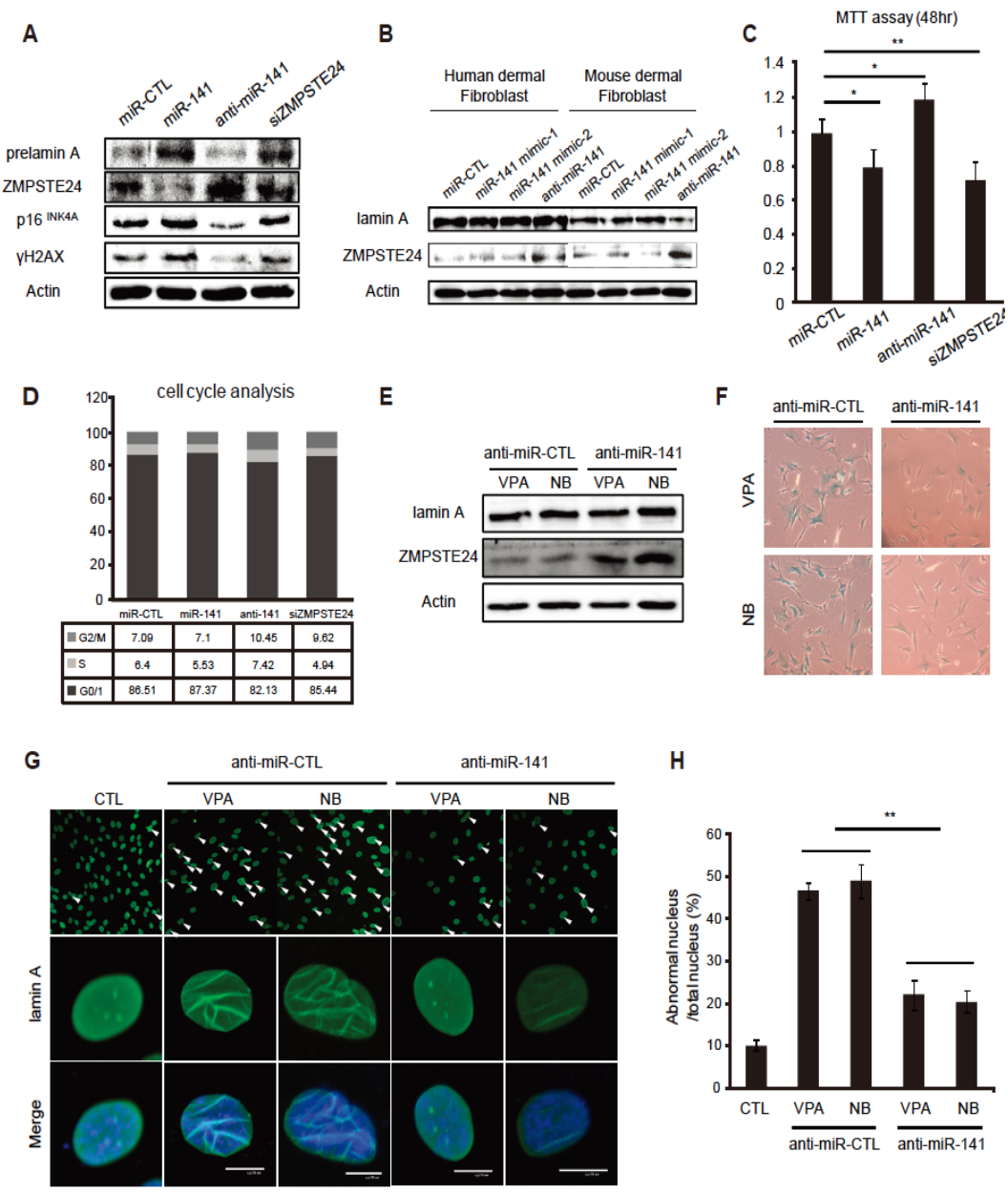

Figure 8. Anti-miRNA-141 up-regulates ZMPSTE24 expression and prevents hMSCs from HDAC inhibitor-induced changes in nuclear morphology.

(A) Western blot analysis was performed to determine prelamin A, ZMPSTE24, $p16^{INK4A}$ and γH2AX protein expression after 72 hr of transfection with miR-CTL, miR-141, anti-miR-141 and siZMPSTE24. **(B)** Lamin A and ZMPSTE24 protein expression levels were confirmed by western blot analysis in human and mouse dermal fibroblasts after the transfection of control miRNA or miR-141 mimic-1, -2 or anti-miR-141. **(C)** MTT cell proliferation assay was performed after 48 hr of transfection with miR-CTL, miR-141, anti-miR-141 or siZMPSTE24. (*$P < 0.05$; **$P < 0.01$) **(D)** Cell cycle distribution profiles showing the percentage of cells in G0/G1, S, and G2/M phases after the transfection of the control miRNA, miR-141, anti-miR-141 or siZMPSTE24. **(E-H)** Western blot analysis was conducted on anti-miR-CTL- or anti-miR-141-transfected cells. Each group was treated with VPA/NB, and the expression levels of lamin A and ZMPSTE24 were analyzed (E). Each group was SA β-gal stained (F), and immunostained using an lamin A antibody and DAPI (G). The graph represents the ratio of cells that show an abnormal nucleus per total nuclear-stained cells (H). (**$P < 0.01$)

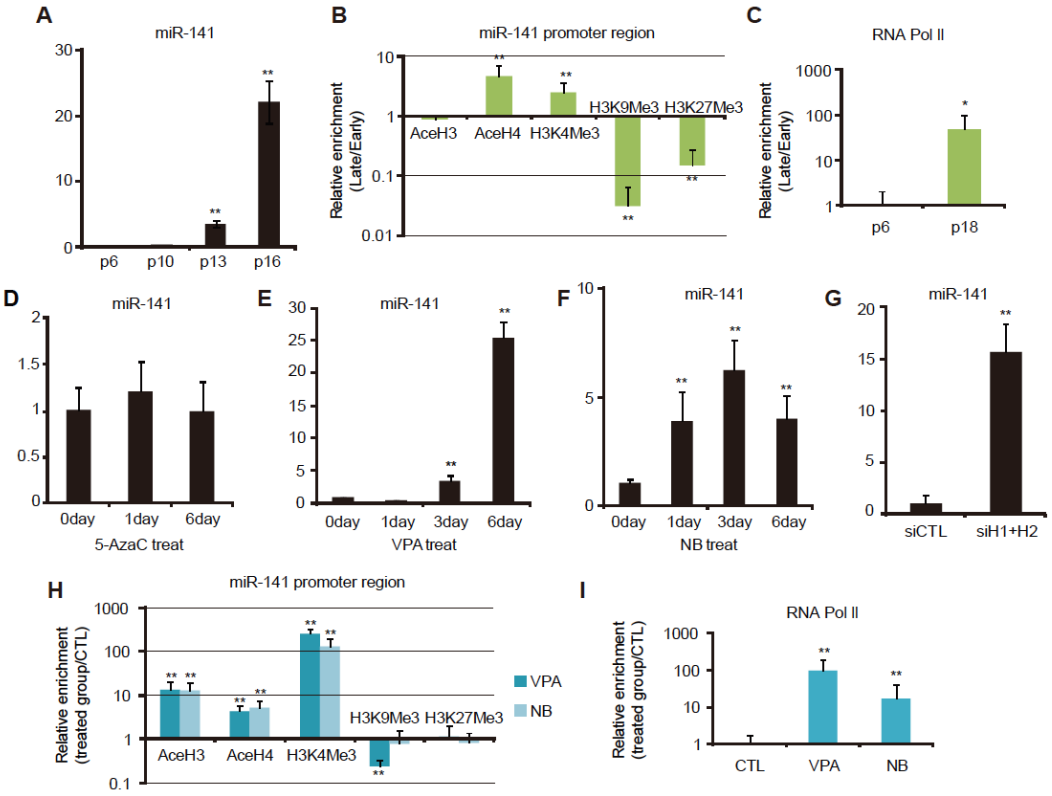

Figure 9. Replicative- and HDAC inhibitor-induced senescent cells show increased miR-141 expression with active histone marks at the miR-141 promoter.

(A) miR-141 expression levels were investigated following consecutive passages. (**P < 0.01) **(B, C)** In replicative senescent cells, ChIP analysis was performed using antibodies targeted to the indicated proteins (AcetylH3, AcetylH4, H3K4Me3, H3K9Me3, H3K27Me3 and RNA polymerase II). The fold enrichment of AcetylH3, AcetylH4, H3K4Me3, H3K9Me3, H3K27Me3 (B) and RNA polymerase II (C) proteins in the vicinity of the miR-141 genomic region was investigated by real-time qPCR. (*P < 0.05; **P < 0.01) **(D)** miR-141 expression levels were investigated following the 5-AzaC treatment. **(E, F)** miR-141 expression levels were investigated in HDAC inhibitor

(VPA/NB)-treated cells. (G) After transfection with siHDAC1 and siHDAC2, the iR-141 expression levels were investigated. (**$P < 0.01$) **(H, I)** In HDAC inhibitor-treated cells, ChIP analysis was performed using antibodies targeted to the indicated proteins (AcetylH3, AcetylH4, H3K4Me3, H3K9Me3, H3K27Me3 and RNA polymerase II). The fold enrichment of AcetylH3, AcetylH4, H3K4Me3, H3K9Me3, H3K27Me3 (H) and RNA polymerase II (I) proteins in the vicinity of the miR-141 genomic region was investigated by real-time qPCR. The graph represents the relative expression of cells treated with VPA or NB compared to control cells. (**$P < 0.01$).

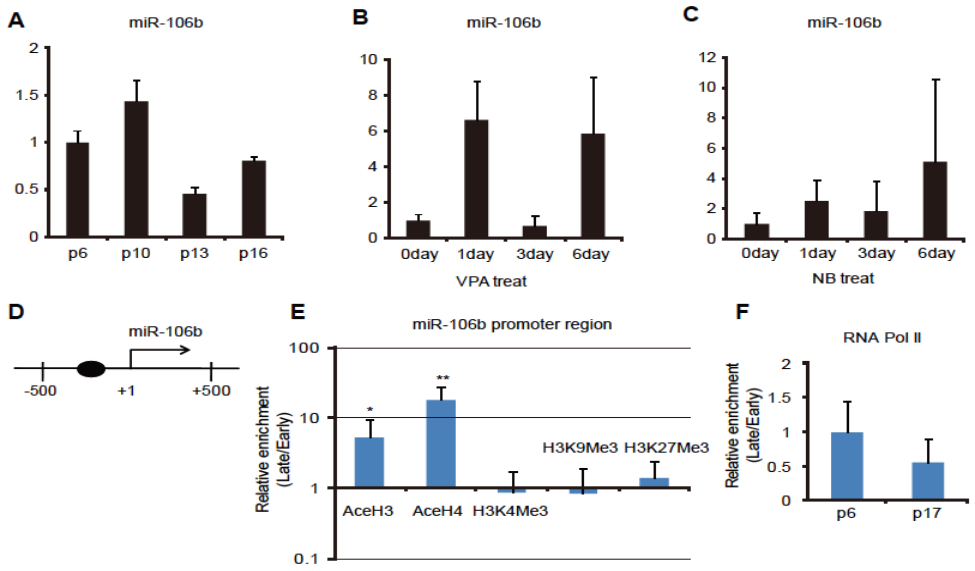

Figure 10. Replicative- and HDAC inhibitor-induced senescent cells show no changes in miR-106b expression, with inactive histone marks at the miR-141 promoter.

(A) The miR-106b expression levels were investigated following consecutive passages. **(B-C)** The miR-141 expression levels were investigated in HDAC inhibitor (VPA/NB)-treated cells. **(D)** Schematic diagram indicating the location of the primer in the vicinity of the miR-141 genomic region. **(E, F)** In replicative senescent cells, ChIP analysis was performed using antibodies targeting the indicated proteins (AcetylH3, AcetylH4, H3K4Me3, H3K9Me3, H3K27Me3 and RNA polymerase II). The fold enrichment of AcetylH3, AcetylH4, H3K4Me3, H3K9Me3, H3K27Me3 (E) and RNA polymerase II (F) in the vicinity of the miR-106b genomic region was investigated by real-time qPCR. (*$P < 0.05$; **$P < 0.01$)

3.4 DISCUSSION

This study provides insights into the mechanisms of prelamin A accumulation and ZMPSTE24 down-regulation in replicative- and HDAC inhibition-induced cellular senescence. My results suggest an epigenetic regulatory model of ZMPSTE24 through miRNA expression that can be modulated during the senescence of hMSCs through histone modification patterns via HDAC activity.

It has been demonstrated previously that the introduction of progerin, a mutant form of lamin A, into hMSCs accelerated aging and caused adult stem cell dysfunction (Scaffidi and Misteli, 2008). Furthermore, differentiation study in HGPS fibroblast-iPSCs demonstrate that MSCs are preferentially affected in HGPS (Zhang et al., 2011). I find that progerin-expressing hMSCs and replicative senescent hMSCs show similar senescent phenotypes, as determined by SA-β-gal activity, defects in proliferation and an abnormal nuclear morphology. These observations led us to investigate the expression of prelamin A during the aging process of adult stem cells. Prelamin A accumulated to high levels in replicative senescent hMSCs, whereas the processing enzyme, ZMPSTE24, a protein that catalyzes the cleavage of prelamin A to generate mature lamin A, was decreased (Fig. 1). Indeed, the accumulation of prelamin A in the nuclear envelope results in the onset of such cellular toxicity as the induction of DNA damage, growth defects and an abnormal nuclear membrane phenotype (Candelario et al., 2011; Liu et al., 2005; Liu et al., 2006b).

Furthermore, aged vascular smooth muscle cells rapidly accumulated prelamin A, which coincided with reduced levels of ZMPSTE24 (Ragnauth et al., 2010), growth defects and nuclear abnormality. These effects can be partially rescued by the over-expression of ZMPSTE24 in cells showing an up-regulation in wild-type prelamin A (Candelario et al., 2008). These data suggest that ZMPSTE24 is largely responsible for the regulation of the toxicity caused by prelamin A accumulation during aging. However, it remains to be determined whether the increase of $p16^{INK4A}$ in the siZMPSTE24-transfected cells is due to ZMPSTE24 itself or the accumulation of prelamin A.

The inhibition of HDACs induces the accumulation of acetylated histone forms, which modulates gene transcription by altering the chromatin structure and transcription factor complexes (Xu et al., 2007), and different phenotypes are induced in various cell types by the treatment with HDAC inhibitors. In hMSCs, HDAC inhibitors decrease stemness and induce cellular senescence by affecting the expression of c-MYC, polycomb group genes and $p16^{INK4A}$ (Jung et al., 2010). In this study, I present direct evidence that HDAC inhibitors significantly inhibit ZMPSTE24 activity, leading to an accumulation of prelamin A after 6 days of treatment. I also demonstrate that, among the multiple targets of HDAC inhibitors, HDAC1 and -2 can specifically affect the expression of ZMPSTE24 and prelamin A. My findings can partly explain the observations of Miller et al., who recently reported that HDAC1 and HDAC2 are involved in the DNA-damage response and are required for double-stranded break repair (Miller et al., 2010).

Although some reports have shown that ZMPSTE24 expression is decreased in senescent cells or tissues (Ragnauth et al., 2010; Ukekawa et al., 2007), the signaling pathways that modulate the ZMSPTE24 expression levels during aging have not yet been elucidated. To address this issue, I searched for miRNAs that target ZMPSTE24 during the aging process. Using computational algorithms for predicting miRNA targets and the evaluation with a luciferase assay, I revealed that ZMPSTE24 transcripts have a functional binding site for miR-141 and that ZMPSTE24 translation can be repressed by the induction of miR-141. Importantly, I was able to reduce the S phase of the cell cycle and induce DNA damage, two important features of the aging process, by transfecting mature miR-141 mimics (Figs. 4 and 8). These phenotypes are similar to those of cells transfected with ZMPSTE24-targeting siRNA, suggesting the induction of a proliferation defect and DNA damage in the miR-141-transfected cells that is caused by the inhibition of ZMPSTE24. Furthermore, I performed experiments aimed at further evaluating the opposing effect of anti-miR-141 on the hMSCs and confirmed that a reduction in the miR-141 expression level through the transfection of anti-miR-141 could up-regulate ZMPSTE24 and the potential for proliferation while down-regulating prelamin A, $p16^{INK4A}$ and γ-H2AX. I also demonstrated that the transfection of anti-miR-141 prevented the reduction in ZMPSTE24 by blocking the significant increase of miR-141 in VPA/NB treated cells. The anti-miR-141-mediated maintenance of the ZMPSTE24 expression levels resulted in the suppression of an abnormal nuclear phenotype in the HDAC inhibitor-treated cells.

Because the expression of ZMPSTE24-targeting miRNA was dramatically increased following consecutive passages, I analyzed the changes in histone modifications between the senescent hMSCs and early-passage hMSCs (Fig. 9). I demonstrated that RNA polymerase II actively binds to the coding regions of miR-141 during replicative or HDAC inhibitor-mediated senescence. An active gene transcription pattern was observed in the senescent cells within the context of histone modification in the miR-141 coding region. I showed that HDAC and DNMT expression were down-regulated in the senescent cells and that only the HDAC inhibitor could reduce the ZMPSTE24 expression (Fig. 3). These findings led us to hypothesize that miR-141 elevation and epigenetic changes in cellular senescence are the result of a decrease in HDAC. Several lines of evidence have demonstrated that miRNA transcription might be regulated through an epigenetic mechanism (Bandres et al., 2009; Saito et al., 2006; Scott et al., 2006). Tsai et al. reported that a large miRNA cluster (C19MC) on human chromosome 19 is up-regulated through the de-methylation of a CpG-rich region (Tsai et al., 2009). In addition, another report demonstrated that 22 miRNA species were decreased and 5 miRNAs were increased in response to treatment with the HDAC inhibitor, LAQ824, in the breast cancer cell line, SKBr3 (Scott et al., 2006). In the present study, I found that the miR-141 expression levels are increased following HDAC inhibitor treatment or in HDAC1- and 2-inhibited hMSCs, suggesting that miR-141 expression is affected by HDAC activity during the aging process (Fig. 9).

In summary, I investigated the roles of ZMPSTE24, prelamin A and miR-141 during cellular senescence related to HDAC activity. These results demonstrate that mutagenesis can affect the aging process, as in the case of progeria, but and that epigenetic changes can also induce senescence in adult stem cells. Furthermore, given the finding of the activation of miR-141 in the senescent hMSCs, miR-141 expression could be a predictive marker for adult stem cell aging. These results may provide a clue to understanding the adult stem cell aging process and the biological relevance of prelamin A in normal aging.

GENERAL CONCLUSION

Adult stem cells, found throughout the organs after development, play essential roles in the maintenance and repair of the organs by its properties of self-renewal and multipotency. Thus, it is important to understand the regulation mechanism of stemness and aging in human adult stem cells. Integrins are the major cellular receptors and known to regulate signaling pathways involved in stem cell survival and proliferation, such as focal adhesion kinases (FAK) and the phosphatidylinositol 3-kinase (PI3K)/AKT pathways. However, the role of CD49f (integrin subunit alpha 6) in regulating the differentiation and pluripotency of stem cells has not been fully investigated. In the first part of this study, I described the role of CD49f cell surface molecule in multipotency determination and maintenance. Specifically, I showed that the expression of CD49f confers hMSCs enhanced proliferation and differentiation capacities, through the activation of the PI3K/AKT/p53 signaling pathway. I also indicate CD49f is induced by pluripotency markers, OCT4 and SOX2, and results to be down-regulated as soon differentiation of hESCs occurs. Altogether, these evidences suggest the CD49f surface protein is a key factors in determining differentiation potential of MSCs and may have an important role in regulation of the balance between pluripotency and differentiation signals in pluripotent stem cells.

HMGA2 is a non-histone chromosomal high-mobility group A (HMGA) family

protein that alters chromatin structure through DNA binding. As an architectural transcription factor, HMGA2 regulates transcription during embryogenesis and in embryonic stem cells. Recently, several studies reported that HMGA2 is able to promote fetal neural stem cell self-renewal through its ability to repress $p16^{INK4A}$ and $p19^{Arf}$ expression. In the second part of this study, I demonstrate that the overexpression of HMGA2 enhances proliferation and reduces the SA-β-gal activity in replicative senescent hMSCs. These data indicate that the inhibition of the decrease in HMGA2 expression during the aging process may increase the proliferation of hMSCs in part by repressing $p16^{INK4A}$, $p19^{ARF}$ and $p21^{CIP1/WAF1}$. I conducted a molecular/cellular functional analysis of microarray data using a pathway analysis program and discovered that HMGA2 overexpression activated the PI3K/AKT/mTOR/p70S6K signaling pathway. In the first part of study, I showed that PI3K/AKT signaling plays an important regulatory role in hMSCs. In agreement with these data, my present results show that the mTOR/p70S6K signaling pathway is involved in repressing the expression of $p16^{INK4A}$, $p19^{ARF}$ and $p21^{CIP1/WAF1}$. My results provide novel insights into the mechanism by which HMGA2 promotes the proliferation of hMSCs through the PI3K/AKT/mTOR/p70S6K signaling pathway.

In the third part of this study, I show the relationships between ZMPSTE24, prelamin A and miRNA during adult stem cell senescence. The zinc metalloproteinase, ZMPSTE24, is involved in the post-translational maturation step of lamin A. I demonstrate that the down-regulation of ZMPSTE24 and the induction of prelamin A

accumulation during the replicative and HDAC inhibitor-mediated senescence of hMSCs are regulated by miR-141, which is over-expressed during the senescence process. The introduction of miR-141 was able to decrease the ZMPSTE24 expression levels effectively and led to an up-regulation of prelamin A and a DNA damage marker in adult stem cells. I also demonstrate that the histone configuration of the coding region of miR-141 was changed to an active form, followed by an enrichment of RNA polymerase II during replicative and HDAC inhibitor-mediated senescence. To my knowledge, I am the first to elucidate a novel function for miR-141 that induces adult stem cell aging by directly targeting ZMPSTE24. These results demonstrate that both mutagenesis, which can affect the aging process (as in the case of progeria), and epigenetic changes can induce senescence in mesenchymal stem cells.

I anticipate that these results might provide a clue to understanding the regulation mechanism of stemness and the biological aging process of human mesenchymal stem cells.

REFERENCES

Aebi, U., J. Cohn, L. Buhle, and L. Gerace, 1986. The nuclear lamina is a meshwork of intermediate-type filaments. Nature 323, 560-564.

Ailles, L.E., and I.L. Weissman, 2007. Cancer stem cells in solid tumors. Curr Opin Biotechnol 18, 460-466.

Alon, U., 2007. Network motifs: theory and experimental approaches. Nat Rev Genet 8, 450-461.

Armesilla-Diaz, A., G. Elvira, and A. Silva, 2009. p53 regulates the proliferation, differentiation and spontaneous transformation of mesenchymal stem cells. Exp Cell Res 315, 3598-3610.

Armstrong, L., O. Hughes, S. Yung, L. Hyslop, R. Stewart, I. Wappler, H. Peters, T. Walter, P. Stojkovic, J. Evans, M. Stojkovic, and M. Lako, 2006. The role of PI3K/AKT, MAPK/ERK and NFkB signalling in the maintenance of human embryonic stem cell pluripotency and viability highlighted by transcriptional profiling and functional analysis. Hum Mol Genet 15, 1894-1913.

Baksh, D., R. Yao, and R.S. Tuan, 2007. Comparison of proliferative and multilineage differentiation potential of human mesenchymal stem cells derived from umbilical cord and bone marrow. Stem Cells 25, 1384-1392.

Bandres, E., X. Agirre, N. Bitarte, N. Ramirez, R. Zarate, J. Roman-Gomez, F. Prosper, and J. Garcia-Foncillas, 2009. Epigenetic regulation of microRNA expression in colorectal cancer. Int J Cancer 125, 2737-2743.

Bartel, D.P., 2004. MicroRNAs: genomics, biogenesis, mechanism, and function. Cell 116, 281-297.

Bennecke, M., L. Kriegl, M. Bajbouj, K. Retzlaff, S. Robine, A. Jung, M.C. Arkan, T. Kirchner, and F.R. Greten, 2010. Ink4a/Arf and oncogene-induced senescence prevent tumor progression during alternative colorectal tumorigenesis. Cancer Cell 18, 135-146.

Bibikova, M., L.C. Laurent, B. Ren, J.F. Loring, and J.B. Fan, 2008. Unraveling epigenetic regulation in embryonic stem cells. Cell Stem Cell 2, 123-134.

Boiani, M., and H.R. Scholer, 2005. Regulatory networks in embryo-derived pluripotent stem cells. Nat Rev Mol Cell Biol 6, 872-884.

Bonab, M.M., K. Alimoghaddam, F. Talebian, S.H. Ghaffari, A. Ghavamzadeh, and B. Nikbin, 2006. Aging of mesenchymal stem cell in vitro. BMC Cell Biol 7, 14.

Bouvard, C., B. Gafsou, B. Dizier, I. Galy-Fauroux, A. Lokajczyk, C. Boisson-Vidal, A.M. Fischer, and D. Helley, 2010. alpha6-integrin subunit plays a major role in the proangiogenic properties of endothelial progenitor cells. Arterioscler Thromb Vasc Biol 30, 1569-1575.

Boyer, L.A., T.I. Lee, M.F. Cole, S.E. Johnstone, S.S. Levine, J.P. Zucker, M.G. Guenther, R.M. Kumar, H.L. Murray, R.G. Jenner, D.K. Gifford, D.A. Melton, R. Jaenisch, and R.A. Young, 2005. Core transcriptional regulatory circuitry in human embryonic stem cells. Cell 122, 947-956.

Candelario, J., S. Borrego, S. Reddy, and L. Comai, 2011. Accumulation of distinct prelamin A variants in human diploid fibroblasts differentially affects cell homeostasis. Exp Cell Res 317, 319-329.

Candelario, J., S. Sudhakar, S. Navarro, S. Reddy, and L. Comai, 2008. Perturbation of wild-type lamin A metabolism results in a progeroid phenotype. Aging Cell 7, 355-367.

Cao, Y., D. Li, C. Shang, S.T. Yang, J. Wang, and X. Wang, 2010. Three-dimensional culture of human mesenchymal stem cells in a polyethylene terephthalate matrix. Biomed Mater 5, 065013.

Chao, Y.H., H.P. Wu, C.K. Chan, C. Tsai, C.T. Peng, and K.H. Wu, 2012. Umbilical cord-derived mesenchymal stem cells for hematopoietic stem cell transplantation. J Biomed Biotechnol 2012, 759503.

Chiappetta, G., V. Avantaggiato, R. Visconti, M. Fedele, S. Battista, F. Trapasso, B.M. Merciai, V. Fidanza, V. Giancotti, M. Santoro, A. Simeone, and A. Fusco, 1996. High level expression of the HMGI (Y) gene during embryonic development. Oncogene 13, 2439-2446.

Chou, M.M., J.M. Masuda-Robens, and M.L. Gupta, 2003. Cdc42 promotes G1 progression through p70 S6 kinase-mediated induction of cyclin E expression. J Biol Chem 278, 35241-35247.

Cicalese, A., G. Bonizzi, C.E. Pasi, M. Faretta, S. Ronzoni, B. Giulini, C. Brisken, S. Minucci, P.P. Di Fiore, and P.G. Pelicci, 2009. The tumor suppressor p53

regulates polarity of self-renewing divisions in mammary stem cells. Cell 138, 1083-1095.

Cocciadiferro, L., V. Miceli, K.S. Kang, L.M. Polito, J.E. Trosko, and G. Carruba, 2009. Profiling cancer stem cells in androgen-responsive and refractory human prostate tumor cell lines. Ann N Y Acad Sci 1155, 257-262.

Collado, M., M.A. Blasco, and M. Serrano, 2007. Cellular senescence in cancer and aging. Cell 130, 223-233.

Corrigan, D.P., D. Kuszczak, A.E. Rusinol, D.P. Thewke, C.A. Hrycyna, S. Michaelis, and M.S. Sinensky, 2005. Prelamin A endoproteolytic processing in vitro by recombinant Zmpste24. Biochem J 387, 129-138.

Cruet-Hennequart, S., S. Maubant, J. Luis, P. Gauduchon, C. Staedel, and S. Dedhar, 2003. αv integrins regulate cell proliferation through integrin-linked kinase (ILK) in ovarian cancer cells. Oncogene 22, 1688-1702.

Danen, E.H., and K.M. Yamada, 2001. Fibronectin, integrins, and growth control. J Cell Physiol 189, 1-13.

Dechat, T., T. Shimi, S.A. Adam, A.E. Rusinol, D.A. Andres, H.P. Spielmann, M.S. Sinensky, and R.D. Goldman, 2007. Alterations in mitosis and cell cycle progression caused by a mutant lamin A known to accelerate human aging. Proc Natl Acad Sci U S A 104, 4955-4960.

Eriksson, M., W.T. Brown, L.B. Gordon, M.W. Glynn, J. Singer, L. Scott, M.R. Erdos, C.M. Robbins, T.Y. Moses, P. Berglund, A. Dutra, E. Pak, S. Durkin, A.B. Csoka, M. Boehnke, T.W. Glover, and F.S. Collins, 2003. Recurrent de novo point

mutations in lamin A cause Hutchinson-Gilford progeria syndrome. Nature 423, 293-298.

Fedele, M., D. Palmieri, and A. Fusco, 2010. HMGA2: A pituitary tumour subtype-specific oncogene? Mol Cell Endocrinol 326, 19-24.

Frith, J.E., B. Thomson, and P.G. Genever, 2010. Dynamic three-dimensional culture methods enhance mesenchymal stem cell properties and increase therapeutic potential. Tissue Eng Part C Methods 16, 735-749.

Fujita, T., Y. Azuma, R. Fukuyama, Y. Hattori, C. Yoshida, M. Koida, K. Ogita, and T. Komori, 2004. Runx2 induces osteoblast and chondrocyte differentiation and enhances their migration by coupling with PI3K-Akt signaling. J Cell Biol 166, 85-95.

Fusco, A., and M. Fedele, 2007. Roles of HMGA proteins in cancer. Nat Rev Cancer 7, 899-910.

Gambaletta, D., A. Marchetti, L. Benedetti, A.M. Mercurio, A. Sacchi, and R. Falcioni, 2000. Cooperative signaling between α6β4 integrin and ErbB-2 receptor is required to promote phosphatidylinositol 3-kinase-dependent invasion. J Biol Chem 275, 10604-10610.

Gao, N., D.C. Flynn, Z. Zhang, X.S. Zhong, V. Walker, K.J. Liu, X. Shi, and B.H. Jiang, 2004. G1 cell cycle progression and the expression of G1 cyclins are regulated by PI3K/AKT/mTOR/p70S6K1 signaling in human ovarian cancer cells. Am J Physiol Cell Physiol 287, C281-291.

Gao, N., Z. Zhang, B.H. Jiang, and X. Shi, 2003. Role of PI3K/AKT/mTOR signaling in the cell cycle progression of human prostate cancer. Biochem Biophys Res Commun 310, 1124-1132.

Greco, S.J., K. Liu, and P. Rameshwar, 2007. Functional similarities among genes regulated by OCT4 in human mesenchymal and embryonic stem cells. Stem Cells 25, 3143-3154.

Grosschedl, R., K. Giese, and J. Pagel, 1994. HMG domain proteins: architectural elements in the assembly of nucleoprotein structures. Trends Genet 10, 94-100.

Hall, P.E., J.D. Lathia, N.G. Miller, M.A. Caldwell, and C. ffrench-Constant, 2006. Integrins are markers of human neural stem cells. Stem Cells 24, 2078-2084.

Hayflick, L., 1965. The Limited in Vitro Lifetime of Human Diploid Cell Strains. Exp Cell Res 37, 614-636.

Hayflick, L. 1994. How and why we age. Ballantine Books, New York. xxii, p.377

He, L., and G.J. Hannon, 2004. MicroRNAs: small RNAs with a big role in gene regulation. Nat Rev Genet 5, 522-531.

Horwitz, E.M., K. Le Blanc, M. Dominici, I. Mueller, I. Slaper-Cortenbach, F.C. Marini, R.J. Deans, D.S. Krause, and A. Keating, 2005. Clarification of the nomenclature for MSC: The International Society for Cellular Therapy position statement. Cytotherapy 7, 393-395.

Hutchison, C.J., and H.J. Worman, 2004. A-type lamins: guardians of the soma? Nat Cell Biol 6, 1062-1067.

Hynes, R.O., 1987. Integrins: a family of cell surface receptors. Cell 48, 549-554.

Ikeda, K., P.J. Mason, and M. Bessler, 2011. 3'UTR-truncated Hmga2 cDNA causes MPN-like hematopoiesis by conferring a clonal growth advantage at the level of HSC in mice. Blood 117, 5860-5869.

Ilic, D., E.A. Almeida, D.D. Schlaepfer, P. Dazin, S. Aizawa, and C.H. Damsky, 1998. Extracellular matrix survival signals transduced by focal adhesion kinase suppress p53-mediated apoptosis. J Cell Biol 143, 547-560.

Iovino, N., and G. Cavalli, 2011. Rolling ES Cells Down the Waddington Landscape with Oct4 and Sox2. Cell 145, 815-817.

Janzen, V., R. Forkert, H.E. Fleming, Y. Saito, M.T. Waring, D.M. Dombkowski, T. Cheng, R.A. DePinho, N.E. Sharpless, and D.T. Scadden, 2006. Stem-cell ageing modified by the cyclin-dependent kinase inhibitor p16INK4a. Nature 443, 421-426.

Javazon, E.H., K.J. Beggs, and A.W. Flake, 2004. Mesenchymal stem cells: paradoxes of passaging. Exp Hematol 32, 414-425.

Jung, J.W., S.D. Cho, N.S. Ahn, S.R. Yang, J.S. Park, E.H. Jo, J.W. Hwang, J.Y. Jung, S.H. Kim, K.S. Kang, and Y.S. Lee, 2005. Ras/MAP kinase pathways are involved in Ras specific apoptosis induced by sodium butyrate. Cancer Letters 225, 199-206.

Jung, J.W., S. Lee, M.S. Seo, S.B. Park, A. Kurtz, S.K. Kang, and K.S. Kang, 2010. Histone deacetylase controls adult stem cell aging by balancing the expression of polycomb genes and jumonji domain containing 3. Cell Mol Life Sci 67, 1165-1176.

Kang, S., C.N. Bennett, I. Gerin, L.A. Rapp, K.D. Hankenson, and O.A. Macdougald, 2007. Wnt signaling stimulates osteoblastogenesis of mesenchymal precursors by suppressing CCAAT/enhancer-binding protein α and peroxisome proliferator-activated receptor gamma. J Biol Chem 282, 14515-14524.

Kasper, G., L. Mao, S. Geissler, A. Draycheva, J. Trippens, J. Kuhnisch, M. Tschirschmann, K. Kaspar, C. Perka, G.N. Duda, and J. Klose, 2009. Insights into mesenchymal stem cell aging: involvement of antioxidant defense and actin cytoskeleton. Stem Cells 27, 1288-1297.

Kirkwood, T.B., 2005. Understanding the odd science of aging. Cell 120, 437-447.

Kohn, A.D., S.A. Summers, M.J. Birnbaum, and R.A. Roth, 1996. Expression of a constitutively active Akt Ser/Thr kinase in 3T3-L1 adipocytes stimulates glucose uptake and glucose transporter 4 translocation. J Biol Chem 271, 31372-31378.

Koul, D., R. Shen, S. Bergh, Y. Lu, J.F. de Groot, T.J. Liu, G.B. Mills, and W.K. Yung, 2005. Targeting integrin-linked kinase inhibits Akt signaling pathways and decreases tumor progression of human glioblastoma. Mol Cancer Ther 4, 1681-1688.

Lawson, D.A., Y. Zong, S. Memarzadeh, L. Xin, J. Huang, and O.N. Witte, 2010. Basal epithelial stem cells are efficient targets for prostate cancer initiation. Proc Natl Acad Sci U S A 107, 2610-2615.

Le Belle, J.E., N.M. Orozco, A.A. Paucar, J.P. Saxe, J. Mottahedeh, A.D. Pyle, H. Wu, and H.I. Kornblum, 2011. Proliferative neural stem cells have high endogenous

ROS levels that regulate self-renewal and neurogenesis in a PI3K/Akt-dependant manner. Cell Stem Cell 8, 59-71.

Lee, R.H., M.J. Seo, A.A. Pulin, C.A. Gregory, J. Ylostalo, and D.J. Prockop, 2009a. The CD34-like protein PODXL and α6-integrin (CD49f) identify early progenitor MSCs with increased clonogenicity and migration to infarcted heart in mice. Blood 113, 816-826.

Lee, S., J.W. Jung, S.B. Park, K. Roh, S.Y. Lee, J.H. Kim, S.K. Kang, and K.S. Kang, 2011. Histone deacetylase regulates high mobility group A2-targeting microRNAs in human cord blood-derived multipotent stem cell aging. Cell Mol Life Sci 68, 325-336.

Lee, S., J.R. Park, M.S. Seo, K.H. Roh, S.B. Park, J.W. Hwang, B. Sun, K. Seo, Y.S. Lee, S.K. Kang, J.W. Jung, and K.S. Kang, 2009b. Histone deacetylase inhibitors decrease proliferation potential and multilineage differentiation capability of human mesenchymal stem cells. Cell Prolif 42, 711-720.

Lee, Y., M. Kim, J. Han, K.H. Yeom, S. Lee, S.H. Baek, and V.N. Kim, 2004. MicroRNA genes are transcribed by RNA polymerase II. EMBO J 23, 4051-4060.

Lewis, B.P., C.B. Burge, and D.P. Bartel, 2005. Conserved seed pairing, often flanked by adenosines, indicates that thousands of human genes are microRNA targets. Cell 120, 15-20.

Li, O., D. Vasudevan, C.A. Davey, and P. Droge, 2006. High-level expression of DNA architectural factor HMGA2 and its association with nucleosomes in human embryonic stem cells. Genesis 44, 523-529.

Lin, A.W., M. Barradas, J.C. Stone, L. van Aelst, M. Serrano, and S.W. Lowe, 1998. Premature senescence involving p53 and p16 is activated in response to constitutive MEK/MAPK mitogenic signaling. Genes Dev 12, 3008-3019.

Liu, B., J. Wang, K.M. Chan, W.M. Tjia, W. Deng, X. Guan, J.D. Huang, K.M. Li, P.Y. Chau, D.J. Chen, D. Pei, A.M. Pendas, J. Cadinanos, C. Lopez-Otin, H.F. Tse, C. Hutchison, J. Chen, Y. Cao, K.S. Cheah, K. Tryggvason, and Z. Zhou, 2005. Genomic instability in laminopathy-based premature aging. Nat Med 11, 780-785.

Liu, S., G. Dontu, I.D. Mantle, S. Patel, N.S. Ahn, K.W. Jackson, P. Suri, and M.S. Wicha, 2006a. Hedgehog signaling and Bmi-1 regulate self-renewal of normal and malignant human mammary stem cells. Cancer Res 66, 6063-6071.

Liu, T.M., Y.N. Wu, X.M. Guo, J.H. Hui, E.H. Lee, and B. Lim, 2009. Effects of ectopic Nanog and Oct4 overexpression on mesenchymal stem cells. Stem Cells Dev 18, 1013-1022.

Liu, Y., A. Rusinol, M. Sinensky, Y. Wang, and Y. Zou, 2006b. DNA damage responses in progeroid syndromes arise from defective maturation of prelamin A. J Cell Sci 119, 4644-4649.

Lu, L.L., Y.J. Liu, S.G. Yang, Q.J. Zhao, X. Wang, W. Gong, Z.B. Han, Z.S. Xu, Y.X. Lu, D. Liu, Z.Z. Chen, and Z.C. Han, 2006. Isolation and characterization of human umbilical cord mesenchymal stem cells with hematopoiesis-supportive function and other potentials. Haematologica 91, 1017-1026.

Ma, S., T.K. Lee, B.J. Zheng, K.W. Chan, and X.Y. Guan, 2008. CD133+ HCC cancer stem cells confer chemoresistance by preferential expression of the Akt/PKB survival pathway. Oncogene 27, 1749-1758.

Macleod, K.F., N. Sherry, G. Hannon, D. Beach, T. Tokino, K. Kinzler, B. Vogelstein, and T. Jacks, 1995. p53-dependent and independent expression of p21 during cell growth, differentiation, and DNA damage. Genes Dev 9, 935-944.

Majore, I., P. Moretti, R. Hass, and C. Kasper, 2009. Identification of subpopulations in mesenchymal stem cell-like cultures from human umbilical cord. Cell Commun Signal 7, 6.

Mantovani, F., S. Covaceuszach, A. Rustighi, R. Sgarra, C. Heath, G.H. Goodwin, and G. Manfioletti, 1998. NF-kappaB mediated transcriptional activation is enhanced by the architectural factor HMGI-C. Nucleic Acids Res 26, 1433-1439.

Maraldi, N.M., C. Capanni, V. Cenni, M. Fini, and G. Lattanzi, 2011. Laminopathies and lamin-associated signaling pathways. J Cell Biochem 112, 979-992.

Martelli, A.M., C. Evangelisti, M.Y. Follo, G. Ramazzotti, M. Fini, R. Giardino, L. Manzoli, J.A. McCubrey, and L. Cocco, 2011. Targeting the phosphatidylinositol 3-Kinase/Akt/Mammalian target of rapamycin signaling network in cancer stem cells. Curr Med Chem.

Meng, Y., S. Eshghi, Y.J. Li, R. Schmidt, D.V. Schaffer, and K.E. Healy, 2010. Characterization of integrin engagement during defined human embryonic stem cell culture. FASEB J 24, 1056-1065.

Miller, K.M., J.V. Tjeertes, J. Coates, G. Legube, S.E. Polo, S. Britton, and S.P. Jackson, 2010. Human HDAC1 and HDAC2 function in the DNA-damage response to promote DNA nonhomologous end-joining. Nat Struct Mol Biol 17, 1144-1151.

Misteli, T., and P. Scaffidi, 2005. Genome instability in progeria: when repair gets old. Nat Med 11, 718-719.

Miyazaki, T., S. Futaki, K. Hasegawa, M. Kawasaki, N. Sanzen, M. Hayashi, E. Kawase, K. Sekiguchi, N. Nakatsuji, and H. Suemori, 2008. Recombinant human laminin isoforms can support the undifferentiated growth of human embryonic stem cells. Biochem Biophys Res Commun 375, 27-32.

Morgensztern, D., and H.L. McLeod, 2005. PI3K/Akt/mTOR pathway as a target for cancer therapy. Anticancer Drugs 16, 797-803.

Mounkes, L., S. Kozlov, B. Burke, and C.L. Stewart, 2003. The laminopathies: nuclear structure meets disease. Curr Opin Genet Dev 13, 223-230.

Mukherjee, A., and P. Rotwein, 2009. Akt promotes BMP2-mediated osteoblast differentiation and bone development. J Cell Sci 122, 716-726.

Narita, M., 2007. Cellular senescence and chromatin organisation. Br J Cancer 96, 686-691.

Navarro, C.L., A. De Sandre-Giovannoli, R. Bernard, I. Boccaccio, A. Boyer, D. Genevieve, S. Hadj-Rabia, C. Gaudy-Marqueste, H.S. Smitt, P. Vabres, L. Faivre, A. Verloes, T. Van Essen, E. Flori, R. Hennekam, F.A. Beemer, N. Laurent, M. Le Merrer, P. Cau, and N. Levy, 2004. Lamin A and ZMPSTE24 (FACE-1)

defects cause nuclear disorganization and identify restrictive dermopathy as a lethal neonatal laminopathy. Hum Mol Genet 13, 2493-2503.

Nishino, J., I. Kim, K. Chada, and S.J. Morrison, 2008. Hmga2 promotes neural stem cell self-renewal in young but not old mice by reducing p16Ink4a and p19Arf Expression. Cell 135, 227-239.

Notta, F., S. Doulatov, E. Laurenti, A. Poeppl, I. Jurisica, and J.E. Dick, 2011. Isolation of single human hematopoietic stem cells capable of long-term multilineage engraftment. Science 333, 218-221.

Ogawara, Y., S. Kishishita, T. Obata, Y. Isazawa, T. Suzuki, K. Tanaka, N. Masuyama, and Y. Gotoh, 2002. Akt enhances Mdm2-mediated ubiquitination and degradation of p53. J Biol Chem 277, 21843-21850.

Ohtani, N., K. Yamakoshi, A. Takahashi, and E. Hara, 2004. The p16INK4a-RB pathway: molecular link between cellular senescence and tumor suppression. J Med Invest 51, 146-153.

Oren, M., 2003. Decision making by p53: life, death and cancer. Cell Death Differ 10, 431-442.

Orkin, S.H., J. Wang, J. Kim, J. Chu, S. Rao, T.W. Theunissen, X. Shen, and D.N. Levasseur, 2008. The Transcriptional Network Controlling Pluripotency in ES Cells. Cold Spring Harb Symp Quant Biol.

Oshima, K., P. Senn, and S. Heller, 2009. Isolation of sphere-forming stem cells from the mouse inner ear. Methods Mol Biol 493, 141-162.

Park, S.B., K.W. Seo, A.Y. So, M.S. Seo, K.R. Yu, S.K. Kang, and K.S. Kang, 2012. SOX2 has a crucial role in the lineage determination and proliferation of mesenchymal stem cells through Dickkopf-1 and c-MYC. Cell Death Differ 19, 534-545.

Pfannkuche, K., H. Summer, O. Li, J. Hescheler, and P. Droge, 2009. The high mobility group protein HMGA2: a co-regulator of chromatin structure and pluripotency in stem cells? Stem Cell Rev 5, 224-230.

Pittenger, M.F., A.M. Mackay, S.C. Beck, R.K. Jaiswal, R. Douglas, J.D. Mosca, M.A. Moorman, D.W. Simonetti, S. Craig, and D.R. Marshak, 1999. Multilineage potential of adult human mesenchymal stem cells. Science 284, 143-147.

Prockop, D.J., 2009. Repair of tissues by adult stem/progenitor cells (MSCs): controversies, myths, and changing paradigms. Mol Ther 17, 939-946.

Ragnauth, C.D., D.T. Warren, Y. Liu, R. McNair, T. Tajsic, N. Figg, R. Shroff, J. Skepper, and C.M. Shanahan, 2010. Prelamin A acts to accelerate smooth muscle cell senescence and is a novel biomarker of human vascular aging. Circulation 121, 2200-2210.

Rao, M.S., and M.P. Mattson, 2001. Stem cells and aging: expanding the possibilities. Mech Ageing Dev 122, 713-734.

Rayess, H., M.B. Wang, and E.S. Srivatsan, 2012. Cellular senescence and tumor suppressor gene p16. Int J Cancer 130, 1715-1725.

Rodin, S., A. Domogatskaya, S. Strom, E.M. Hansson, K.R. Chien, J. Inzunza, O. Hovatta, and K. Tryggvason, 2010. Long-term self-renewal of human pluripotent stem cells on human recombinant laminin-511. Nat Biotechnol 28, 611-615.

Rommel, B., P. Rogalla, A. Jox, C.V. Kalle, B. Kazmierczak, J. Wolf, and J. Bullerdiek, 1997. HMGI-C, a member of the high mobility group family of proteins, is expressed in hematopoietic stem cells and in leukemic cells. Leuk Lymphoma 26, 603-607.

Rowland, T.J., L.M. Miller, A.J. Blaschke, E.L. Doss, A.J. Bonham, S.T. Hikita, L.V. Johnson, and D.O. Clegg, 2009. Roles of Integrins in Human Induced Pluripotent Stem Cell Growth on Matrigel and Vitronectin. Stem Cells Dev.

Saito, Y., G. Liang, G. Egger, J.M. Friedman, J.C. Chuang, G.A. Coetzee, and P.A. Jones, 2006. Specific activation of microRNA-127 with downregulation of the proto-oncogene BCL6 by chromatin-modifying drugs in human cancer cells. Cancer Cell 9, 435-443.

Scaffidi, P., and T. Misteli, 2008. Lamin A-dependent misregulation of adult stem cells associated with accelerated ageing. Nat Cell Biol 10, 452-459.

Scott, G.K., M.D. Mattie, C.E. Berger, S.C. Benz, and C.C. Benz, 2006. Rapid alteration of microRNA levels by histone deacetylase inhibition. Cancer Res 66, 1277-1281.

Shaw, L.M., I. Rabinovitz, H.H. Wang, A. Toker, and A.M. Mercurio, 1997. Activation of phosphoinositide 3-OH kinase by the alpha6beta4 integrin promotes carcinoma invasion. Cell 91, 949-960.

Shibata, K.R., T. Aoyama, Y. Shima, K. Fukiage, S. Otsuka, M. Furu, Y. Kohno, K. Ito, S. Fujibayashi, M. Neo, T. Nakayama, T. Nakamura, and J. Toguchida, 2007. Expression of the p16INK4A gene is associated closely with senescence of human mesenchymal stem cells and is potentially silenced by DNA methylation during in vitro expansion. Stem Cells 25, 2371-2382.

Shimizu, R., K. Okabe, Y. Kubota, A. Nakamura-Ishizu, H. Nakajima, and K. Kishi, 2011. Sphere formation restores and confers hair-inducing capacity in cultured mesenchymal cells. Exp Dermatol 20, 679-681.

Shukla, V., T. Vaissiere, and Z. Herceg, 2008. Histone acetylation and chromatin signature in stem cell identity and cancer. Mutat Res 637, 1-15.

Shumaker, D.K., T. Dechat, A. Kohlmaier, S.A. Adam, M.R. Bozovsky, M.R. Erdos, M. Eriksson, A.E. Goldman, S. Khuon, F.S. Collins, T. Jenuwein, and R.D. Goldman, 2006. Mutant nuclear lamin A leads to progressive alterations of epigenetic control in premature aging. Proc Natl Acad Sci U S A 103, 8703-8708.

Shumaker, D.K., E.R. Kuczmarski, and R.D. Goldman, 2003. The nucleoskeleton: lamins and actin are major players in essential nuclear functions. Curr Opin Cell Biol 15, 358-366.

Silva, H., and I.M. Conboy, 2008. Aging and stem cell renewal.

Smukler, S.R., M.E. Arntfield, R. Razavi, G. Bikopoulos, P. Karpowicz, R. Seaberg, F. Dai, S. Lee, R. Ahrens, P.E. Fraser, M.B. Wheeler, and D. van der Kooy, 2011. The adult mouse and human pancreas contain rare multipotent stem cells that express insulin. Cell Stem Cell 8, 281-293.

So, A.Y., J.W. Jung, S. Lee, H.S. Kim, and K.S. Kang, 2011. DNA methyltransferase controls stem cell aging by regulating BMI1 and EZH2 through microRNAs. PLoS One 6, e19503.

Sperka, T., J. Wang, and K.L. Rudolph, 2012. DNA damage checkpoints in stem cells, ageing and cancer. Nat Rev Mol Cell Biol 13, 579-590.

Tao, L., A.L. Roberts, K.A. Dunphy, C. Bigelow, H. Yan, and D.J. Jerry, 2011. Repression of mammary stem/progenitor cells by p53 is mediated by Notch and separable from apoptotic activity. Stem Cells 29, 119-127.

Thanos, D., and T. Maniatis, 1992. The high mobility group protein HMG I(Y) is required for NF-kB-dependent virus induction of the human IFN-β gene. Cell 71, 777-789.

Tondreau, T., N. Meuleman, A. Delforge, M. Dejeneffe, R. Leroy, M. Massy, C. Mortier, D. Bron, and L. Lagneaux, 2005. Mesenchymal stem cells derived from CD133-positive cells in mobilized peripheral blood and cord blood: proliferation, Oct4 expression, and plasticity. Stem Cells 23, 1105-1112.

Tormin, A., J.C. Brune, E. Olsson, J. Valcich, U. Neuman, T. Olofsson, S.E. Jacobsen, and S. Scheding, 2009. Characterization of bone marrow-derived mesenchymal stromal cells (MSC) based on gene expression profiling of functionally defined MSC subsets. Cytotherapy 11, 114-128.

Tsai, K.W., H.W. Kao, H.C. Chen, S.J. Chen, and W.C. Lin, 2009. Epigenetic control of the expression of a primate-specific microRNA cluster in human cancer cells. Epigenetics 4, 587-592.

Tzatsos, A., and N. Bardeesy, 2008. Ink4a/Arf regulation by let-7b and Hmga2: a genetic pathway governing stem cell aging. Cell Stem Cell 3, 469-470.

Ukekawa, R., K. Miki, M. Fujii, H. Hirano, and D. Ayusawa, 2007. Accumulation of multiple forms of lamin A with down-regulation of FACE-1 suppresses growth in senescent human cells. Genes Cells 12, 397-406.

Varela, I., J. Cadinanos, A.M. Pendas, A. Gutierrez-Fernandez, A.R. Folgueras, L.M. Sanchez, Z. Zhou, F.J. Rodriguez, C.L. Stewart, J.A. Vega, K. Tryggvason, J.M. Freije, and C. Lopez-Otin, 2005. Accelerated ageing in mice deficient in Zmpste24 protease is linked to p53 signalling activation. Nature 437, 564-568.

Veevers-Lowe, J., S.G. Ball, A. Shuttleworth, and C.M. Kielty, 2011. Mesenchymal stem cell migration is regulated by fibronectin through alpha5beta1-integrin-mediated activation of PDGFR-beta and potentiation of growth factor signals. J Cell Sci 124, 1288-1300.

Watanabe, S., H. Umehara, K. Murayama, M. Okabe, T. Kimura, and T. Nakano, 2006. Activation of Akt signaling is sufficient to maintain pluripotency in mouse and primate embryonic stem cells. Oncogene 25, 2697-2707.

Welham, M.J., E. Kingham, Y. Sanchez-Ripoll, B. Kumpfmueller, M. Storm, and H. Bone, 2011. Controlling embryonic stem cell proliferation and pluripotency: the role of PI3K- and GSK-3-dependent signalling. Biochem Soc Trans 39, 674-678.

Xu, J., and K. Liao, 2004. Protein kinase B/AKT 1 plays a pivotal role in insulin-like growth factor-1 receptor signaling induced 3T3-L1 adipocyte differentiation. J Biol Chem 279, 35914-35922.

Xu, W.S., R.B. Parmigiani, and P.A. Marks, 2007. Histone deacetylase inhibitors: molecular mechanisms of action. Oncogene 26, 5541-5552.

Young, A.R., and M. Narita, 2007. Oncogenic HMGA2: short or small? Genes Dev 21(9), 1005-1009.

Young, S.G., L.G. Fong, and S. Michaelis, 2005. Prelamin A, Zmpste24, misshapen cell nuclei, and progeria--new evidence suggesting that protein farnesylation could be important for disease pathogenesis. J Lipid Res 46, 2531-2558.

Yu, K.R., S.R. Yang, J.W. Jung, H. Kim, K. Ko, D.W. Han, S.B. Park, S.W. Choi, S.K. Kang, H. Scholer, and K.S. Kang, 2012. CD49f enhances multipotency and maintains stemness through the direct regulation of OCT4 and SOX2. Stem Cells 30, 876-887.

Zhang, J., Q. Lian, G. Zhu, F. Zhou, L. Sui, C. Tan, R.A. Mutalif, R. Navasankari, Y. Zhang, H.F. Tse, C.L. Stewart, and A. Colman, 2011. A human iPSC model of Hutchinson Gilford Progeria reveals vascular smooth muscle and mesenchymal stem cell defects. Cell Stem Cell 8, 31-45.

국문 초록

인간 중간엽줄기세포의 줄기세포능 및 노화 조절 연구

서울대학교 대학원

수의과대학 수의공중보건학 전공

유 경 록

(지도교수: 강경선)

성체줄기세포는 성체의 각 기관에 존재하며 기관의 기능을 유지하고 손상을 회복시킨다. 성체줄기세포는 정교하게 조절되는 분자적 신호를 통해 각 조직이나 기관의 항상성을 유지시킨다. 따라서 이 연구의 첫번째 부분에서는 성체줄기세포의 줄기세포능을 유지시키며, 다분화능을 향상시키는 표지인자를 밝히는 것에 촛점을 두었다. 먼저, 성체줄기세포 중 하나인,

중간엽줄기세포 (MSC)를 이차원적 배양이 아닌 삼차원적으로 배양하였다. 일부 세포는 구모양의 스피어 (sphere)를 형성하였고, 스피어 유래 세포에는 CD49f 의 발현이 높았으며 PI3K/AKT 신호가 향상되어 있는 것을 확인하였다. 인위적으로 CD49f 를 과발현시킬 경우, PI3K/AKT 신호가 활성화되며 동시에 p53 발현은 억제되었다. 전분화능 인자인 OCT4 와 SOX2 는 CD49f 의 프로모터 부분에 직접적인 결합을 하며, 이를 통해 CD49f 의 발현을 조절하였다. CD49f 의 역할을 배아줄기세포에서도 관찰하였으며, CD49f 의 발현이 배아줄기세포의 전분화능을 유지하는데도 기여함을 확인하였다. 배아줄기세포를 배상체 (embryoid body) 형성을 유도해 분화시킬 경우 CD49f 의 발현은 급격히 감소하였고, siRNA 를 통한 CD49f 발현 억제는 PI3K/AKT 신호 억제와 p53 발현 증가를 가져왔다. 이러한 결과를 통해서 CD49f 가 중간엽줄기세포의 분화능과 배아줄기세포의 전분화능 유지에 중요한 역할을 함을 증명하였다.

일반 체세포와 마찬가지로 성체줄기세포는 일생을 거쳐 다양한 스트레스 요인에 노출되며, 수와 기능이 수명과 반비례하여 떨어지게 된다. 이 연구의 두번째, 세번째 부분에서는 중간엽줄기세포 노화의 중요한 조절인자인 HMGA2 와 ZMPSTE24 의 분자적 조절 기전을 조사하였다. HMGA2 (human high-mobility group protein A2)는 DNA 와의 결합을 통해 크로마틴 구조를 변형시키는 구조적 전사 인자이며, 최근 HMGA2 가 태아의 신경줄기세포에서

높게 발현하며 줄기세포능을 조절한다는 연구결과가 발표되었다. 이 연구에서는 HMGA2 가 세포 노화 및 증식능에 미치는 직접적인 영향과 그 잠재적 조절 기전에 대해 분석하였다. 실험을 수행한 결과, HMGA2 의 과발현이 중간엽줄기세포의 증식능을 높이고 노화를 억제하는 것을 관찰하였다. 이 효과는 cyclin E 와 CDC25A 의 발현 증가 및 cyclin 의존적 효소 억제제들의 발현 감소와 함께 발생하였다. 또한, HMGA2 의 발현을 억제시키면 증식능이 감소하며 지방분화능이 저해되었다. microarray 데이터를 이용해 분자적/세포적 기능 분석을 실시한 결과, HMGA2 과발현은 PI3K/AKT/mTOR/p70S6K 신호를 증가시키며, 이를 통해 노화 표지인자인 $p16^{INK4A}$ 와 $p21^{CIP1/WAF1}$ 의 발현을 억제 시킴을 확인하였다.

ZMPSTE24 는 핵막 단백질인 라민 A 의 단백질 번역 후 성숙 과정에 연관된 인자이다. ZMPSTE24 의 기능적 결함이 발생하면 프리라민 A 가 핵막에 축적되며 세포의 조로(早老)가 유도된다. 세포의 반복계대에 의한 노화 혹은 HDAC 억제제에 의한 노화 현상에서 ZMPSTE24 가 감소되며 프리라민 A 가 축적되었다. 세포 노화 현상 진행 중 증가하는 miRNA-141 은 ZMPSTE24 를 표적하는 것으로 증명되었고, 과발현을 통해 프리라민 A 의 축적을 유도하였다. VPA/SB 처치를 통한 세포 노화 중에 anti miRNA-141 을 처치하면 비정상적 핵형의 발생이 억제됨을 확인하였다. 또한 miRNA-141 프로모터 부분의 후성학적 히스톤 표지인자들이 노화 과정에서 활성형으로 변화되었다.

이 결과들을 토대로 다음과 같은 결론을 도출하였다.

i) OCT4, SOX2 의 직접적 조절을 통한 CD49f 발현은 중간엽줄기세포 구형성능과 분화능을 결정함에 중요한 역할을 한다.

ii) HMGA2 는 PI3K/AKT/mTOR/p70S6K 신호를 증가시키며, $p16^{INK4A}$, $p21^{CIP1/WAF1}$ 발현을 억제한다. 이를 통해 in vitro 노화를 조절한다.

iii) 히스톤 아세틸화효소는 miRNA-141 을 통해 ZMPSTE24 의 발현을 조절하며 프리라민 A 축적을 유도한다.

이 연구를 통해 CD49f, HMGA2, ZMPSTE24 의 발현이 인간 중간엽줄기세포의 줄기세포능 및 노화 과정을 조절함을 증명하였고 관련 분자, 생물학적 기전을 규명하였다.

주요단어 : 중간엽줄기세포, CD49f, PI3K/AKT/p53 신호, HMGA2, $p16^{INK4A}$, 노화, 라민 A, ZMPSTE24, miRNA-141

학번 : 2008-21748

감사의 글

처음 대학원 진학을 결정하던 시간들이 떠오릅니다. 줄기세포를 처음으로 접했던 건, 생명공학을 공부하던 대학교 재학시절이었습니다. 우리 몸을 구성하고 있는 거의 모든 종류의 세포로 분화 가능한, 줄기세포의 능력에서 무한한 가능성을 발견했고, 내가 지금 하고 있는 생명공학과 관련된 일이 미래 질병 치료에 획기적인 길을 제시할 수 있다는 사실에 심장이 뛰었습니다.

그 후 줄기세포 연구를 시작하였고, 어느덧 6년이 흘렀습니다. 그동안 보내왔던 시간들이 결코 수월하지는 않았습니다. 다만 매순간 적당히 타협하지 않고, 주어진 상황에서 최선을 다할 수 있기를 기도하고, 노력했습니다. 열심히 일할 수 있도록 이 모든 환경을 제게 예비하시고 허락해 주신 하나님께 감사드립니다. 건강한 몸과 마음을 주신 부모님께도 감사를 드립니다. 준비 없이 맞이한 기회는 놓쳐버리기 쉽기에, 항상 깨어있는 상태에서 준비하고 겸손하게 살라고 하셨던 두 분의 말씀을 앞으로도 가슴에 새기고 살겠습니다. 부족한 동생을 많이 아끼고 사랑해준 누나와, 언제나 든든하게 응원해준 매형께 감사드립니다.

항상 곁에서 6년간, 때로는 엄한 선생님처럼, 때로는 자상한 아버지처럼 도와주시고 연구에 매진할 수 있게 지도해주신 강경선 교수님께 감사의 말씀을 드리고 싶습니다. 교수님께서는 차별 없이 공평하게, 있는 그대로 저희를 대해주셨습니다. 앞으로 저 역시 그런 지도자가 되고 싶습니다. 퇴임하신 이영순 교수님께도 감사의 인사를 드립니다. 또한, 학위논문의 방향을 잡아주시고 지도해주신 서울대학교 생명과학대학 정진하 교수님과 이건수 교수님, 서울대학교 수의과대학 한호재 교수님께도 감사드립니다. 독일 Max Planck 연구소에서부터 물심양면으로 도와주신 건국대학교 고기남 교수님, 한동욱 교수님, 감사드립니다. 실험과 관련하여 다양하게 논의해주신 서울대학교 Andreas Kurtz 교수님, 국립보건연구원의 정지원 박사님, 한양대학교 김형범 교수님, 강원대학교 양세란 교수님께 감사드립니다.

서울대학교 수의과대학 공중보건학교실 식구들에게 진심으로 감사하다는 말씀을 드리고 싶습니다. 많은 조언과 격려해주신 홍인선 박사님, 최순원 박사님, 민수형, 경환이형, 상범이형, 힘든 시간들을 함께 한 동기들, 승희 누나, 형식이형, 유진누나, 여러모로 부족한 선배를 믿고 열심히 따라준 지희씨, 진영이, 항상 많은 도움을 받았고 앞으로 교실을 이끌어갈 후배들, 태훈씨, 태욱씨, 영실이, 유영이, 인성씨, 재준이, 병철이, 명근이에게 고마움을 전합니다.

학위과정은 끝이 났지만 앞으로 해 나가야할 일들이 많이 남았기에 기대되고, 할 수 있는 일들이 많기에 행복합니다. 현실에 안주하지 않고 철저마침 (鐵杵磨針)의 노력으로 학문에 정진하고 목표를 향해 나아가겠습니다. 다시 한 번 도움주신 분들께 감사의 말씀을 전합니다.

2013 년 2 월

유경록 드림